Université de Liège

Faculté des Sciences Appliquées

Calculation of internal forces in axially and rotationally restrained beams under natural fire

Travail de fin d'études présenté par

François HANUS

en vue de l'obtention du diplôme d'Etudes Approfondies en Sciences Appliquées

Année académique 2007-2008

Acknowledgements

Professor J. M. Franssen, promoter of this work, is gratefully acknowledged for having supervised this work and for his helpful advices.

I am also grateful to my colleagues who, by the way of scientific discussions and an unfailing friendship, help me everyday to overcome new obstacles.

Finally, I would like to thank my family and best friends for their indispensable support

François Hanus

Faculté des Sciences Appliquées 3ème cycle

Année académique 2007-2008

” Determination of internal forces in axially and rotationally restrained beams submitted to a natural fire “

When a constituent of a frame is subjected to fire, the thermal dilatation and bowing of this element is limited by the action of the surrounding frame. The reduction of steel mechanical properties and restrained thermal deformations induce a new distribution of internal forces in the frame. Generally, the stability of structures is calculated by the use of recommended temperature-time curves that do not considered the cooling phase of the fire. After being submitted to high compressive forces and experiencing significant plastic deformations, heated elements become in tension. As it was observed experimentally, the failure of bolts due to an excess of tensile forces may occur during the cooling phase of the fire.

That is the reason why a research project on the design of connections subjected to natural fire (COSSFIRE) has been funded by the Research Fund for Coal and Steel (RFCS). The objective of this project is to provide experimental data and to propose guidelines for designing the joints including both the heating and cooling phases.

This work describes a part of the contribution of the University of Liège in the project COSSFIRE. It is focused on the determination of the internal forces experienced by axially and rotationally restrained beams submitted to a natural fire. This preliminary step is essential for an optimised design of connections in similar conditions.

This work is subdivided three parts. Firstly, some experimental tests have been modelled numerically with the homemade finite element software SAFIR in order to validate it and the models used to analyse this type of problem. Secondly, a set of parametrical analyses have been performed in order to better understand the influence of several factors on the induced internal forces and provide some reference results for the last part of the work. Finally, some simplified methods, based on Wang’s method, have been defined to allow determining the internal forces in a given case without requiring any numerical simulation in finite element packages.

Promoteur : J. M. Franssen

Membres du jury :

J. M. Franssen J.C. Dotreppe J.P. Jaspart O. Vassart

1 Introduction

1.1 Context

For about fifty years, scientists and engineers have been focussing on the structural behaviour of buildings submitted to fire and have been investigating on improvements that enable to fulfil demands aiming at insuring the humans' safety and reducing material damages. These purposes can only be accomplished if the stability of constructions is guaranteed during a sufficient period of time in order to make possible the evacuation of persons and the intervention of firemen. The expansion of fire to other parts of the devastated building has also to be avoided.

Steel constructions lose rather quickly their stability when submitted to elevated temperatures. The main explanations to this are the relative thinness of individual elements and the high conductibility of steel. The fast heating of structural elements induces an important reduction of their mechanical properties. Consequently, it is often necessary to protect steel structures thermally with sheets of insulating materials or intumescent paintings.

The evolution of the mechanical behaviour of beams and columns at elevated temperatures is quite widely known. However, the joints behaviour under fire loading has not been studied so extensively.

In the first European design codes, it was considered as unnecessary to focus on the behaviour of joints under fire conditions because of the less severe exposition to fire and the presence of more material in the joint zone. The large amount of joints typologies, the large number of parameters influencing their behaviour and the difficulty to realize some tests are other explanations to the lack of sufficient knowledge of joints behaviour under fire conditions.

As the response of joints is very important in global frames analyses, some investigations were conducted during the last few years, mainly in Europe. The first design rules have been stated from the Component Method developed initially for joints at room temperature. This method has been adapted later to accommodate with the design of joints under fire loading. More recently, some real-scale tests performed in Cardington and Vernon have shown that the failure of steel or steel-concrete composite structures may occur in connection components during the cooling phase due to the tensile forces created in steel beams after significant plastic deformations have been undergone during the heating phase.

A research project, supported by the Research Fund for Coal and Steel (RFCS), is aiming at enhancing the scientific findings and to develop efficient, practical and economic design rules on steel connections when exposed to real fire conditions as a result of experimental, numerical and analytical investigations. The present work reports a part of the numerical and analytical developments carried out at the University of Liège as a partner of this research project still in progress. The objectives and the content of this study are briefly described in the following paragraph.

1.2 Objectives

The failure of steel and steel-concrete composite structures may happen during the cooling phase of a natural fire owing to the incapacity of joints to resist applied tensile forces. The evaluation of the axial load applied to joints depends on a range of parameters: fire loading, mechanical loading, axial and rotational restraints provided by the surrounding structure, beam stiffness and resistance. The main objective of this work consists in analysing the structural behaviour of steel and composite structures and quantifying the axial thrusts created during both the heating and cooling phases in function of the above-mentioned parameters. The work is divided in the following steps:

Chapter 2 is a large overview of the available knowledge in the behaviour and the design of connections at room and elevated temperature. The classification of joints and the design method proposed in the recent European standards are reported. The experimental and analytical works undertaken in the scope of determining internal forces in restrained elements are shortly described.

Chapter 3 is a more detailed description of experimental tests that have been simulated numerically in order to validate the homemade software SAFIR and the type of model used later in the parametrical analysis.

SAFIR and CoP programs are presented in Chapter 4. A special attention is given to the new material laws defined in SAFIR in order to improve the modelling of the behaviour of connections in structural analyses.

In Chapter 5, numerical analyses of experimental tests performed in SAFIR program are presented.

Chapter 6 is dedicated to the description of the parametrical analyses. One-dimensional and two-dimensional are successively considered. In both cases, reference cases are chosen and

analysed accurately and then, the influence of several parameters is studied.

Chapter 7, based on the Wang's method and the results provided by the parametrical analyses, consists in the definition of a simplified method to calculate the internal forces and evaluate the displacements of a restrained beam submitted to natural fire. Some improvements to the Wang's method and an extension to cooling phase are proposed.

Conclusions and output of the present work are presented in Chapter 8. Perspectives for future studies are also listed in this section.

2 State-of-the-art

2.1 Introduction

The present paragraph aims at producing a state-of-the-art about the fire safety engineering and natural fire concept, the design and the behaviour of steel and composite steel-concrete connections at room temperature and elevated temperatures and the evaluation of internal forces in restrained elements submitted to fire.

2.2 Fire Safety Engineering and Natural Fire Concept

The overall purpose of fire safety is to reduce the risk of life and property losses, the main concern being the safety of lives. Fire Safety Engineering is a global discipline aiming at determining safety strategy for buildings submitted to fire conditions, in which structural stability and control of fire spread are achieved by providing adequate active and/or passive fire protection.

Structural Fire Engineering is the part of that discipline dealing with the thermo-mechanical analyses of structures submitted to fire and the design of members that ensures a sufficient load bearing resistance and controls the fire spread. A fire analysis consists of four successive steps:

- Selection of the design fire scenarios
- Modelling of the fire
- Thermal Analysis
- Structural analysis

The starting point of a fire is the presence of three elements simultaneously: oxygen, fuel and a heat source. The evolution of temperature during a real fire can be divided in five phases:

i. Smouldering phase: ignition and smouldering fire at very low temperature (not considered in calculations and tests) ;

ii. Growing phase: the fire remains localised up to a possible flashover ;

iii. Flashover: formation of a generalised fire (very short period of time) ;

iv. Post-flashover: combustion of the combustible materials (variable duration) ;

v. Decreasing phase: combustible materials have completely burnt and temperature decreases.

The duration of the post-flashover phase depends on the fire loading (total energy released by the complete combustion of materials situated in the compartment divided by the floor area), the surface of openings and the characteristics of walls.

Many experimental and theoretical investigations undertaken more than 25 years ago have lead to the definition of a unique ISO standard temperature-time curve:

$$T - T_{ini} = 345 \log_{10} (8\,t + 1)$$

- t is expressed in minutes ;
- T_{ini} is the initial temperature in the room or the furnace ;
- T is the ambient temperature.

This ISO-834 curve is considered as quite severe for fires in buildings and is one of the numerous standard temperature-time curves (ASTM-E.119 [ASTM, 1998], JIS A 1304 [JIS, 1982]). However, these curves do not describe natural fires realistically. A more rational approach to fire engineering design of buildings requires methods based on actual fire exposure conditions. By example, Annex A of EN 1991-1-2 [CEN, 2002] proposes some parametrical temperature-time curves.

2.3 Thermal analysis of steel elements

2.3.1 Steel thermal properties at elevated temperatures

The specific heat c is the measure of the heat energy required to increase the temperature of a material during a certain temperature interval.

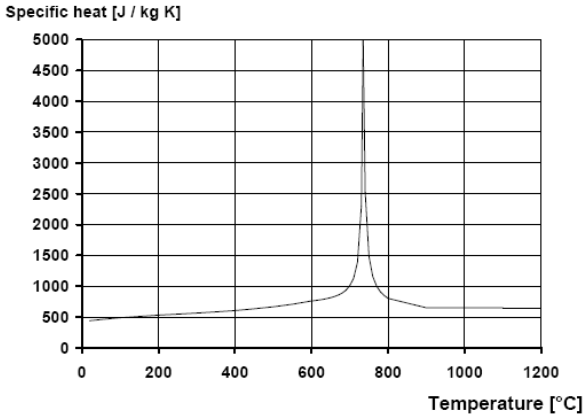

Figure 2-1 : Specific heat of carbon steel as a function of temperature (EN 1993-1-2)

The thermal conductivity λ of a material characterizes its ability to conduct heat. It is defined as the quantity of heat transmitted during a period of time per unit of length.

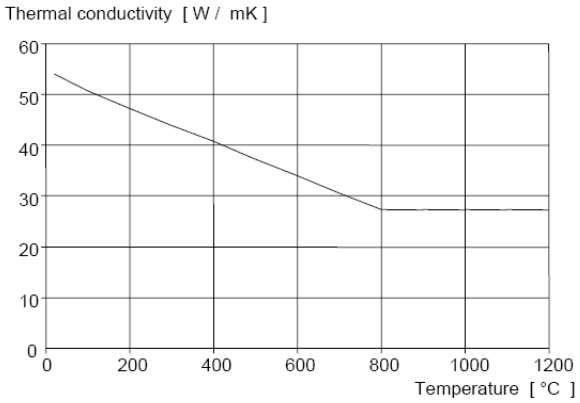

Figure 2-2 : Thermal conductivity of carbon steel as a function of temperature (EN 1993-1-2)

The emissivity of a given material is the ratio between the radiative heat absorbed by a surface made of this material and that of a black body surface. In general, the emissivity of structural materials may be taken as equal to 0.8 according to EN 1991-1-2 [CEN, 2002] recommendations but the EN 1993-1-2 [CEN, 2005] allows to consider a value equal to 0.8.

The relative thermal elongation is the ratio between the variation of length ΔL undergone by a steel element owing to thermal variation and the length L of the element at room temperature. This parameter is approximately linear until 750°C, remains constant in the range [750°C ; 860°C] and increases linearly after this plateau (Figure 2-3).

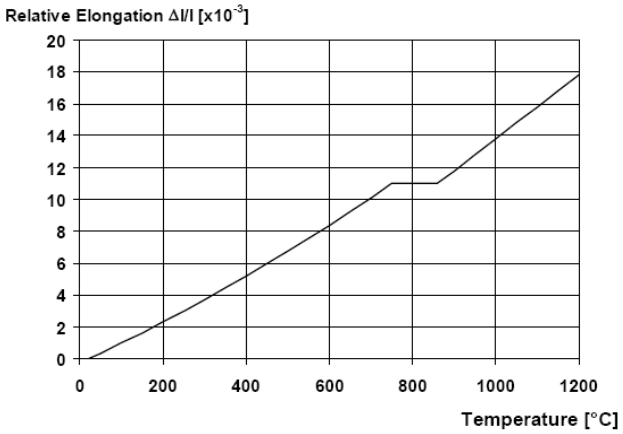

Figure 2-3 : Relative thermal elongation of carbon steel as a function of temperature

2.4 Joints calculation at room temperature

2.4.1 Definitions

The two different English words “joints” and “connections” are distinguished in the Eurocode 3-1-8 [CEN, 2003]. A connection is a location where two or more elements meet. The most common types of connections are double angle web cleats connections, flange cleats connections, flush and extended end plate connections, fin plate connections and welded connections. For design purposes, the connection is the assembly of the basic components required to represent the behaviour during the transfer of the relevant internal forces and moment at the connection. The joint is the zone where the members are interconnected (Figure 2-4). The most common joint configurations are single-sided and double-sided beam-to-column joints, beam and columns splices and column bases (Figure 2-5). For design purposes, the joint is the assembly of all the basic components required to represent the behaviour during the transfer of the relevant internal forces and moments between the connected members. For example, a beam-to-column joint consists of a web panel and one connection or two connections.

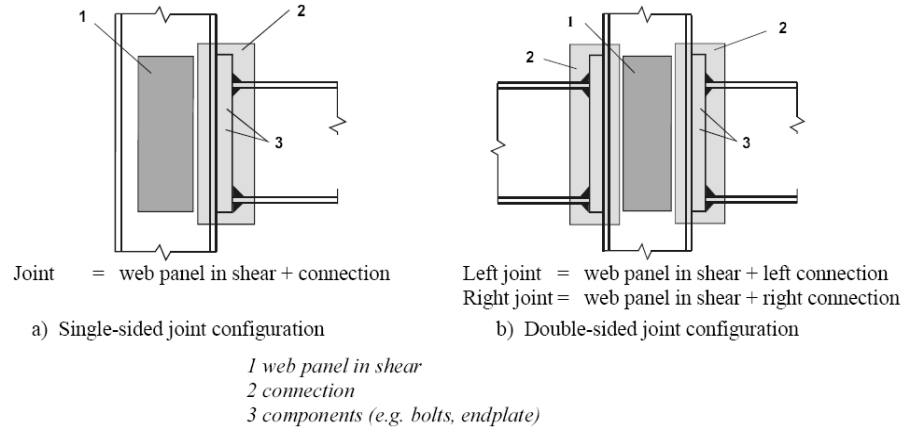

Figure 2-4 : Parts of a beam-to-column configuration

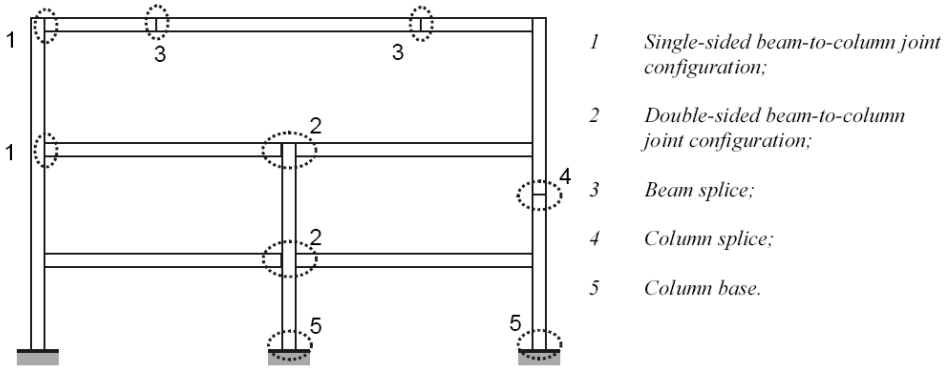

Figure 2-5 : Joint configurations

2.4.2 Classification of joints

Joints may be classified by their stiffness and by their strength.

2.4.2.1 Classification of joints by stiffness

A joint may be classified as rigid, nominally pinned or semi-rigid according to its rotational stiffness by comparing its initial rotational stiffness $S_{j,ini}$ with the classification boundaries defined in Figure 2-6. The rotational stiffness of a joint is the moment required to produce a unit rotation in that joint.

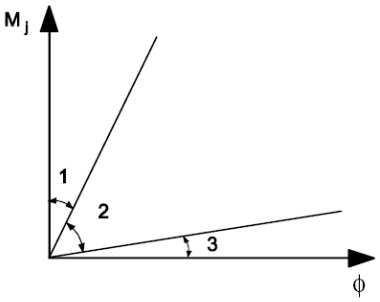

Zone 1: rigid, if $S_{j,ini} \geq k_b EI_b / L_b$

where

k_b = 8 for frames where the bracing system reduces the horizontal displacement by at least 80 %

k_b = 25 for other frames, provided that in every storey $K_b/K_c \geq 0,1$ *)

Zone 2: semi-rigid

All joints in zone 2 should be classified as semi-rigid. Joints in zones 1 or 3 may optionally also be treated as semi-rigid.

Zone 3: nominally pinned, if $S_{j,ini} \leq 0,5 EI_b / L_b$

*) For frames where $K_b/K_c < 0,1$ the joints should be classified as semi-rigid.

Key:

K_b is the mean value of I_b/L_b for all the beams at the top of that storey;
K_c is the mean value of I_c/L_c for all the columns in that storey;
I_b is the second moment of area of a beam;
I_c is the second moment of area of a column;
L_b is the span of a beam (centre-to-centre of columns);
L_c is the storey height of a column.

Figure 2-6 : Classification of joints by stiffness according to prEN 1993-1-8 : 2003

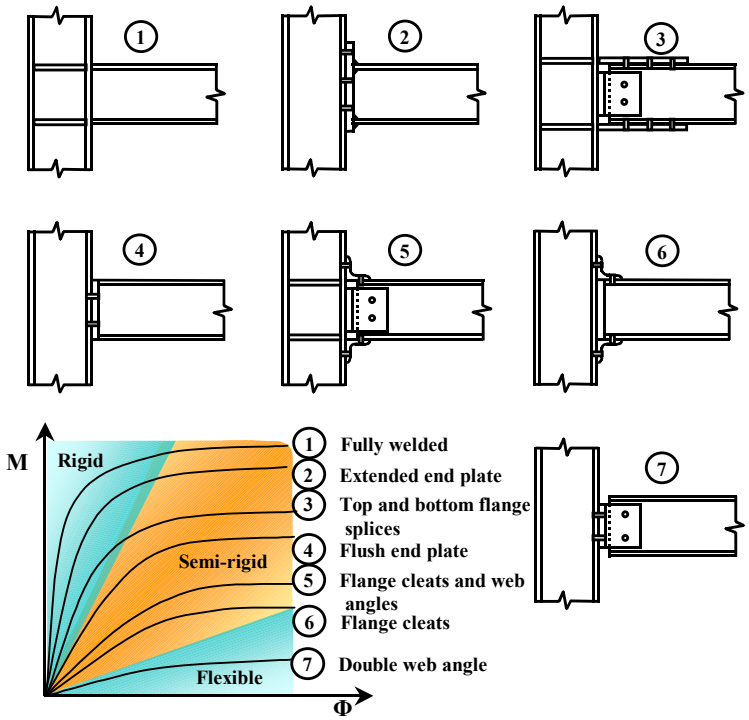

Figure 2-7 : Typical beam-to-column joints and a diagrammatic stiffness classification (S. Spyrou, 2002)

A nominally pinned joint shall be capable of transmitting the internal forces, without developing significant moments which might adversely affect the members or the structure as

a whole and shall be capable of accepting the resulting rotations under the design loads. Joints classified as rigid may be assumed to have sufficient rotational stiffness to justify analysis based on full continuity. A joint which does not meet the criteria for a rigid joint or a nominally pinned joint should be classified as a semi-rigid joint. It should be capable of transmitting the internal forces and moments.

2.4.2.2 *Classification of joints by strength*

A joint may be classified as full-strength, nominally pinned or partial strength by comparing its design moment resistance $M_{j,Rd}$ with the design moment resistances of the members that it connects. When classifying joints, the design resistance of a member should be taken as that member adjacent to the joint.

The design resistance of a full-strength joint shall not be less than that of the connected members. A joint may be classified as full-strength if it meets the criteria given in Figure 2-8. A nominally pinned joint shall be capable of transmitting the internal forces, without developing significant moments which might adversely affect the members or the structure as a whole. It shall be classified as nominally pinned if its design moment resistance $M_{j,Rd}$ is not greater than 0,25 times the design moment resistance required for a full-strength joint, provided that it also has sufficient rotation capacity to accept the resulting rotations under the design loads. A joint which does not meet the criteria for a full-strength joint or a nominally pinned joint should be classified as a partial-strength joint.

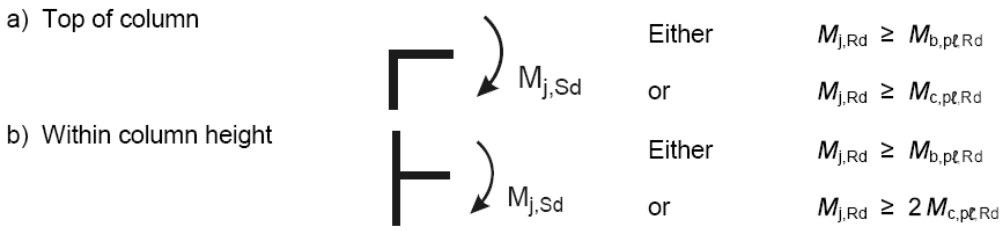

Figure 2-8 : Criteria for full-strength joints

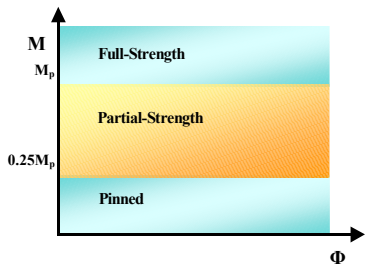

Figure 2-9 : Classification of joints by strength according to prEN 1993-1-8 : 2003 (S. Spyrou, 2002)

2.4.3 Global analysis

To identify whether the effects of joint behaviour on the analysis need to be taken into account, a distinction may be made between three simplified models as follows:

- simple, in which the joint may be assumed not to transmit bending moments;
- continuous, in which the behaviour of the joint may be assumed to have no effects on the analysis;
- semi-continuous, in which the behaviour of the joint needs to be taken into account in the analysis.

Method of global analysis	Classification of joint		
Elastic	Nominally pinned	Rigid	Semi-rigid
Rigid-Plastic	Nominally pinned	Full-strength	Partial-strength
Elastic-Plastic	Nominally pinned	Rigid and full-strength	Semi-rigid and partial-strength Semi-rigid and full-strength Rigid and partial-strength
Type of joint model	Simple	Continuous	Semi-continuous

Table 2-1 : Types of joint models

2.4.3.1 Elastic global analysis

In an elastic global analysis, the joints are classified according to their rotational stiffness and shall have sufficient strength to transmit the forces and moments acting at the joints resulting from the analysis.

In the case of a semi-rigid joint, the rotational stiffness S_j corresponding to the bending moment $M_{j,Ed}$ should generally be used in the analysis. If $M_{j,Ed}$ does not exceed 2/3 $M_{j,Ed}$, the initial rotational stiffness $S_{j,ini}$ may be taken in the global analysis (Figure 2-10a). As a simplification to this, the rotational stiffness may be taken as $S_{j,ini}/\eta$ in the analysis, for all values of the moment $M_{j,Ed}$ (Figure 2-10b) where η is the stiffness modification coefficient shown in Table 2-2.

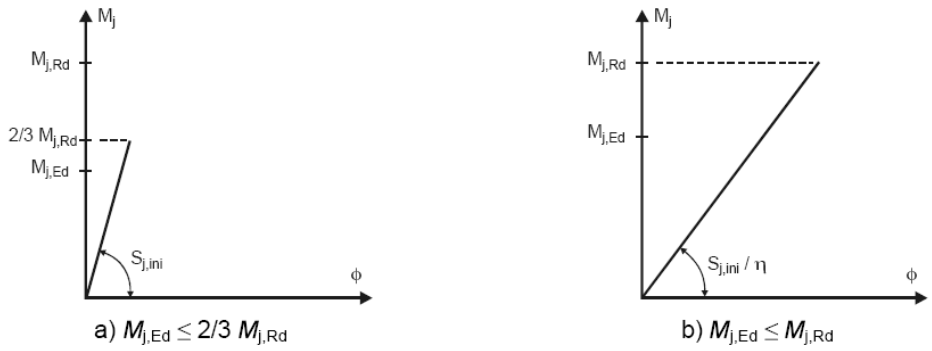

Figure 2-10 : Rotational stiffness to be used in elastic global analysis according to prEN 1993-1-8:2003

Type of connection	Beam-to-column joints	Other types of joints (beam-to-beam joints, beam splices, column base joints)
Welded	2	3
Bolted end-plate	2	3
Bolted flange cleats	2	3,5
Base plates	-	3

Table 2-2 : Stiffness modification coefficient η

2.4.3.2 Rigid-plastic global analysis

In a rigid-plastic analysis, the joints should be classified according to their strength and the rotation capacity of a joint shall be sufficient to accommodate the rotations resulting from the analysis.

2.4.3.3 Elastic-plastic global analysis

The joints should be classified according to both stiffness and strength. The moment-rotation characteristic of the joints should be used to determine the distribution of internal forces and moments. As a simplification, the bi-linear design moment-rotation characteristic shown in Figure 2-10 may be adopted, where η is the stiffness modification coefficient.

2.4.4 Component method

The Component Method is a versatile approach for calculating rotational stiffness, axial stiffness and the capacity of joints. The original feature of this method is to consider any joint as a set of individual basic spring-like components (Figure 2-11). For each component, the non-linear stiffness and maximum force is computed and assembled to form a spring model,

which represent the global behaviour of the joint.

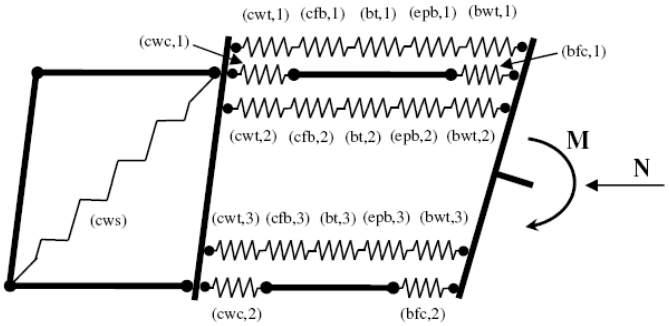

Figure 2-11 : Spring model of an extended end-plate joint for moment and axial force (Cerfontaine, 2004)

The application of this method requires the following three steps:

- Identification of the active components in the considered joint;
- Evaluation of the stiffness and/or resistance characteristics for each individual basic component;
- Assembly of all components and evaluation of the whole joint stiffness and/or resistance characteristic.

2.4.5 Analytical characterisation of joints under bending moment

As shown on Figure 2-7, the actual moment-rotation response of a joint is usually non-linear. Based on the Eurocode prEN 1993-1-8 recommendations [CEN, 2003], COST C1 [J.-P. Jaspart, 1994] suggests three different M-ϕ relationships to characterize the semi-rigid behaviour of connection at room temperature.

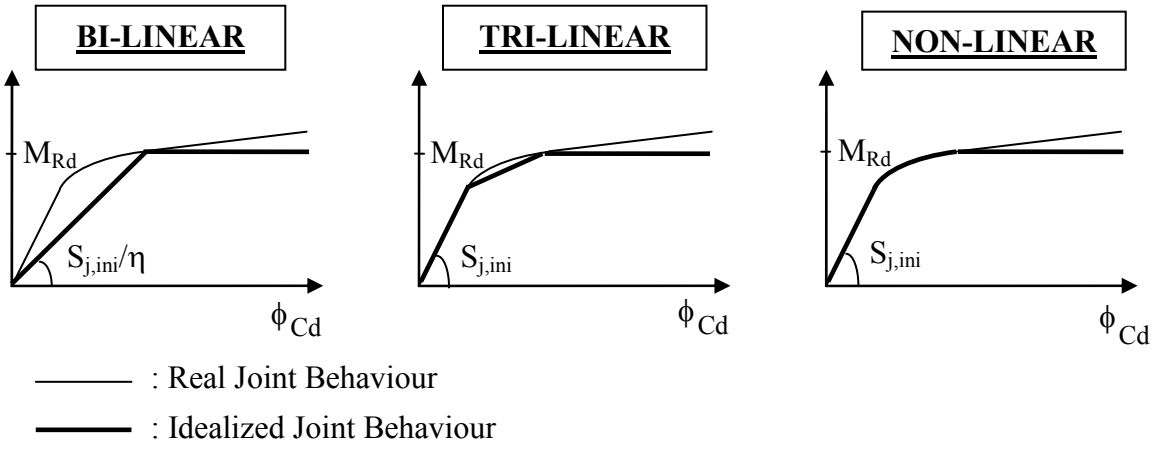

- In the bi-linear law, the stiffness of the joint S_j is assumed to remain constant until the applied bending moment $M_{j,Ed}$ is equal to the resisting bending moment $M_{j,Rd}$. In beam-to-column connections, $S_j = S_{j,ini}/2$;
- In the tri-linear law, the stiffness of the joint is equal to the initial stiffness $S_{j,ini}$ until $M_{j,Ed} = 2/3\ M_{j,Rd}$. For $M_{j,Ed} \in [2/3\ M_{j,Rd}\ ;\ M_{j,Rd}]$, $S_j = S_{j,ini}/7$;
- In the non-linear law, the stiffness of the joint is equal to the initial stiffness $S_{j,ini}$ until $M_{j,Ed} = 2/3\ M_{j,Rd}$. A non-linear function of the stiffness is defined for $M_{j,Ed} \in [2/3\ M_{j,Rd}\ ;\ M_{j,Rd}]$:

$$S_j = \frac{S_{j,ini}}{\left(1,5\, M_{j,Ed} / M_{j,Rd}\right)^{\psi}} \quad \text{where } \Psi = 2,7 \text{ in end-plate and welded connections.}$$

Considering one of these elastic-plastic curves, it is necessary to check if the joint rotation does not exceed its rotation capacity ϕ_{Cd}. Eurocode 3 does not mention any calculation method to evaluate the rotation capacity. Jaspart has proposed a method to evaluate a post-critical stiffness of a joint and to deduce the rotation reached at the ultimate bending moment [Jaspart, 1991].

2.5 Joints calculation at elevated temperature

The summarization of the previous researches and experimental programmes carried out in the field of connections under fire loading is partially based on an article of Al-Jabri published recently [K.S. Al-Jabri and al., 2008]. The design of connections under natural fire necessitates the assessment of internal forces in the joint taking into account the evolution of stiffness during the fire and the verification that the resistance of the joint is sufficient. The evaluation of axial thrusts created by fire in restrained elements during both heating and

cooling phase still needs to be investigated experimentally because few results are currently available. However, several numerical tools predict quite accurately the internal forces produced by fire.

2.5.1 Mechanical behaviour of joints submitted to fire

The first experimental tests on connections under standard fire conditions have been undertaken at CTICM [J. Kruppa, 1976]. This study was not focused on the global behaviour of joints but it showed that the failure of bolts was preceded by important deformations in the other elements. A couple of years later, INSA of Rennes performed some tests on bolts at elevated temperatures to investigate on their behaviour both under tension and shear loading [H. Riaux, 1980]. The creep influence was particularly analysed.

British Steel conducted two fire tests on rigid joints [British Steel, 1982]. These results showed that significant deformations are undergone in the joint during the fire and that the assumption of a rigid behaviour at high temperatures is consequently not valid.

The first tests realized to investigate on the global behaviour of joints have been performed by Lawson on three common types of connections: extended end-plate, flush end-plate and double web-cleats connections [Lawson and al., 1990]. Both bare-steel and steel-concrete composite connections were studied. Lawson observed that significant bending moments are transferred during the fire test. He suggested that composite action in fire contributes to an enhanced moment capacity of joints, which could be estimated by adding the moment capacities of the bare steel joint and the reinforced concrete slab In addition, he proposed a simple method to design simply supported beams submitted to fire and adapted it in order to integrate the effect of moments transferred by joints.

Leston-Jones tests [L. C. Leston-Jones, 1997] was aimed at deriving a set of moment-rotation curves of a unique joint configuration (flush end-plate connections) submitted to five different load ratios at elevated temperature. A modified form of the Ramberg-Osgood equation has been used to define some simplified connection models, based on mathematical curve-fittings procedures. Some numerical simulations made with a software integrating these moment-rotations curves have shown that the fire performance of sub-structures may be significantly enhanced when the real behaviour of common connections, usually considered as pinned, is integrated.

Kirby investigated widely on the behaviour of high-strength 8.8 bolts in fire. He realized series of tests in tension and double shear at temperatures up to 800°C [B.R. Kirby, 1995]. Tests in tensions have highlighted the possible premature failure by thread stripping. The comparison between the performances of high-strength bolts with Eurocodes recommendations for hot rolled structural steel showed that the bolts are far more sensitive

due to the heat treatment methods used in their manufacture. A strength reduction factor was defined for bolts acting in shear and tension.

Al-Jabri conducted series of anisothermal tests to analyse the influence of several parameters on the behaviour of typical joint typologies [K.S. Al-Jabri and al, 1998]: the test series included two full end-plate and one flexible end-plate bare steel connections, and two flexible end-plate composite connections. Moment-rotation temperature curves were derived for each type of connection [K.S. Al-Jabri and al, 2005].

In 2001, an adaptation of the Component Method was proposed in order to extend its applicability to steel joints submitted to fire loading [L. Simões da Silva and al., 2001]. The resistance and the stiffness of each component are multiplied by reduction factors and isothermal moment-rotation diagrams can be obtained at any temperature. That method showed a good agreement with experimental tests already available in literature. A procedure for the evaluation of ductility in steel joints has also been presented [L. Simões da Silva and al., 2002] for end-plate connections.

Spyrou investigated successively on the tension zone and compression zone component within a steel joint at elevated temperature [Spyrou, 2002]. Based on the work previously done by Jaspart [J.P. Jaspart, 1994] at room temperature on T-stubs, he proposed a simplified method to calculate the three failure modes in tension. Concerning the compression zone, Spyrou developed a new method less conservative than those given in BS5950 [BSI, 2000] and ENV 1993: Annex J [CEN, 1994]. The work accomplished on the compression zone was continued by Block: experimental tests at elevated temperatures lead to an improvement of the analytical model [F.M. Block and al., 2005].

2.5.2 Internal forces in restrained elements

The performance of isolated elements in fire is strongly dependent on the boundary conditions. Axial and rotational restraints induce stresses when thermal elongation and thermal bowing are prevented. However, some experiments have shown that the presence of restraints enhance the fire resistance of steel beams. In a study on extended and flush end-plate connections, Liu has shown that the enhancement of the load capacity of an unprotected beam at fire limit state may reach two-thirds of the moment capacity of the beam [T.C.H. Liu, 1999].

In a structure exposed to a real fire, heated elements are successively loaded in compression during the whole heating phase, unloaded during the first part of the cooling phase and loaded in tension until a uniform temperature of 20°C in the structural elements. The first researches were mainly concentrated on the heating phase. Liu conducted an experimental programme, consisting of 16 fire tests on flush end-plate and web-cleat connections, to study the large

deflection behaviour of restrained beams [T.C.H. Liu and al.]. It confirmed that connections can enhance the fire resistance of a beam by reducing some of the mid-span moment during most of the time when temperature is rising, despite the possibility of local buckling in the beam. In web-cleat connections, the transfer of moment is low but a noticeable advantage may be derived from the effect of catenary action.

Wang proposed a simple method to analyse catenary action in steel beams submitted to elevated temperatures [Y.C. Wang and al., 2005a and 2005b]. This method necessitates making an assumption on the beam deflection profile and consists in satisfying the geometric boundary conditions. Uniform and non-uniform temperature distributions have been considered separately but it has been observed that different non-uniform temperature profiles do not have much effect on beam catenary force.

Some full-scale tests have been realised in Cardington in order to reflect the behaviour of a complete building under fire conditions, taking the interaction between structural members into consideration [L. Simões da Silva, 2006]. These tests have shown that the fire resistance predicted by norms is often underestimated. During the tests, it has been observed that the bolts may fail during the cooling phase.

Some tests, based on the results and observations of Cardington tests, have been realised in Coimbra on restrained sub-structures under natural fire [A. Santiago, 2007]. Six different typologies of joints have been tested. The goal of these tests was to deduce some rules for the design of connections that would avoid collapse of structures.

3 Experimental tests

3.1 Tests realized at the University of Manchester

The University of Manchester has carried an experimental programme aimed at examining in detail the role of the connections and axial restraints in the fire resistance of a steel beam when subjected to fire. Twenty fire tests were performed on steel 'Rugby goalpost' frames.

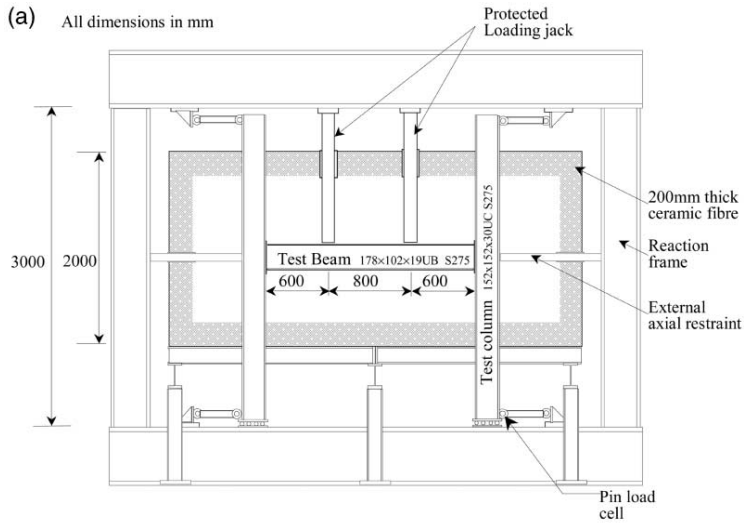

Figure 3-1 : Schematics of the test arrangement of Liu [T.C.H. Liu., 1999]

The beams, with a section 178x102x19UB (S275), were mainly unprotected but top flanges were wrapped with 15 mm thick ceramic fibre blanket in order to simulate the heat-sink effect due to the concrete slab. The columns, with a section 152x152x30UC (S275), together with the connections were generally fire-protected by the use of a 50 mm thickness of ceramic fibre blanket.

Two types of connections were selected as being typical of those commonly used in practice, namely double web-cleats and flush end-plates. The web-cleat connection, which is assumed to have no significant moment capacity, was designed for shear only using angle sections 75x75x8 and M16 Grade 8.8 bolts. A 10 mm thick flush-end plate with M16 Grade 8.8 bolts was used as an alternative connection.

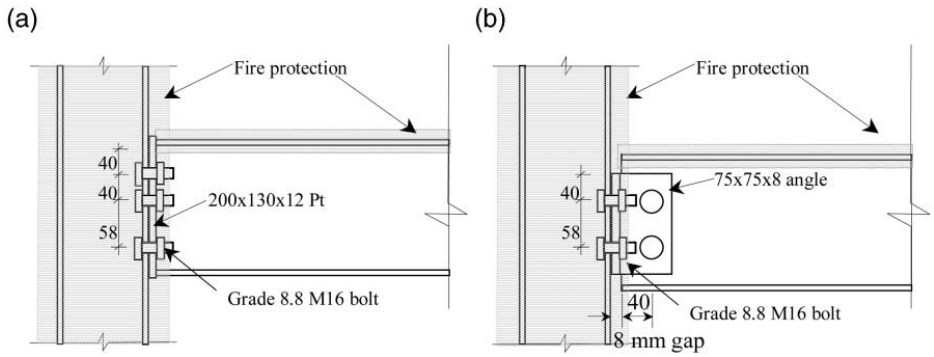

Figure 3-2 : (a) Flush end-plate connection and (b) Web-cleats connection [T.C.H. Liu., 1999]

The beam specimen was subjected to a constant vertical load and the furnace was programmed to follow the ISO834 standard temperature-time curve [CEN, 2002]. Three main level of loading (load ratios of 0.3, 0.5 and 0.7) were tested. The Load Ratio is defined as the ratio of the applied load under fire conditions to the design load-carrying capacity at room temperature of the beam considered as simply-supported.

The 3 meter 152x152x30UC (S275) fire-protected test column alone provided an axial restraint equivalent to a stiffness of 8 kN/mm to the test beam. The possible in-plane restraint imposed by its neighbouring sub-frames has been estimated by Liu and al. to have a range between 10 and about 70 kN/mm. With the use of additional struts spanning between the column of the test frame and the column of the reaction frame (Figure 3-1), two other overall stiffnesses of 35 and 62 kN/mm were achieved.

In the majority of tests performed on flush end-plate connections, Liu observed formation of plastic hinges in the sections where the loading is applied. An exception is the test FUR17, where the Load Ratio is equal to 0.9 and the axial restraint is 8 kN/mm: the excessive material degradation near the connection probably led to local flange buckling causing an almost immediate failure of the specimen.

In tests with web cleat connections, critical temperatures of the beams are 20°C smaller than those obtained with flush end-plate connections. No local buckling was observed closed near to the extremities of the lower flanges. Although usually considered as pinned, web-cleat connections resisted a minimal amount of moment (around 7 kN.m) and the transferred moment still increased after the 8-mm thick gap between the bottom flange of the beam and the column flange was closed.

3.2 Tests realized in the scope of COSSFIRE project

COSSFIRE Project is a European project funded by the Research Fund for Coal and Steel in which the University of Liège is involved. Its main objectives are to enhance the scientific findings and to develop efficient, practical and economic design rules on steel and composite connections when exposed to real fire conditions, including cooling phase. The experimental packages are expected to provide four fire tests on steel structures and four tests on steel and concrete composite structures. In both groups of tests, it was planned to choose one of the three mostly used types of connections (web-cleats, fin-plate and end-plate connections) for a first test under heating up fire exposure condition and a constant applied load to get the critical temperature of this connection. Then, three other fire tests (one with each type of the mostly used connections) are to be carried out under natural fire conditions.

The first two tests have been performed by EFECTIS France. The two used test set-up were identical and are described at (Figure 3-3). The double-sided beam-to-column joint (see blue ring) is composed of two flush end-plate connections whose geometrical characteristics are given in (Figure 3-4). The loaded beam is 5.5 meter-long IPE 300 profile and a portion of 1.7 meter is situated outside the furnace. The HEA 220 column is thermally protected.

The axial restraining system is due to a sub-structure situated outside the furnace and composed of a column and a transversal beam that bends according to its weak axis (Figure 3-3). The mid-span section of the simply-supported transversal beam is connected to the higher extremity of the column that rotates rigidly around its lower pinned support. In order to get an accurate value of the restrained effect, a specific test was carried out. A restrained effect of about 2 kN/mm (1 % of the beam axial stiffness) has been derived.

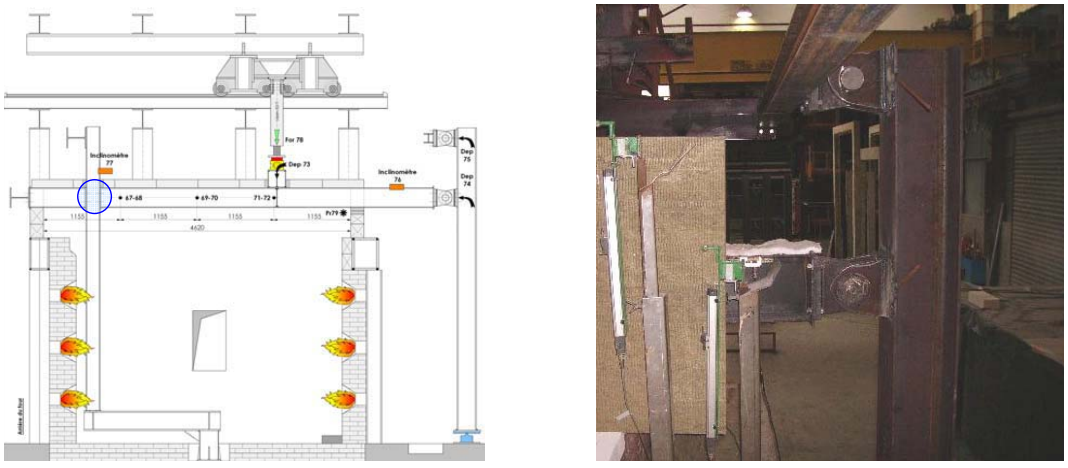

Figure 3-3 : Schematic representation of the test set-up (left) and view of the restraining sub-structure (right)

Figure 3-4 : Geometry of the tested double-sided joint with flush end-plate connections

As these tests are used to investigate on the behaviour of connections including both heating and cooling phases, it is not necessary that the temperature rise of the furnace follows a specific fire curve. It was decided to adopt a temperature rise speed of 10°C/min. During the first test, the specimen was heated increasingly until the steel beam can no longer bear the applied load. For the second test, the specimen was heated up to about 85% of the critical heating obtained with the first test followed by a plateau lasting for about 20 minutes. In both cases, the cooling phase corresponds to the natural cooling condition of the furnace.

4 Tools and software

The numerical simulations of tests and parametrical analyses described in chapters 5 & 6 have been realized with the use of SAFIR program. The analytical calculation of the joints according to the Component Method have been realised with CoP program at room temperature and adapted at elevated temperatures in Excel sheets by assigning time-dependant reduction coefficients on mechanical properties of steel.

4.1 Presentation of SAFIR and description of models

SAFIR is a program based on the Finite Element Method and developed at the University of Liège [J.-M. Franssen, 2007] to analyse the behaviour of two and three-dimensional structures under ambient and elevated temperatures. The available elements are 2-D solid elements, 3-D solid elements, beam elements, shell elements and truss elements.

The analysis procedure is subdivided in a thermal analysis and a structural analysis. A torsional analysis is necessary for beam elements acting in 3-D structures. In the thermal analysis of beam and truss elements, the cross-section is meshed and a non-uniform distribution of temperature is calculated; longitudinal heat transfers are not taken into account. Beam and truss elements are constituted of individual fibres that result from the extrusion of the 2-D finite elements defined in the thermal analysis of the corresponding cross-section. Similarly to this approach, shell elements are constituted of layers and the temperature through the thickness is calculated in a one-dimensional thermal analysis. Both static and dynamic structural analyses are proposed and large displacements are taken into consideration in truss, beam and shell elements.

4.1.1 Joint models

The detailed modelling of joints often requires some 3-D solid and contact elements that have not been developed in SAFIR and necessitates time-consuming calculations. Three proposed models used to substitute the joint behaviour are described below. In a first approach, they are described for 2-D structural applications but the transition to 3-D structural problems would not cause any problem.

4.1.1.1 Three-fibre beam elements

In the first model proposed, not based on the Component Method, the joint is modelled by a unique beam element whose cross-section is composed of three finite elements. The material law is bi-linear for every finite element. The geometry of the cross-section and the material properties are adapted in order to get a mechanical behaviour at room temperature similar to the one calculated analytically. The parameters are the cross-section areas A_1 and A_2, the distance x, the Young's modulus and the elastic limit of the bi-linear material law (Figure 5-1). The equations that have to be filled are the axial stiffness, the resistance to normal forces, the rotational stiffness, the resisting bending moment and the element length.

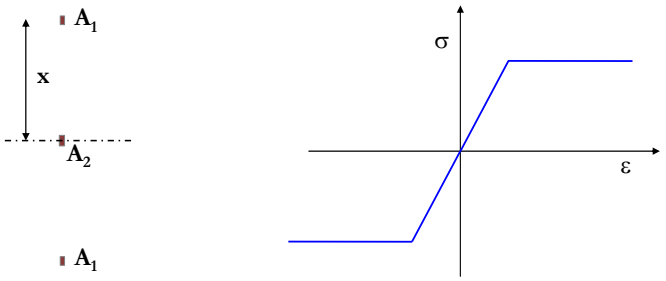

$$\begin{cases} N_{Rd} = A.f_y = (2.A_1 + A_2)\, f_y \\ K_{axial} = \dfrac{EA}{L} = \dfrac{E(2.A_1 + A_2)}{L} \\ M_{Rd} = 2\,x\,A_1\ f_y \\ S_{j,ini} = \dfrac{EI}{L} = \dfrac{2\,E\,A_1\,x^2}{L} \end{cases}$$

Figure 4-1 : Cross-section geometry (left), material law (right) of the three-fibre beam element and equations of compatibility (joint model n°1)

The main advantages of this model are its relative simplicity to evaluate the parameters and the lightness of the numerical calculations. However, the behaviour of this fictitious element differs from the real joint behaviour in many aspects:

- The behaviour is identical in tension and compression so that it is impossible to model accurately and simultaneously the joint response during the heating and the cooling phases ;

- The interaction between bending and normal forces is not accurate ;

- Despite the fact that the bolts resistance and stiffness decrease more rapidly than mechanical characteristics of carbon steel at elevated temperatures, it is impossible to consider different reduction factors under tensile and compression stresses in that model ;

- It is difficult to take account of the thermal gradient present in the joint zone during the fire ;

4.1.1.2 Multi-fibre beam elements

The multi-fibre beam elements are constituted of a number of fibres equal to the number of rows identified by the "Component Method". The resistance and the stiffness of each row are calculated "manually" or with the use of CoP program [J.-P. Jaspart, K. Weynand and al., 1995-2000]. For example, Figure 4-2 shows the cross-section of an extended end-plate connection; the two largest fibres represent the resistance and the stiffness of beam flanges in compression and the three other fibres represent the resistance and the stiffness of bolts rows in tension. The element length and the elastic limit are usually chosen arbitrarily. The cross-section area and the Young modulus are calculated in order to provide the right resistance and stiffness.

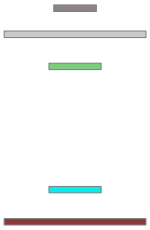

Figure 4-2 : Cross-section of the beam element representing an extended end-plate connection

Some new material laws have been defined in the scope of following the non-symmetric mechanical behaviour of connection rows in the simulations: 'BILIN_TENS' and 'BILIN_COMP' only work in tension or compression respectively. Figure 4-3 shows the mechanical behaviour of the first version of the 'BILIN_TENS' material law when submitted to tensile and compressive stresses. In tension, the law is linearly elastic until the yield limit. A linear hardening branch is defined for tensile stresses higher than the yield limit and the unloading is completely elastic. After a loading-unloading cycle in tension, the $\sigma-\varepsilon$ diagram is translated to the right (yellow axis) to account for plastic deformations ε_{pl}. The proportionality coefficient of the $\sigma-\varepsilon$ diagram in the compression domain is equal to the hardening modulus. It is necessary to give a minimal stiffness to the elements to avoid buckling. Some improvements will be proposed later (see paragraph 4.1.3).

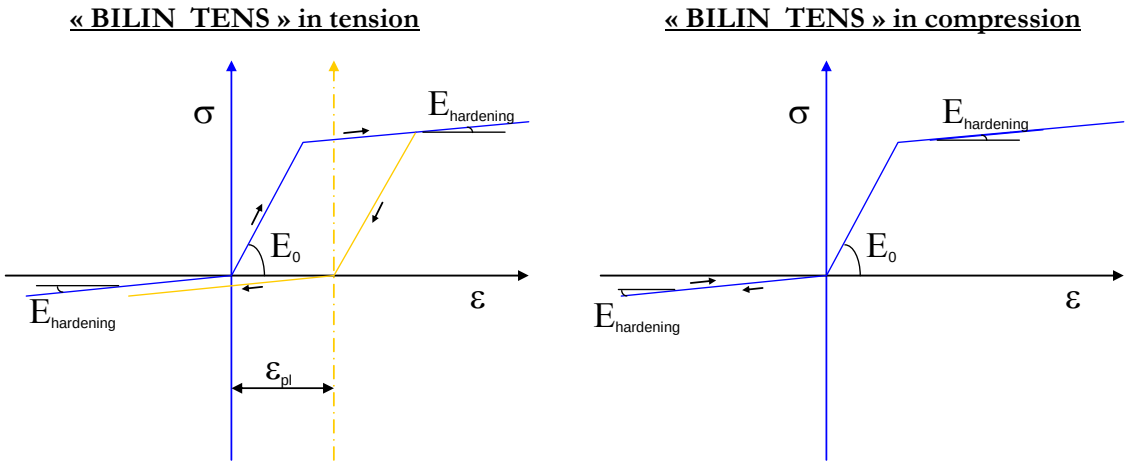

Figure 4-3 : Stress-strain law of BILIN_TENS (Version n°1)

The effect of elevated temperatures on the joint resistance is taken into consideration according to the following approach:

i. Temperature in the joint components is obtained experimentally or numerically ;

ii. Some reduction factors are calculated at each time step for every component ;

iii. The resistances of the components are calculated ;

iv. A fictitious temperature is evaluated in each component to get the right decrease of resistance.

The length of the beam element that represents the effect of the joint is sufficiently short to neglect the thermal elongation in that zone. The necessity to define a fictitious temperature comes from the fact that the reduction of resistance in the component “Bolts in tension” is different from the reduction of resistance in the other components that follow the material law of carbon steel. The bolts resistance decreases quicker than carbon steel due to the thermal treatment they undergo during their fabrication.

The main advantage of the present model is the possibility to follow the individual behaviour of each component, by taking into account the rows activation/deactivation and the presence of plasticity in components. The thermal effect on joint resistance can be accurately considered. This model does not allow getting a realistic evolution of the joint stiffness at elevated temperatures because the “fictitious temperature” defined in a component is evaluated in function of its resistance decrease. The interaction between individual components (group effects) and the resistance in shear can not be considered in that model.

4.1.1.3 *Multi-elements joint model*

Instead of considering an element composed of one fibre per component, the joint may be represented by one truss or beam element per component or row of components (Figure 4-4).

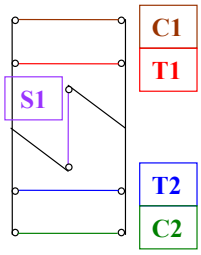

Figure 4-4 : Modelling of a flush end-plate connection

This model allows to define a TRUSS element (S1) that transfers shear forces from beam to columns and to define two elements of a same row in series, allowing the assignment of different material laws in elements of a same row (especially in rows working in tension where end-plate, column and bolts components are put together). However, in comparison with the multi-fibre beam elements, this model necessitates more time for the definition of nodes and elements. Another aspect to investigate is the effect of large displacements: because of the presence of significant deformations during the fire, normal forces create stresses in the shear component and shear forces induce forces in the tension/compression components.

4.1.2 Validation of the BILIN_TENS and BILIN_COMP material laws (Version n°1)

These two new material laws have been inserted in the finite element software SAFIR. In a first approach, BILIN_TENS and BILIN_COMP material laws are defined by four different parameters: Young's modulus, Poisson's ratio, yield limit and hardening coefficient. At elevated temperatures, no thermal elongation is considered but the evolution of mechanical properties is similar to carbon steel as defined in the EN 1993-1-2 [CEN, 2005].

In order to check the validity of the BILIN_TENS and BILIN_COMP material laws and their capacity to model the behaviour of joints components, some simple simulations have been run and compared with the expected results.

4.1.2.1 *Test n°1: single beam in tension (BILIN_TENS) at ambient temperature.*

A one-meter long simply-supported beam has a cross section area equal to 100 cm² and is made of a material that only works in tension. The Young modulus is 210,000 MPa, the

hardening modulus is 1,000 MPa and the elastic limit is 26.72 MPa. This section yields under a load equal to 267.2 kN. The beam is gradually loaded in tension until 300 kN, unloaded, progressively reloaded until 350 kN and unloaded again.

During the first loading cycle of the simulation, the beam elongates elastically until the load is equal to the normal plastic load and the hardening branch is reached. The unloading is completely elastic. The second loading phase is elastic until the load reaches the maximal normal force applied during the first cycle (300 kN) and moves on the hardening branch until N = 350 kN.

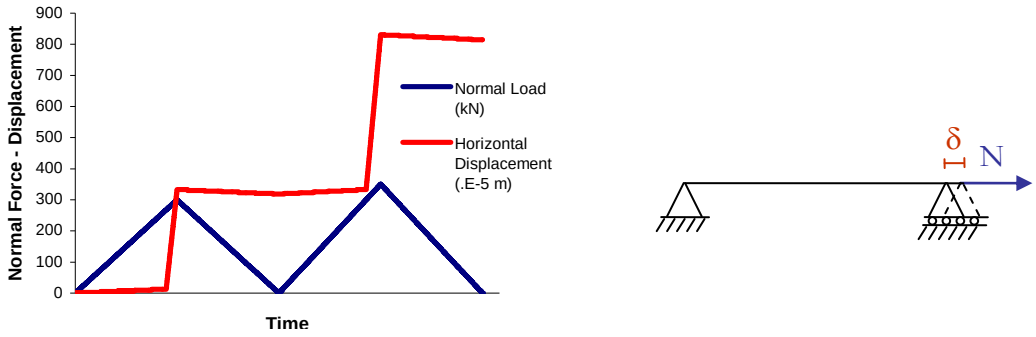

Figure 4-5 : Normal force and horizontal displacement in a BILIN_TENS beam in tension

The same test has been realized with the BILIN_COMP material law that only works in compression. The results are identical and will not be presented here.

4.1.2.2 Test n°2: single beam in tension (BILIN_TENS) at high temperature.

At elevated temperatures, no thermal elongation is considered but resistance and stiffness are reduced. Considering the same geometrical and mechanical data as in Test n°1 at several temperatures, the yield force is proportional to the reduction factor for effective yield strength $k_{y,\theta}$ defined in the Eurocode for carbon steel.

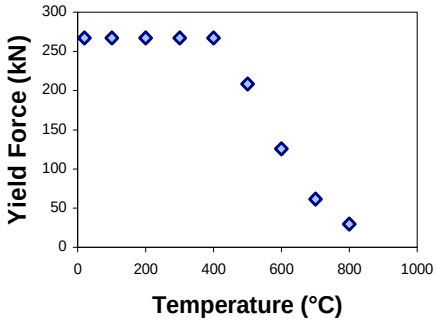

Figure 4-6 : Effect of temperature on yield force

The horizontal displacement at the end of the first loading phase (N = 300 kN) is inversely proportional to the reduction factor for the slope of the elastic range $k_{E,\theta}$ defined for carbon steel until 400°C. For temperatures higher than 400°C, the yielding force is reduced and the hardening branch is reached at a lower load level.

Temperature	δ	$\delta_{20°C} / \delta$	$k_{E,\theta}$
(°C)	($.10^{-6}$ m)	(-)	(-)
20	340.7	1	1
100	340.7	1	1
200	378.6	0.9	0.9
300	425.9	0.8	0.8
400	486.7	0.7	0.7
500	1542.9	0.22	0.6
600	5645.6	0.06	0.31
700	18372.0	0.02	0.13
800	30083.1	0.01	0.09

Table 4-1 : Horizontal displacement at the rolled support (N = 300 kN)

4.1.2.3 Test n°3: three rows in tension-compression at ambient temperature

Three beams are connected rigidly and submitted successively to tensile and compressive forces. All the beams have the same geometry as in Tests n°1 and 2. External beams work in tension (BILIN_TENS) and the middle one works in compression (BILIN_COMP).

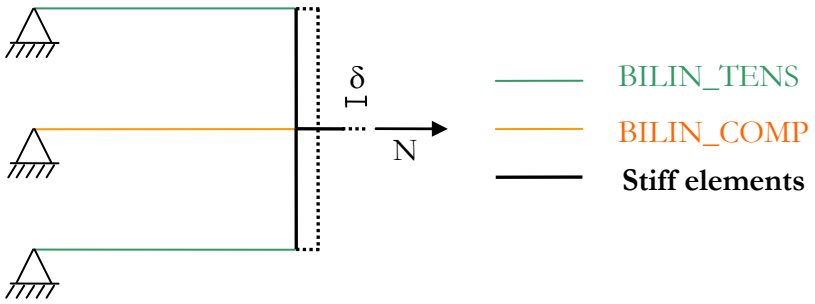

Figure 4-7 : Static scheme of test n°3

Three consecutive loading-unloading cycles are applied to the structure: a first cycle in tension with a peak value equal to 600 kN, a second cycle in compression reaching -600 kN and a third cycle where the maximal load is 1000 kN.

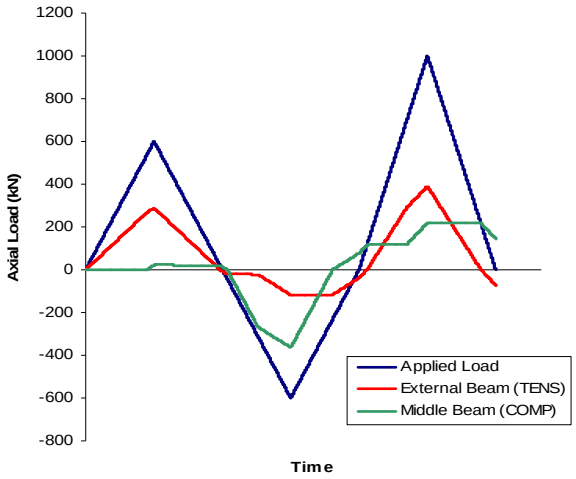

Figure 4-8 : Applied Load and axial forces in the beams

Figure 4-8 shows the branch of the σ–ε diagram on which each beam is situated during the test and gives the axial forces in the beams at relevant moments. When "BILIN_TENS" elements are loaded in compression and "BILIN_COMP" elements are loaded in tension, it is specified that they are not activated. However, it does not mean that the axial force is equal to 0 because the slope of the σ–ε diagram is equal to the hardening modulus.

	Load (kN)	TENS	COMP
1	0 --> 536	Elastic	Not activated
	536	268	0
2	536 --> 600	Hardening	Not activated
	600	289	22
3	600 --> 21	Elastic	Not activated
	21	0	21
4	22 --> 0	Not activated	Not activated
	0	-7	14
5	0 --> -42	Not activated	Not activated
	-42	-21	0
6	-42 --> -312	Not activated	Elastic
	-312	-22	-268
7	-312 --> -600	Not activated	Hardening
	-600	-118	-364
8	-600 --> -232	Not activated	Elastic
	-232	-116	0
9	-232 --> 0	Not activated	Not activated
	0	-39	78
10	0 --> 696	Elastic	Not activated
	696	289	118
11	696 --> 1000	Hardening	Not activated
	1000	390.5	219
12	1000 --> 217	Elastic	Not activated
	217	0	217
13	217 --> 0	Not activated	Not activated
	0	-72.5	145

Table 4-2 : Axial forces in BILIN_TENS and BILIN_COMP elements

Due to that assessment, elements are submitted to significant normal loads in the domain they are not expected to work. Table 4-2 shows that, when the applied load comes back to 0 at the end of a loading-unloading cycle, there is simultaneously significant compressive stresses in "BILIN_TENS" elements and significant tensile stresses in "BILIN_TENS" elements.

4.1.3 Validation of the BILIN_TENS* and BILIN_COMP* material laws (Version 2)

In cross-sections where every finite element is constituted of a unique material law, it is not allowable to assign a zero or very low slope to the "inactivated" domain of the $\sigma-\varepsilon$ diagram. However, assigning a too high value to that slope leads to wrong stresses distributions. In order to prevent from the problems exposed in the paragraph 4.1.2, some adapted "BILIN_TENS*" and "BILIN_COMP*" material laws have been defined in SAFIR program.

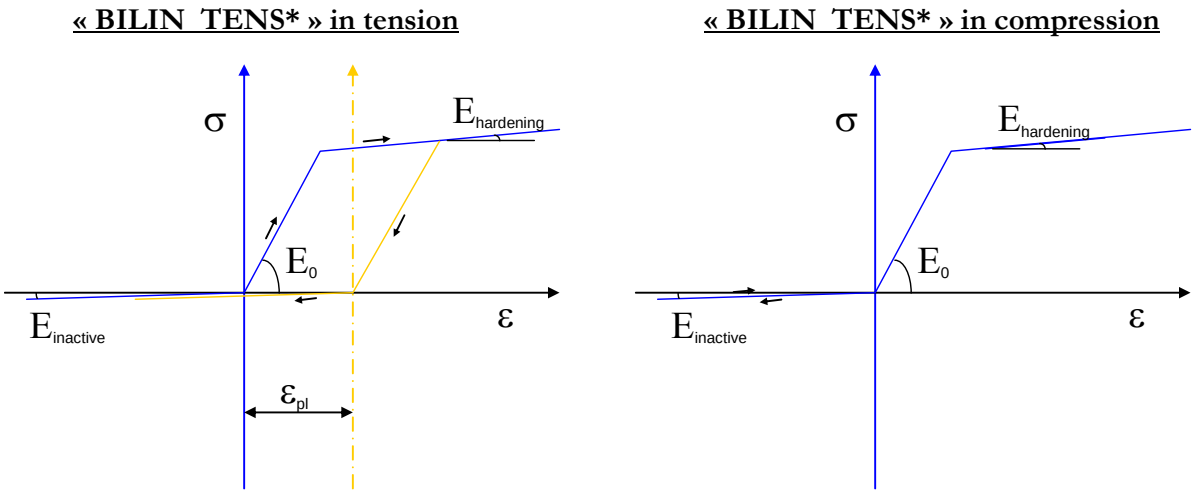

Figure 4-9 : Stress-strain law of BILIN_TENS* (Version n°2)

The same three tests as those performed with the first version of new material laws have been run. The geometrical properties, the mechanical properties and the loading are kept unchanged except the hardening modulus, equal to 5,000 MPa, and the modulus of the "inactive branch", equal to 100 MPa.

Under this assumption, Test n°1 and Test n°2 give identical results in the elastic branch and plastic deformations are five times smaller in the present case.

4.1.3.1 Test n°3: three rows in tension-compression at ambient temperature

The system of three connected beams is submitted to three loading-unloading cycles. In the present case, the ratio between the stiffness of the elements on the hardening branch of the σ–ε diagram and the stiffness of the elements loaded in their "inactive domain" is equal to 50. No more significant "parasitic loads" are observed in "BILIN_TENS*" elements under compressive loading cycles and "BILIN_COMP*" elements under tensile loading cycles (Figure 4-10).

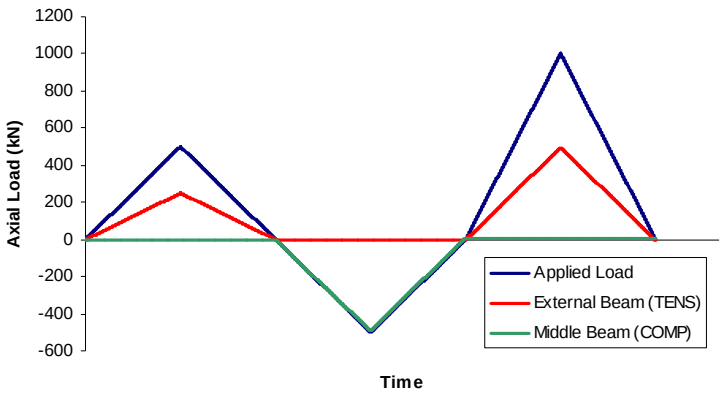

Figure 4-10 : Normal force in the components of the system

The evolution of horizontal displacement is given in Figure 4-11. At the transition between the first two cycles, the resulting displacement comes back to 0 before the BILIN_COMP* beam (middle beam) starts to adopt an elastic behaviour. After the second cycle (compression cycle) and as soon as the tensile loads are applied, the displacement recovers the plastic displacement reached at the end of the first loading cycle in tension.

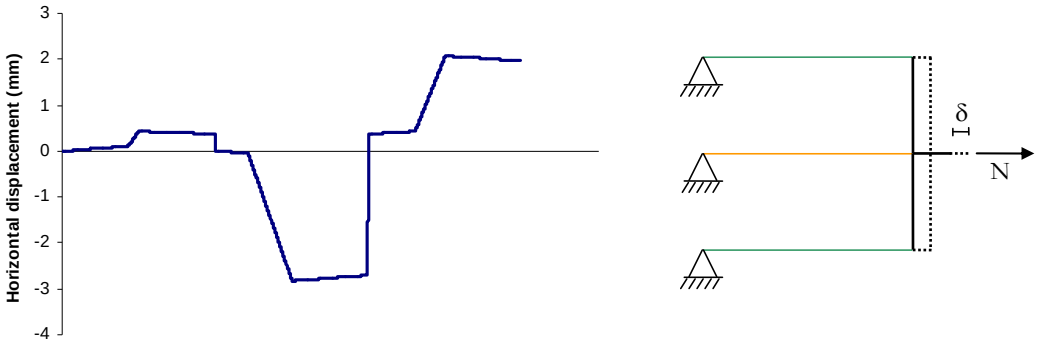

Figure 4-11 : Horizontal displacement at the load position

This is in complete agreement with the realistic behaviour of a joint. In a flush or extended end-plate joint, the bolts rows only work in tension if the bolt nut and bolt head are in contact with the column flange and the end-plate respectively. In compression, the contact between the beam flange and the end-plate is needed to make the load transfer possible.

After successive cycles producing plastic deformations in tension and compression, the contact requested to mobilise a row in tension (respectively in compression) is obtained when the horizontal displacement reaches the maximal plastic displacements undergone during the previous tensile (respectively in compression) cycles. The results obtained with "BILIN_TENS*" and "BILIN_COMP*" material laws defined in SAFIR are in agreement with that reality.

4.2 Presentation of CoP

CoP program [J.-P. Jaspart, K. Weynand and al., 1995-2000] is a tool aimed at designing steel joints submitted to a combination of axial forces, shear forces and hogging or sagging bending moments according to Eurocode 3 recommendations. It was developed at the Universities of Aachen (Germany) and Liège. The calculation of joints resistance and stiffness is based on the analytical Component Method.

For a large variety of connections typologies, the software CoP can calculate:

- the plastic bending resistance M_{Rd} ;
- the elastic bending resistance M_e ;
- the initial stiffness $S_{j,ini}$;
- the shear resistance V_{Rd} ;
- the collapse mode and ductility.

The analytical determination of these results is based on the Component Method, described in chapter 2.4.4 and recommended by the EN 1993-1-8 [CEN, 2003].

5 Numerical Simulations of the experimental tests

5.1 Tests realized at the University of Manchester

In his paper, Liu describes the results of 15 experimental tests [T.C.H. Liu., 1999]:

- 2 tests on simply-supported beams
- 3 tests on substructures with web-cleats connections
- 10 tests on substructures with flush end-plate connections

The three tests on web-cleats connections have not been modelled in the FE software SAFIR because of the difficulty to model the action of this type of joint. As mentioned previously, the resistance of this joint is not negligible and its behaviour is completely modified when the rotation of the joint is sufficient to create a contact zone between the beam lower flange and the column.

5.1.1 Thermal Analyses

In every test, the furnace temperature is controlled to follow the ISO834 standard curve. In order to simulate the heat-sink effect due to concrete slab, the top flanges were wrapped with 15 mm thick ceramic fibre blanket. The column and the connections were fire-protected by a 50 mm thickness of this material.

The distribution of temperature in the beam has been calculated with SAFIR by considering that the upper flange frontiers are adiabatic. This assumption is not completely realistic because the insulating material avoids any heat flux during a limited period of time but the precision is sufficient to make this thermal distribution acceptable in the mechanical analysis (Figure 5-1).

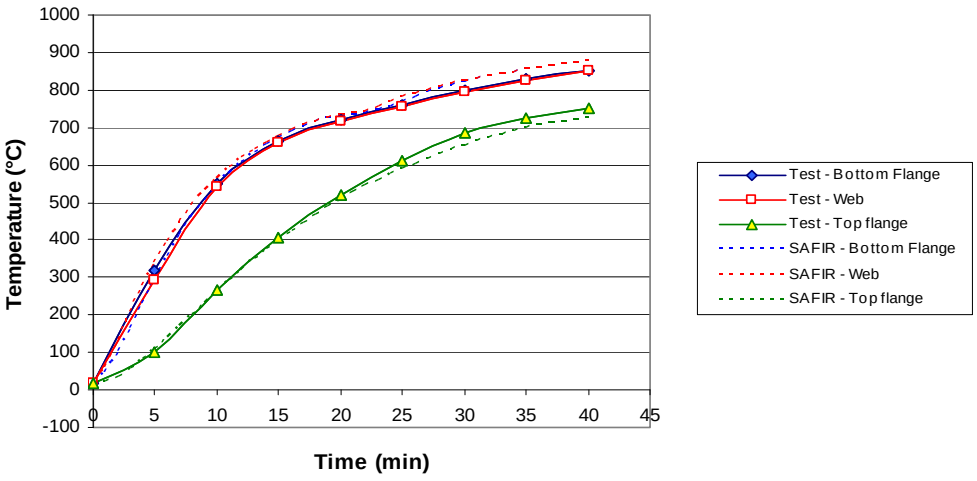

Figure 5-1 : Comparison between numerical and measured temperatures in the mid-span cross-section

5.1.2 Mechanical Analyses

5.1.2.1 Simply-supported beams

The failure of a simply-supported beam is reached when the first plastic hinge is formed in the most critical cross-section or zone. In this case, the analytical calculation of the beam fire resistance consists in evaluating the time where the reduction of the resisting bending moment due to the elevation of temperature is equal to the load ratio. The actual load ratios are lower than the design load ratios because the actual yield strength of steel at room temperature, measured on coupon tests, is higher than 275 MPa.

Assuming that the temperature is constant on the complete beam cross-section, the critical temperature calculated analytically is given in (Table 5-1):

Design Load Ratio	Actual Load Ratio	Critical Temperature
0.5	0.42	620°C
0.7	0.58	565°C

Table 5-1 : Critical temperature of tested simply-supported beams

The comparison between the experimental and numerical results is given in Figure 5-2. The failure of the beam is reached in the numerical simulations for lower temperatures than experimentally. The bottom flange temperature at the failure in the test is about 35°C higher than the one leading to the failure in the numerical model. The mid-span deflection increases more quickly in the numerical simulations.

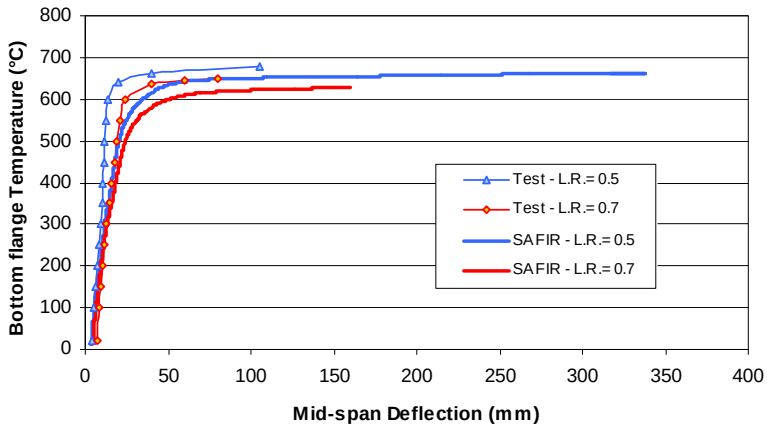

Figure 5-2 : Comparison of numerical and analytical deflections in simply-supported beams

Comparing the numerical and experimental results with the analytical solution is not simple because of the thermal protection on the upper flange and the non-uniform distribution of temperature in the beam cross-section. Figure 5-3 shows the distribution of temperature at failure time for two values of the design load ratio.

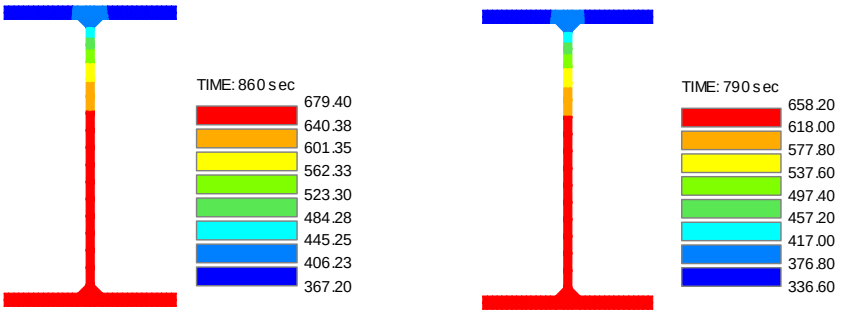

Figure 5-3 : Distribution of temperature in UB 178x102x19 at failure time

(a) Design L. R. = 0.5 - Time = 860 sec (b) Design L. R. = 0.7 - Time = 790 sec

5.1.2.2 Substructures with flush end-plate connections – BEAM elements

The design moment capacity of the flush end-plate connections used in this series of tests has been calculated by Liu as equal to 30 kN.m. The end-plate connections were estimated to provide a rotational stiffness of 14,000 kN.m/rad. By using CoP software and considering unitary partial coefficients on the elastic limit of steel, the design resisting moment is 25.20 kN.m. The failure mode is the column web in shear and the initial rotational stiffness is 2,940 kN.m/rad.

The origin of these significant differences has not been detected because the article describing the experimental tests is the only piece of information available. No more documentation

could be obtained. The question about the plate thickness (10 mm mentioned in the text and 12 mm on the drawing) does not explain such an important divergence on the evaluation of the initial rotational stiffness of the joint.

The numerical simulations of the 10 tests performed on substructures with flush end-plate connections have been modelled with beam elements because no local instabilities have been observed during these tests, except for the test with the highest load ratio and the lowest axial restraints (Load Ratio = 0.9 and k = 8 kN/mm). A shell model has been run in this particular case and will be discussed later.

As the measurements have been stopped at the beginning of the cooling phase, the beam is exclusively subjected to compressive axial thrusts. The presence of group mechanisms in the connections is less likely to happen than under pure bending. The action of the connections has been represented by short beam elements where each row (working in tension or compression) is substituted by a fibre whose section area and material properties are adapted to match with the resistances and the stiffnesses calculated analytically without considering group effects.

The correlation between the vertical deflections measured during the experimentations and those calculated numerically with beam elements are very good (see Appendix B). Similarly to the simply-supported beams, the numerical results give smoother curves; during the real test, the mid-span vertical displacement does not vary much until the formation of the plastic hinges. In every simulation, beam mechanisms lead the structure to failure.

In tests with axial restraints equal to 35 kN/mm and 62 kN/mm, the difference between axial thrusts obtained numerically and experimentally is due to the fact that the restraining system is not fully effective at the beginning of the tests. Therefore, the initial low axial stiffness of the end restraint induces a slower rate of increase in the measured compression force than expected. In tests where the axial restraining system is only due to the stiffness of the column in bending (k = 8 kN/mm), a slight difference is noticed at elevated temperatures. The compression forces are more important in the tests and this is in agreement with the “more rigid” behaviour observed in the displacement curves. For every axial restraint, the influence of the load ratio on the axial thrusts is very low.

The evolution of the hogging bending moments at the junction between the beam and the column is influenced by the connection behaviour. As referred previously, the analytical calculation of the resisting moment and the initial rotational stiffness according to the Component Method lead to lower values than those mentioned by Liu.

5.1.2.3 Substructures with flush end-plate connections – SHELL elements

Numerical simulations using BEAM elements do not allow taking the local instabilities into account because this theory assumes that the cross-section of elements remain planary. The presence of hogging bending moments and compressive axial thrust near the connection increases much the risk of local buckling in the beam lower flanges. Moreover, top flanges are strongly exposed to fire and their stiffness decreases more quickly than the bottom flanges. Figure 5-4 shows the model and the meshing of the sub-structure used to analyze its numerical response in the case with a Load Ratio equal to 0.9 and without any additional struts (k = 8 kN/mm).

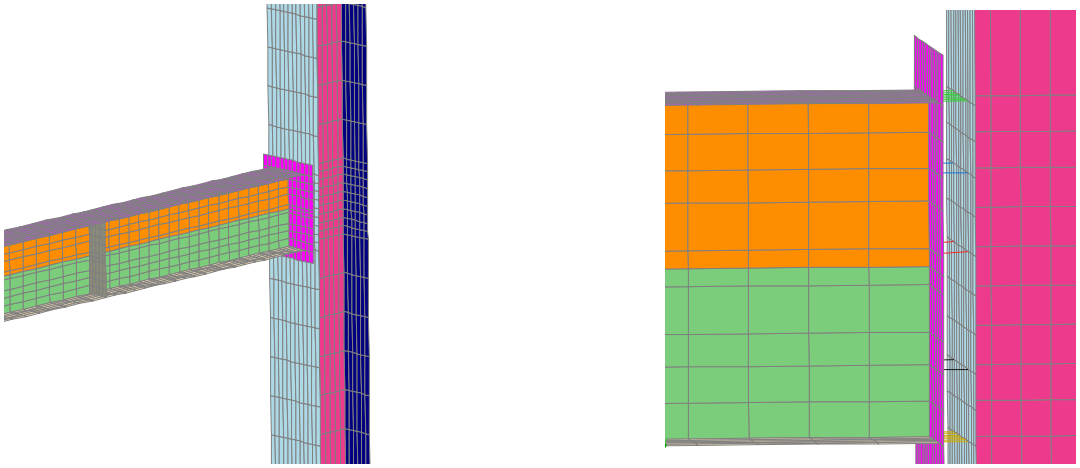

Figure 5-4 : Meshing of the substructure and modelling of the joint

The end-plate connection is modelled according an "adapted version" of the Component method. The components dealing with the resistance and stiffness of the beam, the column and the plate are already taken in consideration with the SHELL finite elements. Two rows infinitely stiff and resistant in compression are defined between the beam flanges and the column for transmission of compression forces. Each row is modelled by seven TRUSS elements. The three rows working in tension are represented by six TRUSS elements whose material and geometrical properties are defined in order to get a mechanical behaviour that matches with the real behaviour of bolts.

The vertical displacements of the two nodes of a TRUSS element are imposed to be identical so that shear forces are transferred from the beam to the column. The effect of shear on the resistance of bolts is consequently not taken into account. This modelling assessment also causes an under-estimation of the joint capacity of rotation and an over-estimation of the joint stiffness because the column is assumed not to rotate at all. In the present test, the column is very stiff and is completely protected.

A stiffener has been added in the cross-section where the load is applied to avoid a failure due to localised stresses that has not been observed during the experimental tests. The temperature in the stiffener has been defined as equal to temperature in the beam so that no thermal stresses are created. The symmetry of the sub-structure has been considered to reduce the number of finite element and the computer calculation-time.

Figure 5-5 shows that the failure is obtained at a lower temperature than expected with the SHELL model. This is due to the model used for the joint. Imposing that the vertical displacements are equivalent at the extremities of the TRUSS elements representing the action of joint components is acceptable for low joint rotations. Under the effect of thermal gradient and vertical loading, significant rotations tend to develop in the joint. Avoiding the rotation of the TRUSS elements increases the rotational stiffness of the joint noticeably. In consequence, the joint is submitted to higher hogging bending moments and the failure is obtained prematurely.

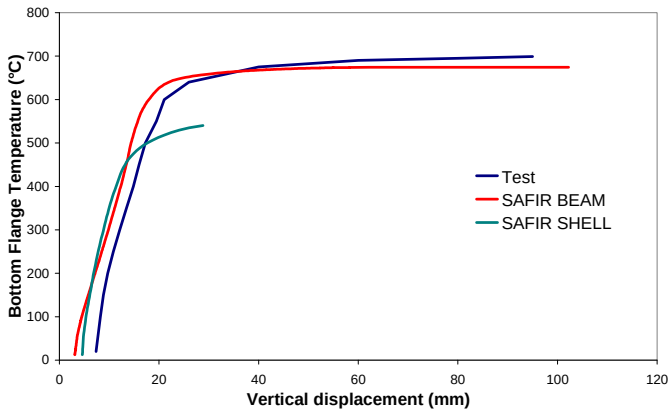

Figure 5-5 : Comparison between vertical displacements with BEAM and SHELL elements

5.2 Tests realized in the scope of COSSFIRE project

5.2.1 Thermal Analyses

The thermal analyses have been realised with 3D solid elements and the shadow effect is taken into account by reducing the materials relative emissivity according to Eurocode recommendations. Three different correction factors for the shadow effect are used in the three following zones: beam and end-plate, part of the column situated below the end-plate and part of the column situated between the end-plates of the joint (Figure 5-6). The emissivity factor is not modified in the slab and the unheated part of the column, situated

above the slab.

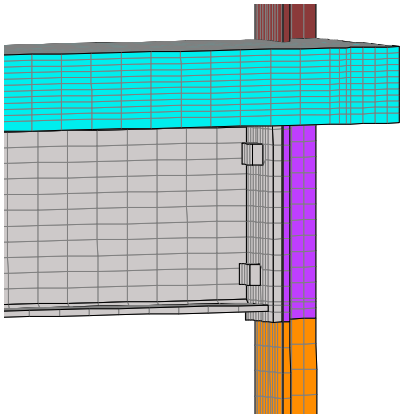

Figure 5-6 : Subdivision of the joint in zones characterised by different "shadow effect" factors

The comparisons between numerical and experimental temperatures in the plate, the beam, the bolts and the column show a good agreement (see Appendix C) in both tests. It should be mentioned that the low heating speed (10°C/min) explains partially why the numerical and experimental curves fit so well on the graphs.

5.2.2 Mechanical Analyses

The geometry of the sub-structure and the 3-D numerical model are shown in Figure 5-7. The system used to provide axial restraints has been substituted by an elastic spring in the numerical simulation. The rotation and the out-of-plane displacement are the beam are fixed at the position of the loading jack.

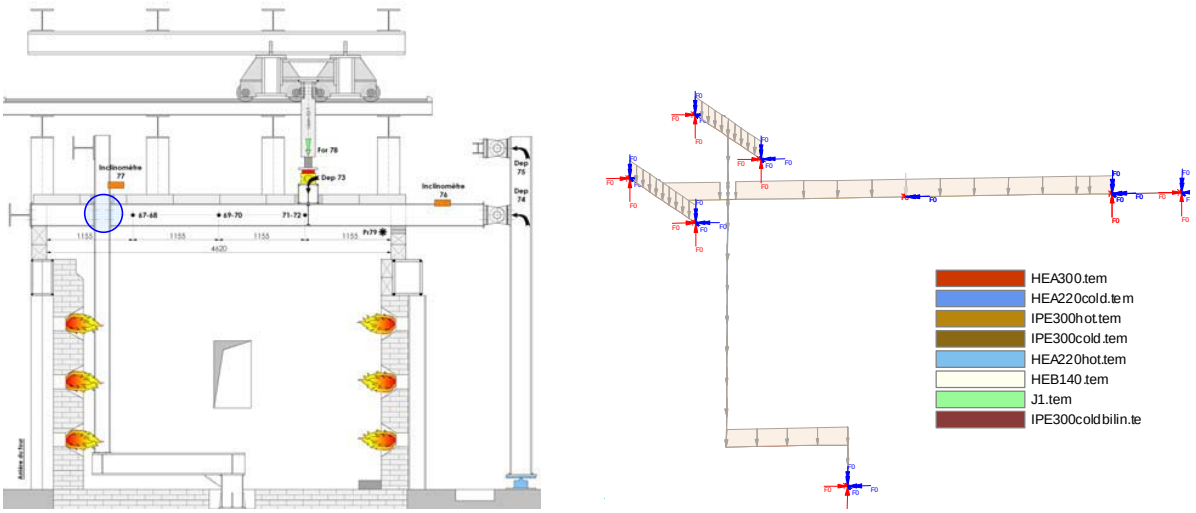

Figure 5-7 : Structural model of the tests n°1&2

The two tests have been modelled with two steel resistances of carbon steel (235 MPa & 355 MPa) because no coupon tests have been performed on the grade S235 steel used. As the real yield strength of S235 steel is usually closer to 355 MPa than 235 MPa, the two simulations have been run. The mean value of the ultimate resistance of bolts measured during the four tests realised at room temperature has been chosen as the bolts resistance in tension.

In Test n°1, the failure is reached when the furnace temperature is equal to 797 °C (t = 4185 sec = 70 min) and the comparisons between numerical and experimental values of the vertical displacement at the jack position and the horizontal displacement at the beam extremity, given in Figure 5-8, are very good. The failure mode is a plastic beam mechanism: two plastic hinges appear in the studied joint and the section where the vertical loading is applied.

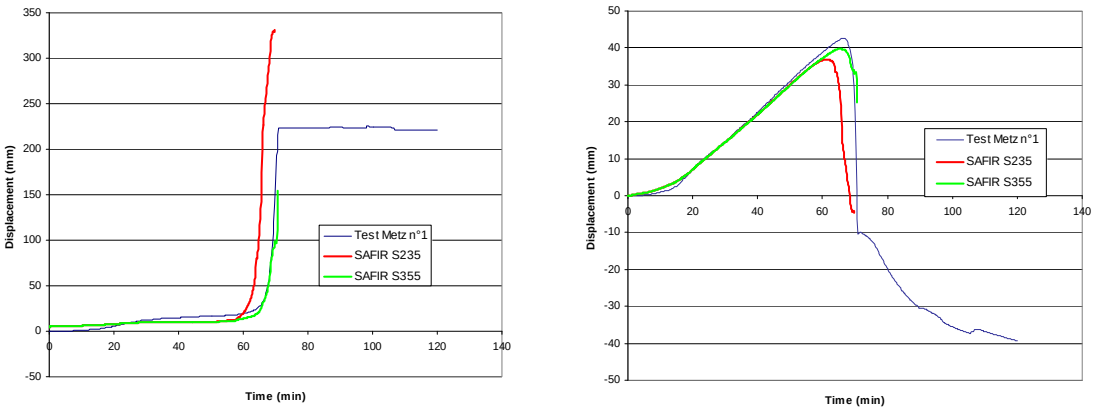

Figure 5-8 : Test n°1 – (a) Loading jack : vertical displacement - (b) Beam extremity : horizontal displacement

In Test n°2, no failure is observed until the end of the test (12550 sec = 209 min). The horizontal displacement of the beam extremity obtained numerically follows the experimental curve with a good precision. However, the vertical displacement at the jack position given by the numerical simulation is lower than the measured displacement, mainly during the cooling phase (Figure 5-9).

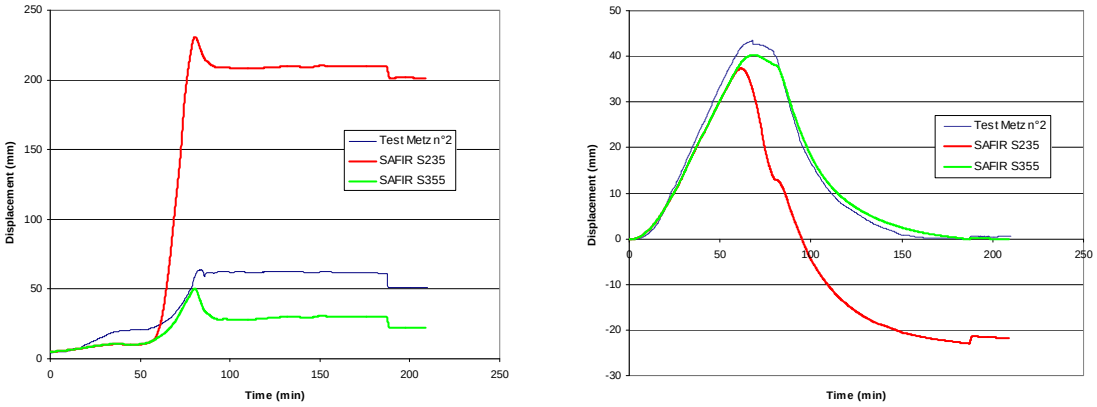

Figure 5-9 : Test n°2 – (a) Loading jack : vertical displacement - (b) Beam extremity : horizontal displacement

The correlation between the results of the mechanical numerical analyses and the experimental results is good for tests n°1 & 2.

6 Parametrical Analyses

This paragraph is aiming at providing numerical results that are the starting point of the next paragraph dedicated to the definition of simplified analytical methods. A step-by-step approach is followed so that the number of parameters and the difficulty to keep simple and accurate calculation methods increases progressively. At each step, the assumptions and the field of application is clearly defined.

Some simple developments aiming at getting realistic values of the studied parameters are reported. This enables to focus the parametrical analysis and the simplified methods on the realistic ranges of values.

6.1 Effect of surrounding frame on boundary conditions of beams

6.1.1 Introduction

When a simply-supported beam without any axial restraints is uniformly heated, it tends to elongate and the thermal loading does not induce any solicitation in the beam. On the contrary, axial deformations are not allowed in the case of a fully restrained beam and thermal strains are equilibrated by mechanical strains. The axial thrusts developed are equal to:

$$P = EA.\varepsilon_{th} = EA.\alpha.\Delta T$$

In a frame, the situation is intermediate between the two extreme cases mentioned previously. The surrounding structure, unheated, is opposed to the heated beam dilatation and creates compression forces in it. The axial thrusts depend on several factors like the ratio between beam extensional stiffness and the frame stiffness, the increase of temperature in the beam and the evolution of the Young's modulus.

Similarly, the presence of vertical loading and asymmetric thermal distribution produce some rotations and/or bending moments at the extremities of the beam. The extreme cases are pinned joints where no bending moments are created at the beam extremities and rigid joints where the rotations of the beam extremities are avoided.

In order to evaluate the normal forces that will appear in any beam of a frame, the considered beam is removed from the initial structure and two opposed unitary loads are applied at each extremity (Figure 6-1). By calculating analytically or numerically the horizontal

displacement at the beam extremities, the extensional stiffness of the equivalent elastic spring at ambient temperature can be deduced. This method is not applicable if the fire acts on the surrounding structure or if some parts of it are yielded.

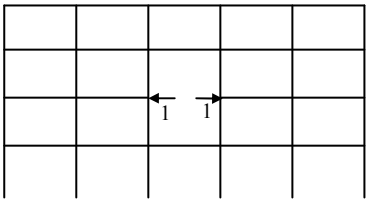

Figure 6-1 : Evaluation of the axial stiffness applied at beam extremities due to surrounding frame

6.1.2 Choice of the elements cross-sections and frame geometry

The choice of the beam cross-section, the column cross-section and the geometry of the frame is essential to get realistic values of the frame stiffness. The restraints applied to a chosen beam increase with the rotational stiffness of columns, the extensional stiffness of beams, the number of storeys and the number of bays. For a given frame geometry, the axial restraints still vary much in function of the location of the beam considered.

In order to take into account the effect of the global frame on the tested elements during the fire tests, the ratio between the extensional stiffness of the beam and the extensional stiffness of the surrounding frame has been calculated for a geometry of beams and columns (IPE 220 beams and HEB 140 columns) chosen after a preliminary analysis. The studied frame is a four-level and five-span frame with spans of 5 m. The calculations have been produced for two different configurations: a braced frame with pinned joints and an unbraced frame with rigid joints. This analysis has underlined that horizontal restraints, as expected, depend strongly on the position of the studied beam. The ratio between the extensional stiffness of the beam and the extensional stiffness of the surrounding frame varies between 0.1 % and 6.3%.

Much higher horizontal restraints have been applied during the tests realised by the University of Coïmbra [L. Simões da Silva and al., 2006]. In the tests performed at the University of Coïmbra on bare-steel elements, 5.7-meter IPE 300 beams and HEA 300 columns are considered. In the RFCS PRECIOUS project [O.S. Bursi and al., 2008] focused on the fire resistance of two types of composite steel-concrete connections after a seismic loading, the high-rise, designed according to Eurocodes, is composed of 7.5-meter and 10-meter IPE 300 beams and 3-meter HEB 260 columns.

Axial restraints have been calculated in the paragraph 6.1.3 with IPE 300 beams, HEB 260 columns and three different beam spans: 5 meters, 8 meters and 10 meters. The height of

columns is equal to 3 meters.

6.1.3 Results and conclusions

	K_{total} (kN/m)	K_{total} (kN/m)	K_{total} (kN/m)	%	%	%
Beam/Span	5 m	8 m	10 m	5 m	8 m	10 m
1 & 3	16.98	15.92	15.41	7.51	11.27	13.64
2	28.90	25.77	24.27	12.79	18.25	21.48
4 & 6	13.19	11.93	11.35	5.84	8.45	10.04
5	22.62	19.16	17.67	10.01	13.56	15.64
7 & 9	11.17	9.82	9.25	4.94	6.95	8.19
8	21.10	17.54	15.97	9.33	12.42	14.14
10 & 12	1.84	1.67	1.59	0.81	1.18	1.41
11	7.01	5.38	4.72	3.10	3.81	4.17

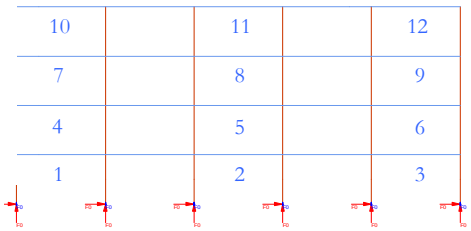

Table 6-1 : Stiffness and relative stiffness of surrounding structure in a moment resisting frame (rigid joints)

	K_{total} (kN/m)	K_{total} (kN/m)	K_{total} (kN/m)	%	%	%
Beam/Span	5 m	8 m	10 m	5 m	8 m	10 m
1	64.10	54.95	50.76	28.36	38.90	44.92
2	36.10	30.58	28.17	15.97	21.65	24.93
3	16.92	15.85	15.29	7.49	11.22	13.53
4	41.67	34.36	31.25	18.44	24.33	27.65
5	24.45	20.24	18.45	10.82	14.33	16.33
6	12.29	11.33	10.85	5.44	8.02	9.60
7	34.13	28.90	26.60	15.10	20.46	23.54
8	19.92	16.89	15.48	8.81	11.96	13.70
9	9.03	8.41	8.09	4.00	5.95	7.16
10	6.21	5.43	5.06	2.75	3.84	4.47
11	3.75	3.29	3.07	1.66	2.33	2.72
12	1.56	1.46	1.41	0.69	1.04	1.25

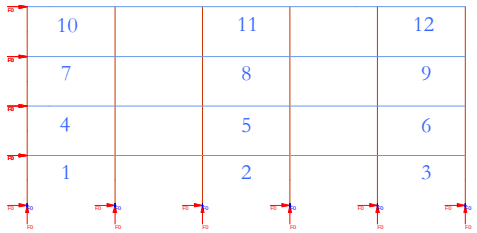

Table 6-2 : Stiffness and relative stiffness of surrounding structure in a braced frame (pinned joints)

- There is a large difference between axial restraints applied to beams located in intermediary spans of lower storeys and those applied to off-centered spans of the upper levels. In the case of braced frames, beams situated near the bracing system are much more restrained than other beams.

- The stiffness of the surrounding structure is not modified much when considering different spans. This is due to the fact that the most influent parameter on the horizontal restraints is the column stiffness in bending, which is constant in all cases considered. Consequently, the ratio between the extensional stiffness of the beam and the extensional stiffness of the surrounding frame when considering each span length differs mainly because of the eigen extensional stiffness of the beam.

6.2 Step 1: One-dimensional analysis

In a first approach, the behaviour of restrained beams is analysed without considering vertical loading and rotational restraints. The distribution of temperature in the beams is assumed to be uniform on its cross-section and along the complete length so that the shielding of top flanges and beam extremities is neglected. The numerical simulations are performed with the use of BEAM elements in SAFIR program in order to reduce significantly the calculation time in comparison with SHELL elements. The axial restraints are supposed to remain constant during the heating and the cooling phases. Local and global instabilities are not considered.

6.2.1 Reference Case

The effect of several parameters is considered in this paragraph: level of axial restraints, beam cross-section, maximal temperature and steel grade. The influence of each parameter is studied separately by comparing a reference case to other simulations results where the unique studied parameter is modified. The influence is the beam length and the cross-section area is negligible because of the uniform thermal distribution and the uni-axial behaviour.

The reference case is a 5-meter long IPE 300 beam restrained horizontally by a spring whose relative stiffness is equal to 20%. The yield limit of steel is 235 N/mm² and σ–ε diagram comes from Eurocode 3 [CEN, 2005]. The temperature of the beam increases linearly until 800°C with a speed of 10°C/min and comes back to 20°C with an identical speed of cooling.

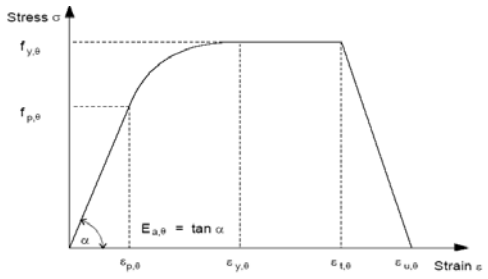

Figure 6-2 : Stress-strain diagram of steel at elevated temperature

The evolution of axial thrust in the beam during the heating-cooling cycle, given in Figure 6-3, may be divided in five zones:

i. Elastic heating: the compression force increases almost proportionally to temperature as thermal elongation of steel is nearly constant until 750 °C. The reduction of Young's modulus due to temperature induces a slight reduction of the

axial force.

ii. Elasto-plastic heating: after the stress has reached the proportional limit, the compression force is stabilized although temperature is still increasing. The diminution of the Young's modulus in the elasto-plastic branch counteracts the effects of thermal elongation and a plateau is usually observed when stress varies from proportional limit to yield strength.

iii. Plastic heating: when the stress reaches its yield limit, the compression force starts to decrease and follows the evolution of the plastic axial load until the maximal temperature has been reached.

iv. Elastic cooling: steel recovers its stiffness as temperature falls and thermal elongation decreases. If no plastic deformations have been undergone during the heating phase, the axial thrust comes back to 0. If not, the beam is subjected to tensile stresses at the end of the cooling phase.

v. In case of significant tensile stresses during the cooling phase, steel may reach yield strength in tension. Then, the axial force follows the yield force until the end of the cooling phase. It means that it remains constant during this phase if the beam yields at a temperature smaller than 400°C.

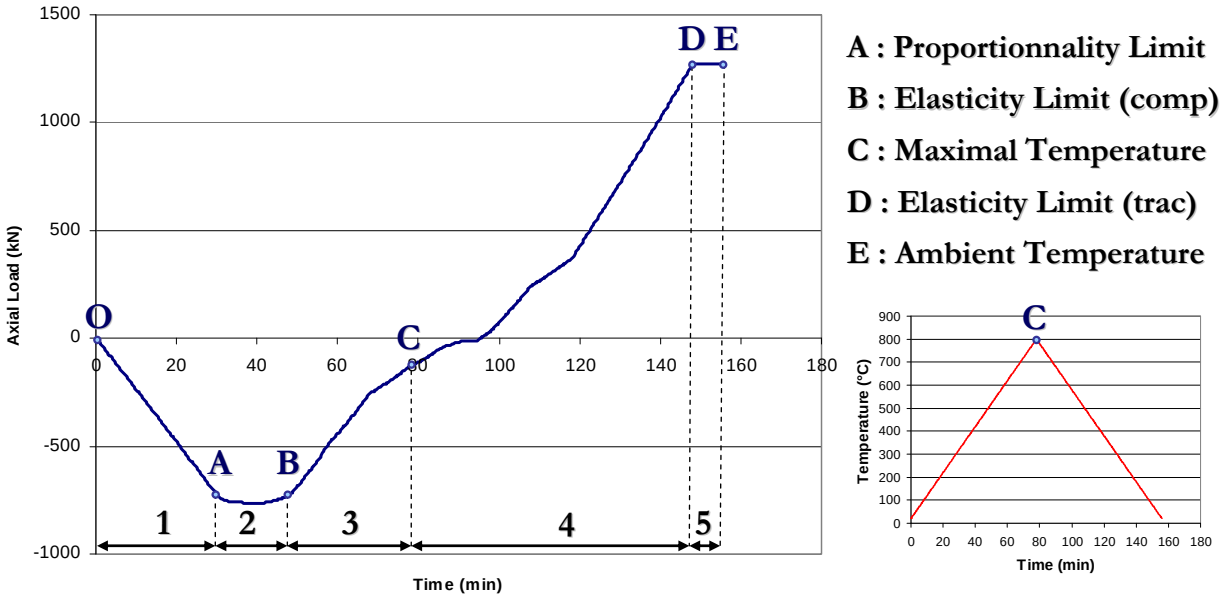

Figure 6-3 : Evolution of axial forces in the restrained beam of the reference case

6.2.2 Parameter n°1: Axial restraints

The preliminary analysis detailed in paragraph 6.1 has shown that the axial restraints applied to a beam depend on many parameters. In the frame considered, the axial restraints are included in the range [1.41 kN/m ; 64.1 kN/m] and the relative stiffness of the spring varies from 0.69 % to 44.92 %. Figure 6-4 shows the evolution of axial forces considering relative spring stiffnesses going from 1 % to 100 %.

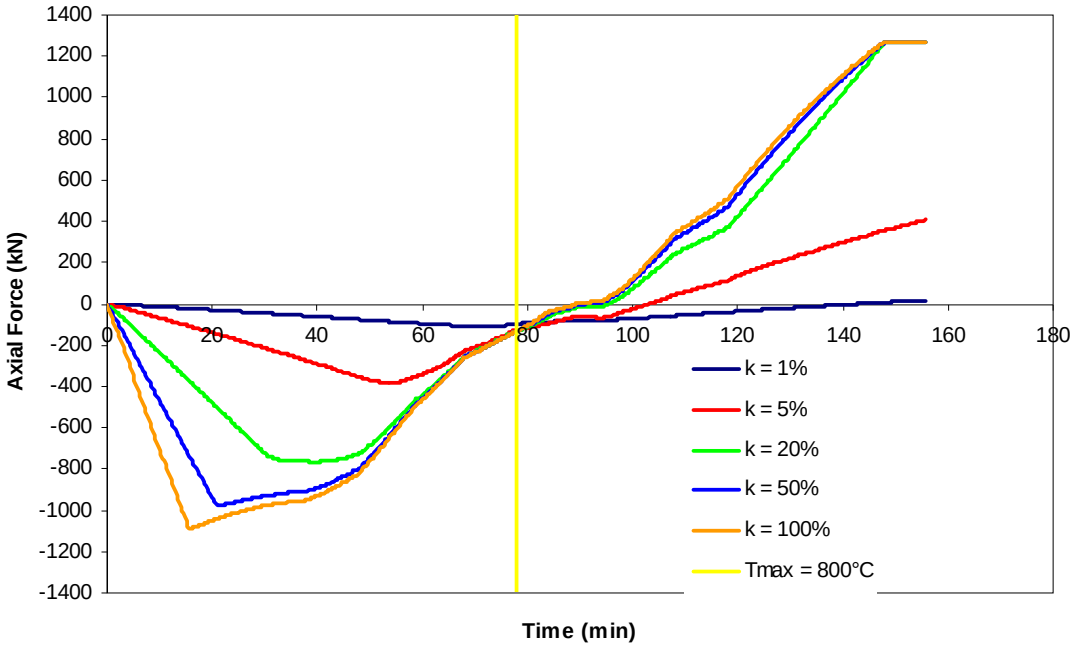

Figure 6-4 : Axial force during heating-cooling cycle in function of horizontal restraints

Critical temperature, defined here as the temperature at which the stresses reach the proportional limit, is decreasing with axial restraints (Table 6-3).

k [-]	T_{cr} [°C]
1%	688°C
5%	532°C
20%	320°C
50%	226°C
100%	175°C

Table 6-3 : Critical temperature for different values of relative spring stiffness

In the hypothetical case of infinite restraints, the critical temperature is the one for which relative thermal elongation is equal to plastic mechanical strain (Equation 6-1).

$$\varepsilon_{th} = 0.4*10^{-8}\,T^2 + 1.2*10^{-5}\,T - 2.416*10^{-4} = \varepsilon_{mec} = \frac{235}{210000} = 0.00112$$
$$\leftrightarrow \quad T \approx 109°C$$

Equation 6-1 : Critical temperature in a completely restrained beam

Inversely, a simply-supported beam allowed to elongate freely will never be loaded in compression. In this theoretical case, the critical temperature is 1200°C because steel loses its stiffness at this temperature.

6.2.3 Parameter n°2: Steel grade/Yield strength

The S235 steel grade is probably the most used one for beams in Belgium but the yield strength is often underestimated noticeably. The effect of yield strength on axial forces during a fire has been studied by considering two other yield strengths, referring to other existing steel grades: 355 N/mm² and 460 N/mm² (Figure 6-5).

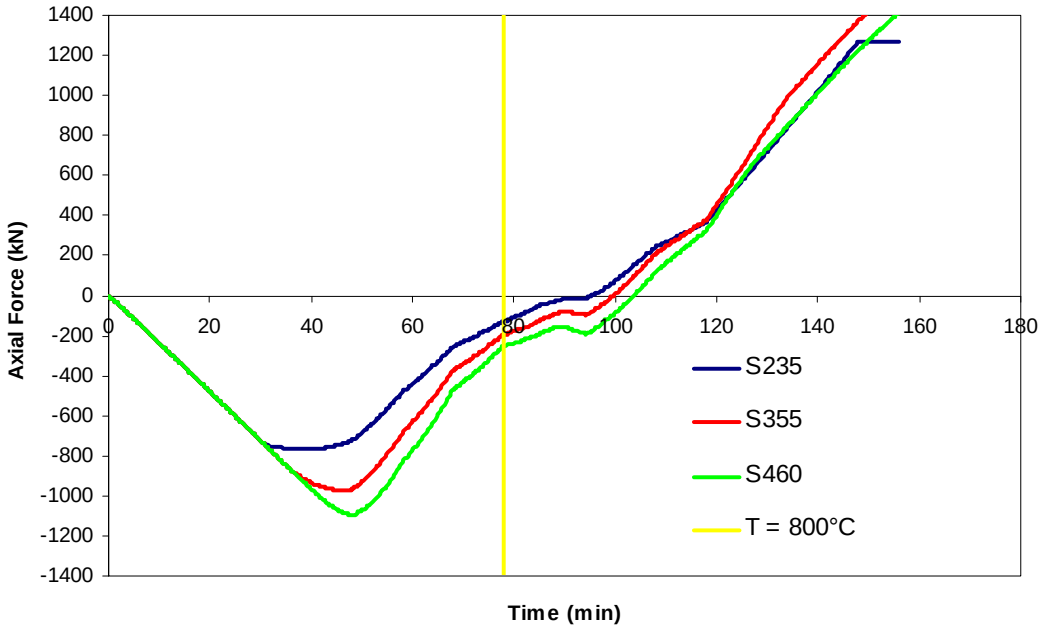

Figure 6-5 : Axial force during heating-cooling cycle for several steel yield strength

The enhancement of the steel yield strength induces a vertical shift of the time-axial force curve in the domain of high compressive forces. The width of the elasto-plastic plateau (see paragraph 6.2.1 ii) is smaller for more resistant steel and the shape of the curve is sharper in the heating phase. When temperature reaches 800°C, the beam is submitted to an axial load equal to its normal plastic load in any case. The cooling phase is mainly influenced by the

evolution of the Young's modulus and the influence of yield strength is slight but the beam is only yields under tensile stresses in the case of f_y = 235 MPa.

6.2.4 Parameter n°3: Maximal temperature

The temperature is supposed to be uniform longitudinally and across the sections so that the effect of fire on the restrained beam is governed by the maximal temperature the beam reaches. Figure 6-6 shows a comparison between four values of T_{max} (400°C, 600°C, 800°C and 1000°C) expressed in function of time. A speed of 10°C/min has been considered for both the heating and cooling phases in every numerical simulation.

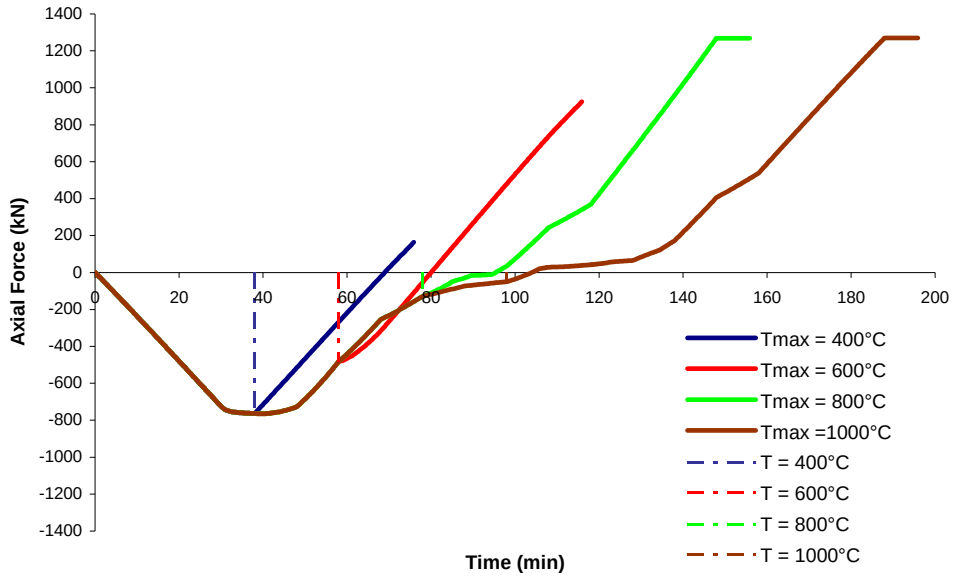

Figure 6-6 : Axial force during heating-cooling cycle for several values of Tmax

As expected, tensile forces are much higher after a heating-cooling cycle reaching elevated temperatures. The beams heated until 800°C and 1000°C are yielded in tension because of the significant plastic deformations experienced during the heating phase. The large plateau of the curve T_{max} = 1000°C relates to a range of temperature where the Young's modulus is very low.

6.3 Step 2: Two-dimensional analysis

The paragraph 6.2 was dedicated to the uni-axial analysis of beams submitted to natural fires. In practice, this situation is scarce and beams are always subjected to vertical loads. The presence of vertical loads makes the prediction of internal forces and deformations in the

element more difficult because of the presence of the interaction M-N and of second order effects. In the scope of investigating the behaviour of beams subjected to vertical loads under natural fire and providing reference results for the validation of the simplified analytical method, some parametrical analyses have been performed. The graphs showing the effect of the different parameters on vertical deflections, bending moments and axial forces are given in Appendix D.

6.3.1 Reference Case

The reference case is similar to the one used in the parametrical analysis of the one-dimensional analysis, except that a uniformly-distributed vertical load is applied. The load ratio, defined as the ratio of the applied load at fire limit state to the load-carrying capacity as a simply-supported beam at room temperature, is chosen as equal to 0.5. As a reminder, the 5-meter long IPE 300 beam is restrained horizontally by a spring of which the relative stiffness is equal to 20%.

Considering that the vertical deflection is not limited and that the yield plateau of the steel material law is infinite, it is always possible to find a position of equilibrium for any values of the vertical load and the temperature (if the residual resistance is not equal to 0). However, the steel material law defined in the EN 1993-1-2 for strains higher than 0.15 %. For this reason, several cases studied in the parametrical analyses fail before reaching 800°C (Load Ratio = 0.7, Beam length = 3m, IPE 360 and IPE 450 cross sections, presence of rotational restraints). Thus, it has been chosen to consider a maximal temperature equal to 700°C for the reference case.

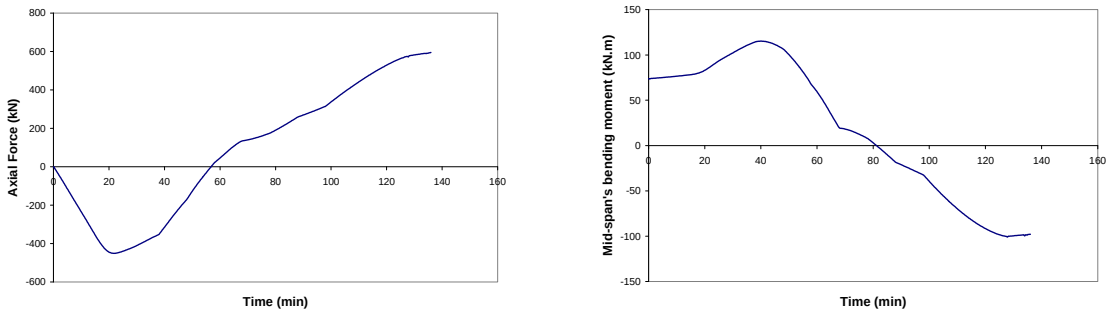

Figure 6-7 : Evolution of axial forces and mid-span's bending moment in the beam of the reference case

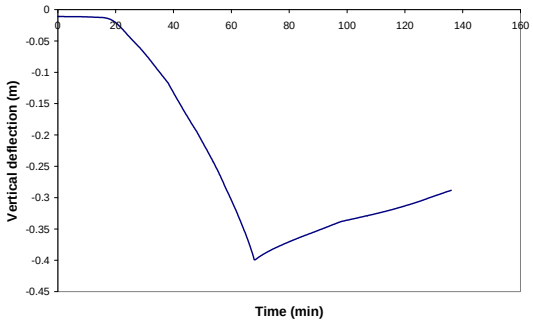

Figure 6-8 : Evolution of vertical displacement in the beam of the reference case

Figure 6-7 and Figure 6-8 describe the behaviour of the beam during the complete heating-cooling cycle. The heating speed and cooling speed are equal to 10°C/min. The cycle may be divided in different steps:

i. During the first 20 minutes, the axial force increases linearly with temperature. The bending moments and the vertical displacement remain constant.

ii. After around 20 minutes, the proportionality limit is reached in steel and the stiffness starts to decrease. This induces a progressive deflection of the beam and the bending moment increases due to second-order effects.

iii. After approximately 40 minutes, a plastic hinge is formed in the mid-span section and the bending moment starts to decrease, following the evolution of the plastic moment. Due to the diminution of the Young's modulus and the large deflections, the compressive force disappears and some tensile forces are experienced before the end of the heating phase.

iv. During the cooling phase, tensile forces increase until the end of the cycle and steel recovers its stiffness. The vertical displacement decreases linearly and gradually. At the end of the cooling phase, some hogging moment are created in the mid-span cross-section because of the second-order effects.

6.3.2 Parameter n°1: Axial restraints

The axial force, that increases linearly until the proportionality limit is reached in steel, is a function of the axial stiffness of the surrounding structure. In consequence, this elastic phase will be longer in less restrained elements. After the proportionality limit is reached, the beam starts to undergo significant vertical deflections and the speed of vertical displacement is higher in less restrained elements because the development of catenary effect requires high axial restraints. At the end of the heating phase, the axial force and the mid-span bending

moment are equal in all cases but the vertical displacement is higher in the less restrained case ($K_{A,spring}/K_{A,beam}$ = 1 %).

During the cooling phase, the very restrained beams are subjected to higher tensile stresses because steel recovers its elastic stiffness. The residual vertical deflection at the end of the heating-cooling cycle varies between L/20 ($K_{A,spring}/K_{A,beam}$ = 50 %) and L/10 ($K_{A,spring}/K_{A,beam}$ = 1%).

6.3.3 Parameter n°2: Rotational restraints

The effect of rotational restraints has been studied on cases with a maximal temperature equal to 600°C. For every value of the rotational stiffness considered (from K_R = 5.000 kN.m/rad to K_R = 50.000 kN.m/rad), the beam fails just before reaching 700°C. In fact, some plastic hinges are formed at each extremity and the failure is obtained when the rotations required at the extremities are higher than the capacity of rotation of the beam cross-section.

It is observed that the vertical deflections and the axial forces obtained in all cases with rotational restraints are similar. The initial value of the bending moment at the beam extremity is the elastic value and this bending moment increases after steel has reached the non-linear branch of the stress-strain law and until the plastic bending moment has been reached.

Extreme compressive forces (at the end of the heating phase) and tensile forces (at the end of the cooling phase) are higher in cases with rotational restraints because the stiffness of the rotational springs limits the vertical deflection and induces axial restraints.

6.3.4 Parameter n°3: Steel grade/Yield strength

Vertical loading is adapted in order to keep the load ratio unchanged and that explains why the vertical deflection and the bending moment are higher in the simulations made with more resistant steel grades. In the elastic zone of the heating phase, the axial force is equal in every case because the same thermal conditions and axial restraints are applied.

The effect of the steel grade on vertical deflections is negligible but more resistant steel grades involve higher compressive forces during the heating phase (beam stiffness starts to decrease at higher temperatures) and higher tensile forces during the cooling phase (higher plastic deformations during the heating phase).

6.3.5 Parameter n°4: Maximal temperature

If no cooling phase is considered, the failure of the reference case is reached at 825°C. The higher the heating phase stops, the higher the vertical deflections and the plastic

deformations will be. In the one-dimensional analysis, it has been shown that higher plastic deformations induce higher tensile forces. This is not necessarily true under vertical loading because the axial stiffness of the beam decreases much when important vertical deflections have been observed. That explains why tensile forces appearing after the complete heating-cooling cycle are higher at 600°C than at 700°C or 800°C.

6.3.6 Parameter n°5: Beam length

In order to analyse the influence of the beam length on its behaviour when submitted to a natural fire and without modifying any other parameter, the spring axial stiffness and the vertical loading have been adapted. When the span is multiplied by two, keeping a same load ratio implies to multiply the load by four. However, vertical deflections are proportional to L^4.

Second-order effects are more noticeable when higher beam spans are considered. In consequence, the mid-span's bending moment increases more rapidly in longer beams, even during the elastic part of the heating phase. The plastic bending moment is reached earlier. Concerning the axial forces, second-order effects tend to reduce compressive forces (the developed length of the beam increases with deflections) and tensile forces (the beam axial stiffness is reduced during the cooling phase because of the deflections).

6.3.7 Parameter n°6: Load Ratio

As expected, higher load ratios induce higher vertical deflections and bending moments at mid-span. Once again, the effect of vertical deflections during the heating phase on the axial stiffness during cooling is observed: despite a significant difference between compressive forces experienced during the heating phase, the residual tensile forces at the end of the complete cycle is comparable.

7 Simplified Method

This chapter is dedicated to the definition of a simplified analytical method based on the numerical simulations described in Chapter 6. The step-by-step approach followed in this previous chapter is kept.

7.1 Step 1: One-dimensional analysis

The method described in this point is founded on the same assessments than the parametrical analysis described in chapter 6.2.

7.1.1 Elastic domain

If we consider a simply-supported beam without any axial restraints, a uniform increase of temperature ΔT produces a thermal elongation equal to:

$$\varepsilon_{th} = \alpha . \Delta T$$

where α is the thermal elongation coefficient of steel.

If horizontal displacements are blocked at the two extremities, the compression force created in the beam is:

$$P = EA . \varepsilon_{th} = EA . \alpha . \Delta T$$

A beam that is not submitted to any external mechanical loading and doesn't yield is loaded in compression only during a fire. When the temperature comes back to 20°C, axial force disappears.

In the intermediary case where the horizontal displacement is regulated by an extensional spring, temperature induces simultaneously a smaller deformation ε than ε_{th} and a compression force N lower than P. These values are linked by:

$$N = EA . \varepsilon$$

The compression force in the beam (and the joint) at a temperature T is obtained from the two

following compatibility conditions:

$$\begin{cases} N_1 = N_2 \\ \Delta L_1 + \Delta L_2 = \varepsilon_{th} . L_{poutre} \end{cases}$$

where N_1 and ΔL_1 are compression force and length variation in the beam;

N_2 and ΔL_2 are compression force and length variation in the spring.

So,

$$\begin{aligned} \varepsilon_{th} . L_{poutre} &= \Delta L_1 + \Delta L_2 \\ &= \left(\frac{NL}{EA} \right)_{poutre} + \left(\frac{NL}{EA} \right)_{ressort} \end{aligned}$$

When the temperature of the steel profile increases, the beam stiffness varies proportionally to its Young modulus. The stiffness of the spring modelling the action of the surrounding frame is assumed to remain constant.

$$\begin{aligned} N &= \frac{\varepsilon_{th} . L_{poutre}}{K_{poutre}^{-1} + K_{ressort}^{-1}} \\ &= \frac{\varepsilon_{th} . L_{poutre}}{K_{poutre,20°C}^{-1} \left(k_E(\theta) + k \right)} \end{aligned}$$

Equation 7-1 : Normal load due to thermal restraints in the elastic domain

where $K_{poutre} = \frac{E(\theta) A}{L}$

$k_E(\theta)$ is the reduction factor on the Young's modulus of steel;

k is the ratio between the beam axial stiffness and the spring axial stiffness at 20°C.

The formulation of the equation stating that the stress reaches the proportionality limit necessitates knowing the analytical expressions of the thermal dilatation ε_{th} and reduction coefficients $k_{p,\theta}$ and $k_{E,\theta}$. In order to get equations easy to solve (degree lower or equal to 2) and to keep a sufficient accuracy, those three parameters are linearised by sections : linear expressions are defined for the reduction coefficients $k_{p,\theta}$ and $k_{E,\theta}$ under 400°C and in the range between 400°C and 800°C (Figure 7-1). As the proportionality limit is equal to 5% of

its value at 20°C, the cases where proportionality limit is reached after 800°C are scarce and not considered here. However, this approach would remain similar to the exposed developments.

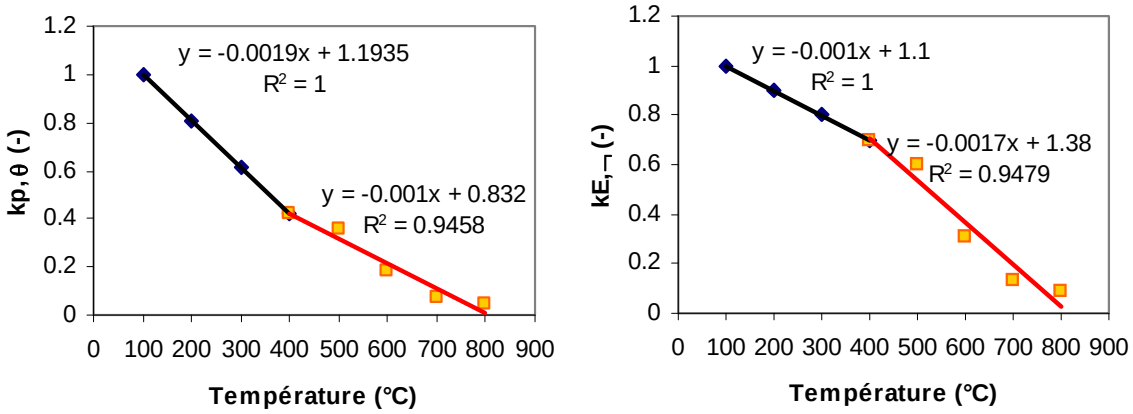

Figure 7-1 : Linearisation of the reduction coefficients on f_p (left) and E (right)

Eurocode 3 gives a quadratic formula for thermal dilatation between 20°C and 750°C and a horizontal plateau between 750°C and 860°C. The linear approached expression on the range [20°C ; 800°C] is sufficiently accurate and it is not necessary to consider several domains separately.

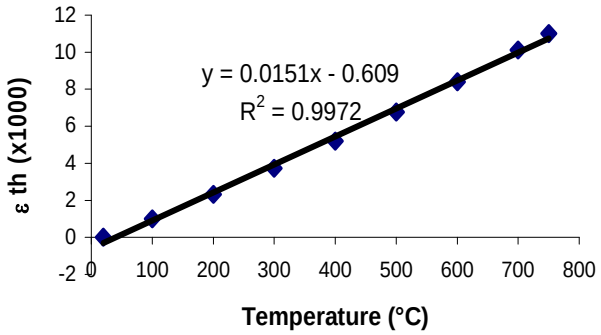

Figure 7-2 : Linearisation of the relative thermal elongation of steel

Temperature T is the only unknown parameter of the equation stated below in order to find the temperature at which the stress reaches the proportionality limit:

$$N_{pl,20°C}.k_{p,\theta}(T) = \frac{\varepsilon_{th}(T).L_{poutre}}{\left(\frac{L}{E(T)A}\right)+\left(\frac{L}{E_{20°C}Ak}\right)}$$

$$\Leftrightarrow \quad \frac{N_{pl,20°C}.k_{p,\theta}(T)}{KL}\left(\frac{1}{k_E(T)}+\frac{1}{k}\right) = \varepsilon_{th}(T)$$

$$\Leftrightarrow \quad \frac{N_{pl,20°C}}{KL}(1.1935-0.0019T) = (1.1-0.001T)\left(1.513*10^{-5}T-6.09*10^{-4}-\frac{N_{pl,20°C}}{kKL}(1.1935-0.0019T)\right)$$

$$\Leftrightarrow \quad 1.1935\frac{N_{pl,20°C}}{KL}-0.0019T\frac{N_{pl,20°C}}{KL} = 1.6643*10^{-5}T-6.7*10^{-4}-1.313*\frac{N_{pl,20°C}}{k.KL}+2.09*10^{-3}.\frac{N_{pl,20°C}}{k.KL}T$$

$$-1.513*10^{-8}T^2+6,09.10^{-7}T+1,1935*10^{-3}*\frac{N_{pl,20°C}}{k.KL}T-1.9*10^{-6}*\frac{N_{pl,20°C}}{k.KL}T^2$$

$$\Leftrightarrow \quad \alpha T^2+\beta T+\gamma = 0$$

with

$$\alpha = 1.513*10^{-8}+1.9*10^{-6}*\frac{N_{pl,20°C}}{k.KL}$$

$$\beta = -1.6643*10^{-5}-6.09*10^{-7}-1.1935*10^{-3}\frac{N_{pl,20°C}}{k.KL}-0.0019\frac{N_{pl,20°C}}{KL}-2.09*10^{-3}*\frac{N_{pl,20°C}}{k.KL}$$

$$\gamma = 6.7*10^{-4}+1.313*\frac{N_{pl,20°C}}{k.KL}+1.193*\frac{N_{pl,20°C}}{KL}$$

In the numerical simulation of the reference case, the geometry of the beam cross-section is IPE 300, its length is equal to 5 m and the ratio k between the spring extensional stiffness and the beam extensional stiffness is equal to 0.2.

Consequently,

$$N_{pl,20°C} = A.f_{y,20°C} = 5381*235*10^{-3} = 1264.53\,kN$$

$$K = \frac{EA}{L} = \frac{210000*5381}{5000} = 226000\,N/mm = 226000\,kN/m$$

The values of parameters of the quadratic equation are:

$$\alpha = 1.513*10^{-8} + 1.063*10^{-8} = 2.576*10^{-8}$$
$$\beta = -1.6643*10^{-5} - 6.09*10^{-7} - 6.678*10^{-6} - 2.126*10^{-6} - 1.169*10^{-5} = -3.7746*10^{-5}$$
$$\gamma = 6.7*10^{-4} + 7.346*10^{-3} + 1.3356*10^{-3} = 9.3516*10^{-3}$$

The analytical solution is 315.8°C. The proportionality limit is reached at a temperature situated between 20°C and 400°C, in agreement with the assumption concerning the expression of $k_{p,\theta}$ and $k_{E,\theta}$.

According to this equation, the proportionality limit is reached when the temperature is equal to 315.8 °C. That solution is in agreement with the assumption made on the expression of $k_{p,\theta}$ and $k_{E,\theta}$ because it is situated between 20°C and 400°C. If it had been in contradiction, it would have been necessary to repeat the same calculations with the equations of $k_{p,\theta}$ and $k_{E,\theta}$ between 400°C and 800°C. The values of α, β and γ are given below for that range:

$$\alpha = 2.0879*10^{-8} + T*10^{-6}.\frac{N_{pl,20°C}}{k.KL}$$
$$\beta = -2.0879*10^{-5} - 1.035*10^{-6} - 1.38*10^{-3}.\frac{N_{pl,20°C}}{k.KL} - 0.001\frac{N_{pl,20°C}}{KL} - 1.4144*10^{-3}.\frac{N_{pl,20°C}}{k.KL}$$
$$\gamma = 8.4042*10^{-4} + 1.148\frac{N_{pl,20°C}}{k.KL} + 0.832\frac{N_{pl,20°C}}{KL}$$

7.1.2 Elasto-plastic domain

As underlined previously, the effect of plasticity has not been taken into account yet. The stress-strain law of steel at elevated temperatures mentioned in Eurocode 3 is a non-linear curve (Figure 6-2), in opposition to the bilinear material law at room temperature. The axial load does not vary noticeably during the elasto-plastic domain because the effect of the increase of thermal elongation is counteracted by the reduction of the Young's modulus.

The elasto-plastic domain starts when the stresses induced by thermal loading (see Equation 7-1) reach the proportional limit of steel. In the present simplified method, the axial force is supposed to remain constant in the elasto-plastic domain between T_A and T_B (see Figure 6-3) where :

$$k_p\left(T_A\right) = k_y\left(T_B\right)$$

7.1.3 Fully plastic domain

When the beam cross-section is integrally yielded, plastic deformations are allowed without any variation of the normal force if the material law does not contain any hardening branch,

like in the general steel law defined in Eurocode 3-1-2*. If the yield strength is reached before the maximal temperature is attained, the normal force keeps decreasing as long as temperature increases and follows the evolution of the normal plastic load.

7.1.4 Elastic unloading phase

When temperature rises to the peak value, three different scenarios may occur depending on the beam length, the beam cross-section area, the stiffness of the surrounding structure and peak temperature T_{max}.

- The longitudinal stress has remained lower than the steel proportional limit during the whole heating phase. No plastic deformations are observed and the normal load evolution during the cooling phase follows the curve followed during the elastic heating phase. When temperature comes back to the initial temperature, the deformation and the load are equal to 0.

- The longitudinal stress has remained lower than the steel yield limit but has risen above the proportional limit during the end of the heating phase. The curves of the normal force during the heating and cooling are not identical because the unloading is elastic (except if the tensile plastic stress is reached later). At 20°C, the beam is in tension and there is a residual deformation.

- The longitudinal stress has risen above the yield limit during the heating phase and deformations are mainly due to plastic deformations. During its cooling, the beam is de-compressed and then, loaded tension. The tension force when temperature comes backs to 20°C is as important as plastic deformations are high during the heating phase.

In the last two cases, the normal force at a chosen temperature T during the heating phase is different from the normal force at the same temperature T during the cooling phase. The normal force during the cooling phase is calculated by adding a tension force $N_{cooling}$ to the

* Annex A of Eurocode 3-1-2 gives an alternative stress-strain relationship for steel allowing for strain-hardening [CEN, 2005].

compression force applied when the temperature reaches the peak value. The calculation of $N_{cooling}$ takes into account the modification of the dilatation coefficient variation and the Young modulus reduction, assuming that this phase is fully elastic.

The force created by a temperature variation ΔT is given by Equation 7-1 in elastic domain. The spring stiffness is independent of temperature. The beam deformability is equal to $L/(E(\theta).A)$ and the force during the cooling phase depends on steel thermal dilatation and steel Young modulus.

In high restrained levels, structures submitted to elevated temperatures undergo some large plastic deformations and tension forces become so important that it can reach the tensile plastic strength during the cooling phase. In order to consider this eventuality, the force at temperature T has to be calculated as the minimal value between those two values:

$$N_{Sd,\theta} = \min\left(N_{Sd,T_{max}} + \frac{\left(\varepsilon_{th,\theta_{max}} - \varepsilon_{th,\theta}\right).L_{poutre}}{\left(\frac{L}{E_\theta.A}\right)+\left(\frac{L}{k.E.A}\right)} \quad ; \quad \frac{A.f_{y,\theta}}{\gamma_{M,fire}} \right)$$

7.2 Step 2: Two-dimensional analysis – Heating (Wang Method)

The structural analysis of a single beam under vertical and axial loading requires considering the equilibrium equation in the deformed configuration in order to account for second order effects. That is the basis of catenary action. Y.C. Wang [Y.C. Wang and al., 2005a and 2005b] developed a method to evaluate the vertical displacement and internal stresses of axially and rotationally restrained steel beams subjected to mechanical loading at elevated temperatures. In this method, the field of displacements is assumed as a function of the mid-span deflection and this value is obtained after the resolution of the equilibrium equation in the mid-span section. This method will be discussed and compared with numerical results. Then, some new developments and proposals will be enunciated in order to extend the field of application to cooling phase.

7.2.1 General method

An isolated steel beam, axially and rotationally restrained, is submitted to symmetrical mechanical and thermal loading (Figure 7-3).

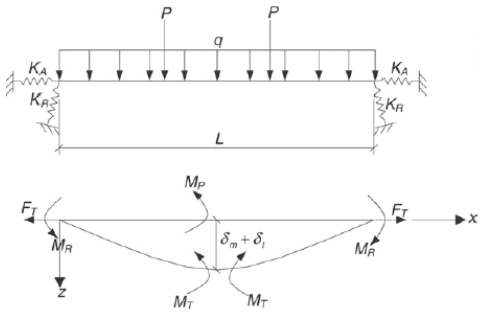

Figure 7-3 : Beam deflection and equilibrium diagrams (Wang, 2005)

The equilibrium equation is

$$F_T\left(\delta_m + \delta_t\right) + M_T + M_R + M_P = 0$$

- F_T is the axial load, supposed constant along the beam length ;
- δ_m is the maximum mechanical deflection due to load ;
- δ_t is the maximum thermal bowing deflection ;
- M_T is the beam's mid-span bending moment ;
- M_R is the restraint bending moment ;
- M_P is the externally applied free bending moment ;

Each of this term can be express as a function of known parameters and the mid-span beam's deflection.

7.2.1.1 Axial force F_T

Assuming that the beam deflection is z(x), the beam shortening due to lateral deflection is

$$\Delta L = \int_0^L \left[1 + \left(\frac{dz}{dx}\right)^2\right]^{1/2} dx - L$$

The beam's thermal expansion is

$$\Delta L_t = \varepsilon_{th}\ L$$

Thus, the axial force is determined by

$$F_t = K'_A \Delta L_m = K'_A \left(\Delta L - \Delta L_t \right)$$

where ΔL_m is the change of the beam length if it was not axially restrained and K'_A is the global axial restraint stiffness defined as

$$\frac{1}{K'_A} = \frac{1}{K_A} + \frac{L}{E_T A} + \frac{1}{K_A}$$

This formula is only valid in the elastic domain.

7.2.1.2 Mid-span bending moment M_T

The beam's mid-span bending moment is

$$M_T = E_T \, I \, \varphi_m \Big|_{x=\frac{L}{2}} = E_T \, I \, \frac{d^2 z_m}{dx^2} \Bigg|_{x=\frac{L}{2}}$$

This formula is only valid in the elastic domain.

7.2.1.3 Support bending moment M_R

The beam's end bending moment is

$$M_R = K_R \, \theta \Big|_{x=0} = K_R \, \frac{dz}{dx} \Bigg|_{x=0}$$

This last formula is only valid in the elastic domain.

7.2.1.4 Inelastic interaction between axial load and bending moment

The last three formulas are only valid in the elastic domain. In order to extend this method to inelastic problems without applying iterative processes, an incremental approach has been proposed. In this approach, the axial force $F_{elastic}$ is calculated according to the formula dedicated to elastic cases and compared to the plastic axial force F_{pl}. If the axial force $F_{elastic}$ is higher than F_{pl}, the axial force is reduced to F_{pl} and the bending resisting moment is equal to 0. If not, the residual bending moment $M_{interaction}$ is calculated with an interaction curve M-N. The bending moment in a cross-section is the minimum value between the bending moment $M_{elastic}$ calculated with the formula applied to elastic cases and $M_{interaction}$ (Figure 7-4).

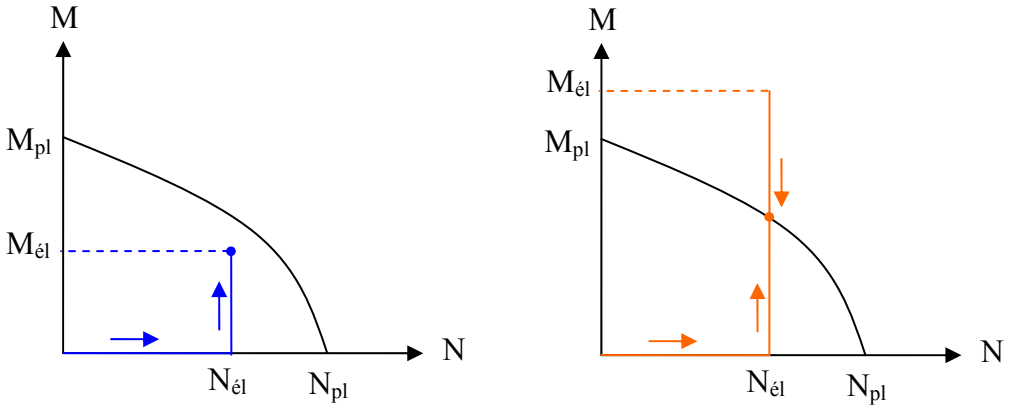

Figure 7-4 : Inelastic interaction between axial load and bending moment

7.2.2 Modifications and improvements with regard to Wang's method

7.2.2.1 Axial stiffness of the beam

The axial stiffness of a beam is equal to EA/L if its Young's modulus and cross-section area is constant along the beam span. When a beam undergoes large deflections, this formula is not valid anymore because second-order effect creates bending moments; deflections increase and tend to reduce the horizontal distance between the beam extremities. In other words, the axial stiffness of the beam is reduced.

More accurate axial stiffness has been calculated in case of simply-supported beams and fully fixed beams deflection profiles. In both cases, the axial stiffness has been evaluated as the ratio between the unitary horizontal loads applied at the beam extremities and the variation of the distance between these extremities. It has been considered that the length reduction is very low in comparison with the beam length ($\delta << L$).

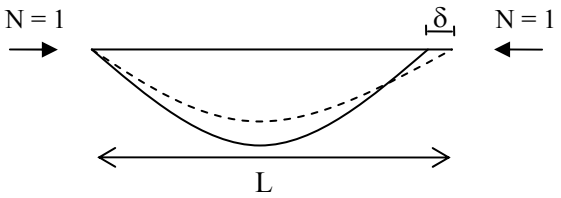

Figure 7-5 : Influence of second order effects on a beam axial stiffness

The complete developments of the calculation of axial stiffness that takes second order effects

into account are given in Appendix F. The results are:

Simply-supported beams deflection profile

$$\int_0^L \frac{M.M_1}{EA}\,dx + \int_0^L \frac{N.N_1}{EA}\,dx = \frac{L}{EA} + \frac{3968\,.\,\delta_{m,\max}^2\,.L}{7875\,EI} - \frac{4352\,.\,\delta_{m,\max}^2}{875\,EA.L}$$

Fully fixed beams deflection profile

$$\int_0^L \frac{M.M_1}{EA}\,dx + \int_0^L \frac{N.N_1}{EA}\,dx = \frac{L}{EA} + \frac{128\,.\,\delta_{m,\max}^2\,.L}{315\,EI} - \frac{512\,.\,\delta_{m,\max}^2}{105\,EA.L}$$

In intermediary cases, the deflection profile will be interpolated linearly between pinned and fully rigid profiles using the coefficient $c_{f,new}$ defined in chapter 7.2.2.2.

7.2.2.2 Rotational restraints at the beam extremities

The presence of rotational restraints implies a modification of the deflection profile. In the case of fully restrained rotations, the boundary conditions are:

$$z\big|_{\substack{x=0\\x=L}} = 0 \qquad z\big|_{x=\frac{L}{2}} = \delta_{m,\max} \qquad \left.\frac{dz}{dx}\right|_{\substack{x=0\\x=L}} = 0$$

and the fourth order polynomial equation that satisfies to these condition is:

$$z_{rigid} = \frac{16\,\delta_{m,\max}}{L^2}\left(\frac{x^4}{L^2} - \frac{2x^3}{L} + x^2\right)$$

For flexible end rotational restraint, Wang proposes to make an interpolation between pinned and fully rigid cases. The beam's deflection profile is:

$$z = \left(1 - c_f\right) z_{pinned} + c_f\; z_{rigid}$$

where

$$c_f = \frac{K'_R}{\frac{EI}{L}} \le 1 \qquad \text{and} \qquad \frac{1}{K'_R} = \frac{1}{K_R} + \frac{L}{E_T\,I} + \frac{1}{K_R}$$

The term K'_R is calculated in a similar way to K'_A and called effective end rotational restraint but it has no physical meaning. Another approach is proposed by the author to calculate the global rotational restraint $K'_{R,new}$ and a coefficient $c_{f,new}$ is defined to make the interpolation between pinned and rigid deflection profiles.

Considering that the beam is supported by two equivalent supports, the global rotational restraint $K'_{R,new}$, defined as the ratio between the moment applied to a flexible support and the rotation of this support, is equal to (see Appendix D):

$$K'_{R,new} = K_R + \left(\frac{L}{3EI} + \frac{\frac{L}{6EI}}{\frac{L}{3EI} + \frac{1}{K_R}} \right)^{-1}$$

This term is equal to $K_b = 3EI/L$ in case of simply-supported beams and is equal to ∞ when beam supports are fully rigid. The coefficient $c_{f,new}$ has to quantify the rotational stiffness of supports in order to approach as much as possible the real deflection profile of the beam. It has to fill two boundary conditions:

$$c_{f,new}\left(K'_R = K_b\right) = 0 \qquad \text{and} \qquad c_{f,new}\left(K'_R = \infty\right) = 1$$

The proposed expression of $c_{f,new}$ is:

$$c_{f,new} = 1 - \frac{2K_b}{K'_R + K_b} \leq 1$$

Some numerical simulations have been performed at several levels of rotational restraints in order to validate Wang's method in elastic cases and compare the influence of c_f and $c_{f,new}$ on the obtained results.

7.2.2.3 Value of Young's modulus integrating the effect of plasticity

The influence of the Young's modulus on the obtained results is huge. In his work, Wang used a bilinear material law for steel and the effect of plasticity is integrated as exposed in chapter 7.2.1.4. However, EN 1993-1-2 [CEN, 2005] recommends a non-linear material law at elevated temperatures. Under the effect of vertical loading, the Young's modulus is not constant in any fibre of a cross-section and varies along the beam length. In order to integrate the effect of plasticity on the value of the Young's modulus considered, the following method has been used:

- The beam is longitudinally divided in 20 slices and the curvature is assessed to be constant in each slice. This curvature is calculated by derivation of the deflection profile.
- The cross-section of the beam is vertically divided in a given number of fibres in which the mechanical strain is supposed to be constant. The mechanical strain of the neutral fibre ε_{mec} is unknown and the mechanical strain in other fibres is obtain by addition of the mechanical strain of the neutral fibre and the mechanical strain due to curvature:

$$\varepsilon_{mec,h} = \varepsilon_{mec,h=0} + h.\chi_{mec}$$

- Knowing the mechanical strain in every fibre constituting every longitudinal slice, the value of the average Young's modulus $E_{average}$ (see explanation below) can be evaluated everywhere in the beam.
- The average Young's modulus of a longitudinal slice is the "balanced average value" of the complete cross-section:

$$E_{slice} = \frac{\sum_{fibres} E_{average,\,fibre}\, A_{fibre}}{\sum_{fibres} A_{fibre}}$$

- The global Young's modulus of the complete beam is obtained by coupling every slices as a springs positioned in a row:

$$E_{global} = \left(\sum_{slices} \left(E_{slice}^{-1} \right) \right)^{-1} \qquad \text{(if every slice have the same width)}$$

The mechanical strain of the neutral fibre is calculated so that the normal load applied to the beam is equal to the one calculated according to geometrical considerations. The consideration of the average Young's modulus is due to the necessity to take the history of the thermal loading into account. The term E_{global} is used to link, in the formulas mentioned previously, the total solicitations to the total displacements.

7.2.2.4 Inelastic interaction between axial loads and bending moments

Paragraph 7.2.1.4 exposes the method used by Wang to find the beam's mid-span bending moment. It has been used in examples with simply-supported beams and showed a good agreement with numerical results. However, this method has been substituted in presence of rotational restraints at the beam extremities. Similarly to what is done in the scope of evaluating the global Young's modulus, the cross-section of the beam is divided in a given number of fibres in which the strain is known by geometrical conditions of compatibility. The bending moment is the sum of the load in each fibre multiplied by its lever arm. This method

is preferred because:

- Wang's method may overestimate the bending moment in a section (mid-span or extremity) because if bending moment calculated "elastically" is higher than the maximal plastic moment obtained by use of the interaction curve, the bending moment in this section is not necessarily equal to the maximal plastic moment that the section, submitted to an axial load N, can resist.

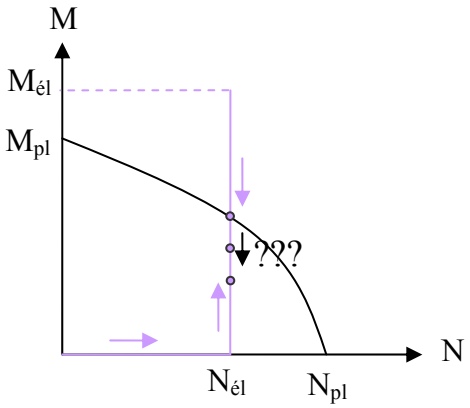

- The beam's end bending moment can not be calculated as the rotational stiffness of the spring multiplied by the slope of the beam at this extremity because this formula is only valid in the elastic domain. The "fibre method" is used in both mid-span and extremity cross-sections ;

- The division of the cross-section in fibres has already been realised to calculate the global Young's modulus and this method does not involve much additional work in the Excel sheet.

7.2.3 Elastic domain – No rotational restraints

The reference case is similar to the one used in the parametrical analysis of the two-dimensional analysis. For reminding, the 5-meter long and simply-supported IPE 300 beam is restrained horizontally by a spring whose relative stiffness is equal to 20% and submitted to a load-ratio equal to 0.5.

The deflection profile has to respect five conditions of compatibility:

$$z\big|_{\substack{x=0\\x=L}} = 0 \qquad z\big|_{x=\frac{L}{2}} = \delta_{m,\max} \qquad \left.\frac{d^2 z}{dx^2}\right|_{\substack{x=0\\x=L}} = 0$$

Thus, a fourth order polynomial expression is used:

$$z_{pinned} = \frac{16\,\delta_{m,\max}}{5\,L}\left(\frac{x^4}{L^3} - \frac{2x^3}{L^2} + x\right)$$

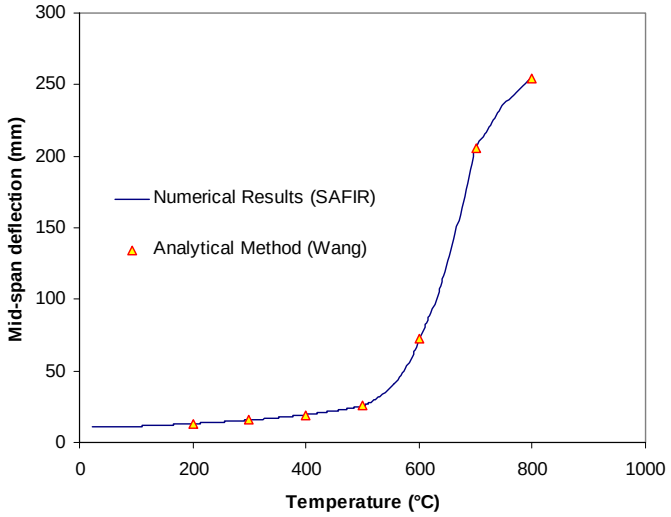

T [°C]	SAFIR	Wang
200	13.09	13.09
300	15.62	15.63
400	19.33	19.38
500	25.38	25.39
600	72.23	73.22
700	205.6	207.4
800	254.7	255.2

Figure 7-6 : Comparison between numerical and analytical method (Elastic – No rotational restraints)

The analytical and numerical results match very well.

7.2.4 Elasto-plastic domain – No rotational restraints

The data of the reference case are kept identical with respect to the elastic case. However, a second case, equivalent to the first one but at 600°C, is analysed in the scope of validating the calculation method and the modifications proposed by the author. In the second case, the beam will undergo some more noticeable plastic deformations compared with the first case and highlight the precision or imprecision of the analytical method.

Owing to the necessity to evaluate a global Young's modulus (described previously), the determination of the equilibrium deflection profile is quite more complicated. Indeed, two conditions of compatibility have to be satisfied simultaneously:

- the global equilibrium equation $F_T\left(\delta_m + \delta_t\right) + M_T + M_R + M_P = 0$

- the compatibility equation on axial load $K'_A\left(\varepsilon_{mec,real}\right)\Delta L_m = \sigma\left(\varepsilon_{mec,real}\right)A$ *

In consequence, it has been chosen to create a short routine that considers independently each value of $\delta_{m,max}$ between 1 mm and 1000 mm (step = 1 mm) and for each value of $\delta_{m,max}$, $\varepsilon_{mec,real}$ that satisfies to the compatibility equation on axial load is calculated. The term $F_T\left(\delta_m + \delta_t\right) + M_T + M_R + M_P$ is evaluated for each value of $\delta_{m,max}$ and the equilibrium is reached when this term is equal to 0. This method is illustrated graphically on Figure 7-7 in the reference case at 400°C.

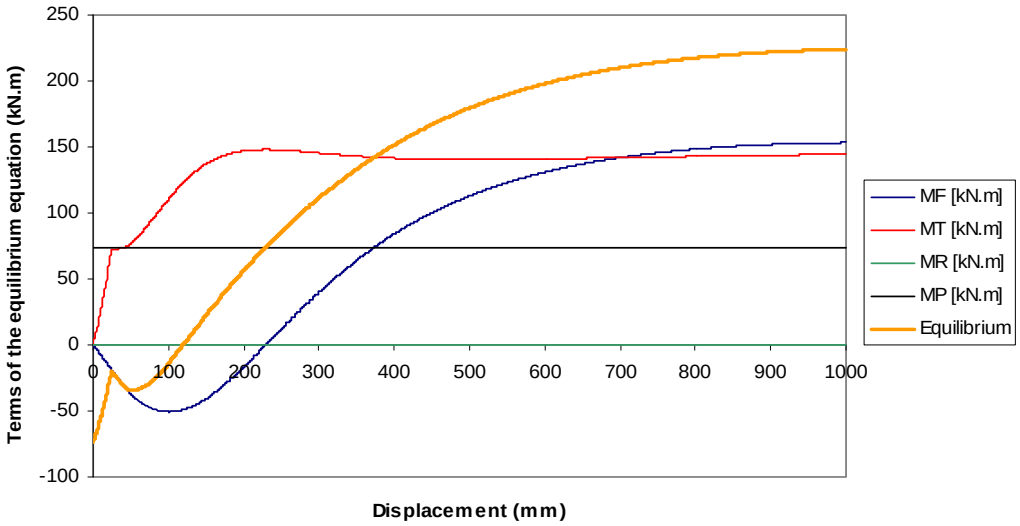

Figure 7-7 : Evolution of the terms of the global equilibrium equation in function of $\delta_{m,max}$

Once more, the results obtained analytically are compared with those given by SAFIR program. Figure 7-8 shows that the vertical deflection is overestimated with the modified Wang's method. As observed in Table 7-1, the precision on the bending moments at the beam mid-span is very good and slight differences between analytical and numerical results are obtained in the axial load and the vertical deflection at mid-span.

* Note that ΔL_m is the variation of length of the beam due to mechanical loading taking axial restraints into account. Thus, it is not equal to $\varepsilon_{mec,real}$ multiplied by the beam length L.

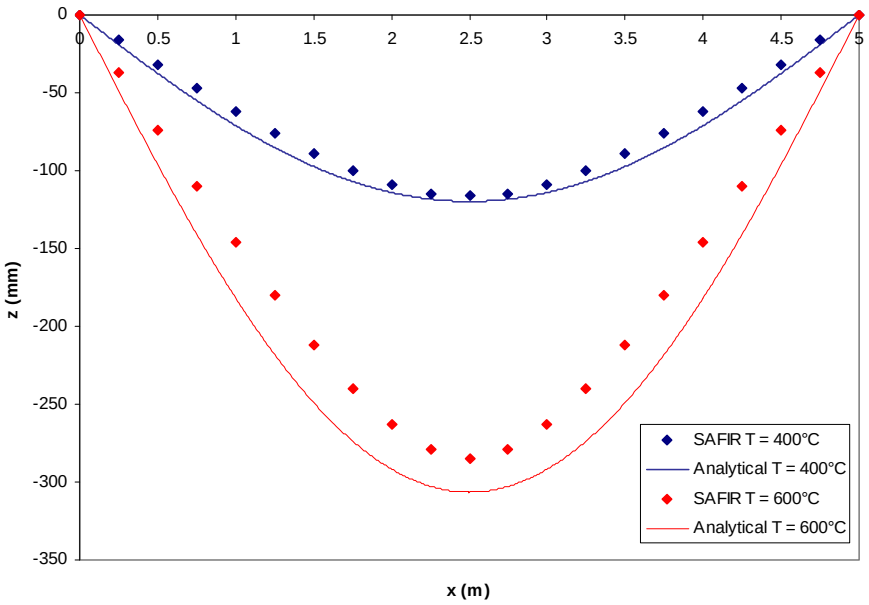

Figure 7-8 : Comparison between numerical and analytical vertical deflections

		SAFIR	Analytical
M (kN.m)	400°C	67.11	69.52
	600°C	114.5	122.84
N (kN)	400°C	21.4	14.03
	600°C	-351.8	-409.8
$\delta_{m,max}$ (mm)	400°C	116.41	119.8
	600°C	284.7	306.5

Table 7-1 : Bending moment, axial load and vertical deflection at the beam mid-span

The analytical method is conservative because the criteria that impose a limited vertical deflection during fire are reached earlier.

7.2.5 Elasto-plastic domain – Rotational restraints

The incorporation of rotational restraints necessitates the calculation of the coefficient $c_{f,new}$ that will determine the shape of the beam deflection profile and the evaluation of the beam's end bending moment M_R. As the global Young's modulus depends on the beam deflection profile and $c_{f,new}$ is a function of the global Young's modulus, it is necessary to add a condition of compatibility in the macro described in the paragraph dedicated to simply-supported beams. The system has been solved in the macro, for a given value of $\delta_{m,max}$, in that way:

- $c_{f,new}$ is calculated with the Young's modulus (taking into account of the reduction due

to temperature) ;

- The compatibility equation on axial load $K'_A\left(\varepsilon_{mec,real}\right)\Delta L_m = \sigma\left(\varepsilon_{mec,real}\right)A$ is solved and leads to a new value of E_{global} ;

- The difference between the initial Young's modulus and E_{global} is calculated ;

- If the ratio between this difference and the Young's modulus used to evaluate $c_{f,new}$ is less than 1%, $c_{f,new}$ is calculated with the new value of E_{global} and the process is reiterated as many times as necessary (one or two iterations are usually sufficient).

Two reference cases have been chosen and the presented method has been used to solve them. A comparison with SAFIR results is given below. The two cases are based on the previous cases without rotational restraints and two elastic rotational springs (K_R = 10,000 kN.m/rad) are positioned at each beam extremity. The complete datas are reminded herein:

Beam length: 5 m

Cross-section geometry: IPE 300

Yield strength of steel: 235 MPa

Young's modulus of steel: 210,000 MPa

Load Ratio: 0.5

Axial stiffness of the extensional spring: 45.2 kN/mm (at 20°C: K_{spring}/K_{beam} = 20 %)

Note: there is only a spring at one extremity and its stiffness is not reduced with T°

Stiffness of rotational springs: 10,000 kN.m/rad

Note: there is one spring at each extremity and the stiffness is not reduced with T°

Temperatures: 400°C (case 1) and 600°C (case 2)

As explained previously, the short routine that considers independently each value of $\delta_{m,max}$ between 1 mm and 1000 mm (step = 1 mm) has been modified in order to solve simultaneously two conditions of compatibility. Obviously, the calculation time has been significantly extended but it remains acceptable: entering the data and making a run takes approximately 4 minutes. Moreover, the range in which $\delta_{m,max}$ varies could be reduced and a higher value of the step between two consecutive values of $\delta_{m,max}$ would give lower calculation times. Figure 7-9 shows the evolution of each term constituting the global equilibrium equation in function of the vertical deflection $\delta_{m,max}$ at the beam's mid-span at

400°C.

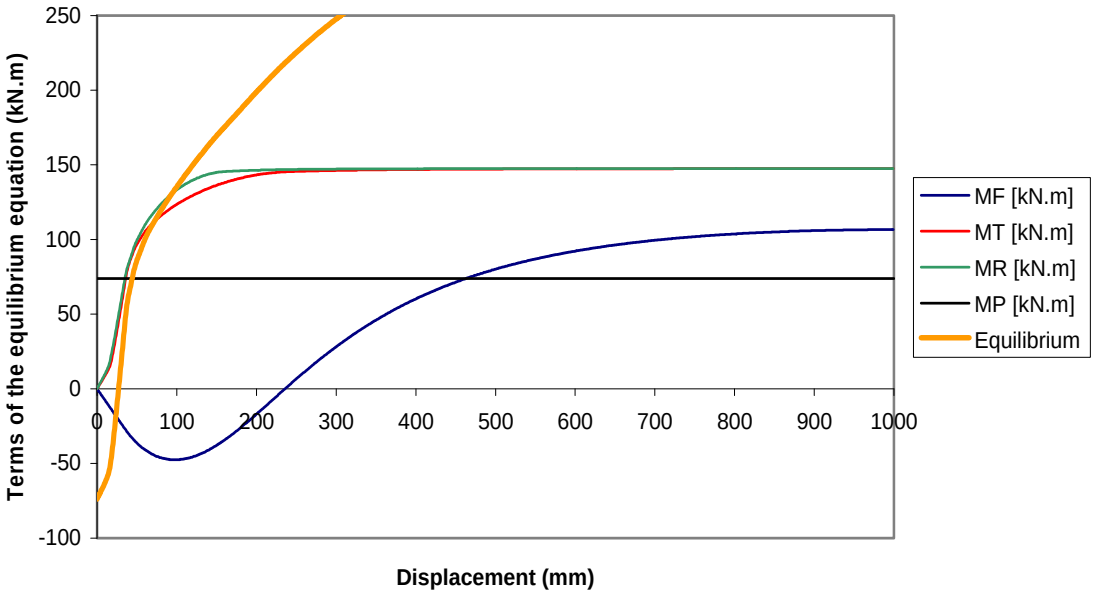

Figure 7-9 : Evolution of the terms of the global equilibrium equation in function of $\delta_{m,max}$ at 400°C

Although the beam's extremity bending moment M_R is a hogging moment and the beam's mid-span bending moment M_T is a sagging moment, both are positive in Figure 7-9 because they tend to counteract the applied bending moment. The moment due to the axial force multiplied by the lever arm produces additional sagging moments by second order effects at low deflections because the axial force is a compressive force when $\delta_{m,max}$ is lower than 225 mm. For higher vertical deflections, the tensile axial load produces hogging moments and counteracts the externally applied bending moments. The equilibrium is obtained when $\delta_{m,max}$ is equal to 27 mm.

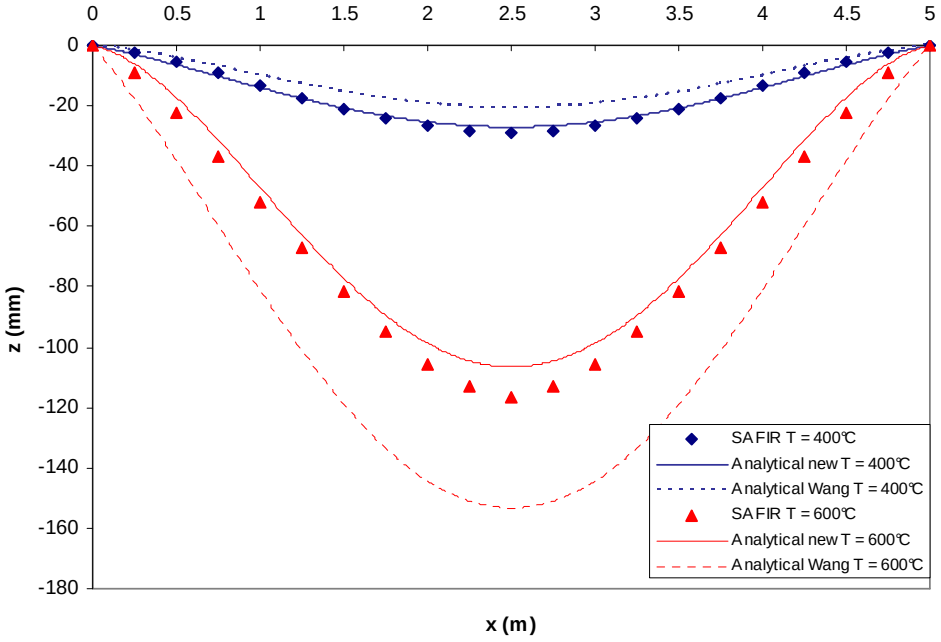

Figure 7-10 : Comparison between numerical and analytical vertical deflections

Figure 7-10 shows the vertical deflection of the beam obtained numerically and analytically at 400°C and 600°C. The shape of the deflection profile given by the new analytical method is very good and the coefficient $c_{f,new}$, used to interpolate linearly between the simply-supported and fully fixed deflection profiles, appears to be a better approximation than the one proposed by Wang. It should be mentioned that the coefficient of interpolation c_f is the only difference between the analytical curves called "new" and "Wang". The other modifications mentioned in Chapter 7.2 are considered in both analytical methods.

		SAFIR	Analyt. new	Analyt. Wang
M_R (kN.m)	400°C	-54.55	-49.62	-59.01
	600°C	-53.62	-64.98	-60.79
M_T (kN.m)	400°C	38.95	44.89	30.41
	600°C	48.52	55.67	61.48
N (kN)	400°C	-685.7	-770.84	-773.47
	600°C	-245.7	-435.67	-315.76
$\delta_{m,max}$ (mm)	400°C	28.86	27	20.6
	600°C	116.28	106.5	153.3

Table 7-2 : Bending moment, axial load and vertical deflection at the beam mid-span

The precision on N, M_R and M_T is acceptable except that the difference between the axial load at 600°C given by SAFIR and the new analytical method is quite important. The compressive axial force is noticeably overestimated because M_R and M_T are simultaneously overestimated

and the equilibrium is consequently obtained for a lower deflection profile and the mechanical strain (shortening) is higher than in the numerical simulations.

7.3 Step 2: Two-dimensional analysis – Cooling (Wang Method)

In the uni-dimensional case and the parametrical analyses of the two-dimensional case, it was observed that the cooling phase consists in an elastic unloading: compressive forces, sagging bending moments and vertical displacements decrease linearly. Thus, the calculation of the internal forces during the cooling phase will be based on the simple method established for elastic cases.

7.3.1 Evaluation of the General method terms after cooling

After having solved the General method at the maximum temperature T_{max}, it is chosen to find the global equilibrium by just considering the variation of each term. The sum of the variation must be found equal to 0. This equation is valid for any value of the temperature T_{cool} included between T_{max} and 20°C.

$$\Delta\left(F_T.\delta_m\right) + \Delta M_T + \Delta M_R + \Delta M_P = 0$$
$$\Leftrightarrow\ \Delta\left(F_T.\delta_m\right) + \Delta M_T + \Delta M_R = 0$$

7.3.1.1 Axial force F_T

The variation of the axial force F_T during the cooling phase is due to the variation of the beam shortening (modification of $\delta_{m,max}$) and the reduction of the thermal expansion:

$$\Delta F_T = K'_{A,T=Tcool}\left(\Delta L_{total,T\max} - \Delta L_{total,Tcool} - \Delta L_{t,T\max} + \Delta L_{t,Tcool}\right)$$
$$F_{T,Tcool} = F_{T,T\max} + \Delta F_T$$
$$\Delta M_F = F_{T,Tcool}.\delta_{m,\max,Tcool} - F_{T,T\max}.\delta_{m,\max,T\max}$$

K'_A is the axial stiffness at $T = T_{cool}$, taking the influence of the vertical deflection into account (see 7.2.2.1). It will be checked that the axial force remains lower than the plastic axial force in tension.

7.3.1.2 Mid-span bending moment M_T

The variation of the beam's mid-span bending moment is

$$\Delta M_T = \left(\frac{E_{T=T\max}}{2} + \frac{E_{T=Tcool}}{2} \right) I \left(\varphi_m \Big|_{x=\frac{L}{2},T=Tcool} - \varphi_m \Big|_{x=\frac{L}{2},T=T\max} \right)$$

It will be checked that the beam's mid-span bending moment remains lower than the maximal bending moment respect the M-N interaction criteria.

7.3.1.3 Support bending moment M_R

The variation of the beam's end bending moment is

$$\Delta M_R = K_R \left(\theta \Big|_{x=0,T=Tcool} - \theta \Big|_{x=0,T=T\max} \right)$$

It will be checked that the beam's mid-span bending moment remains lower than the maximal bending moment respect the M-N interaction criteria.

7.3.2 Proposed method of resolution

Assuming that the behaviour of axially and rotationally restrained beams submitted to natural fire is elastic during the cooling phase, it is proposed to evaluate vertical displacements and internal forces in the following way:

- Resolution of the General equilibrium equation at T = T_{max} (including plastic deformations) ;

- Resolution of the General equilibrium equation based on terms variations at T = T_{cool} without considering the plastic axial force and the interaction between axial force and bending moments ;

- Verification that the normal force at T = T_{cool} remains lower than the plastic axial force during the cooling phase ;

- Verification that the mid-span's bending moment and the beam's end bending moment obtained by linear interpolation between at T = T_{cool} remain lower than the maximal bending moment given by the M-N interaction criteria ;

Parametrical analyses have shown that the evolution of the vertical displacement remains linear even when tensile forces and bending moments induce some plasticization. In that case, the diagrams of normal forces and bending moments will be modified as shown on Figure 7-11.

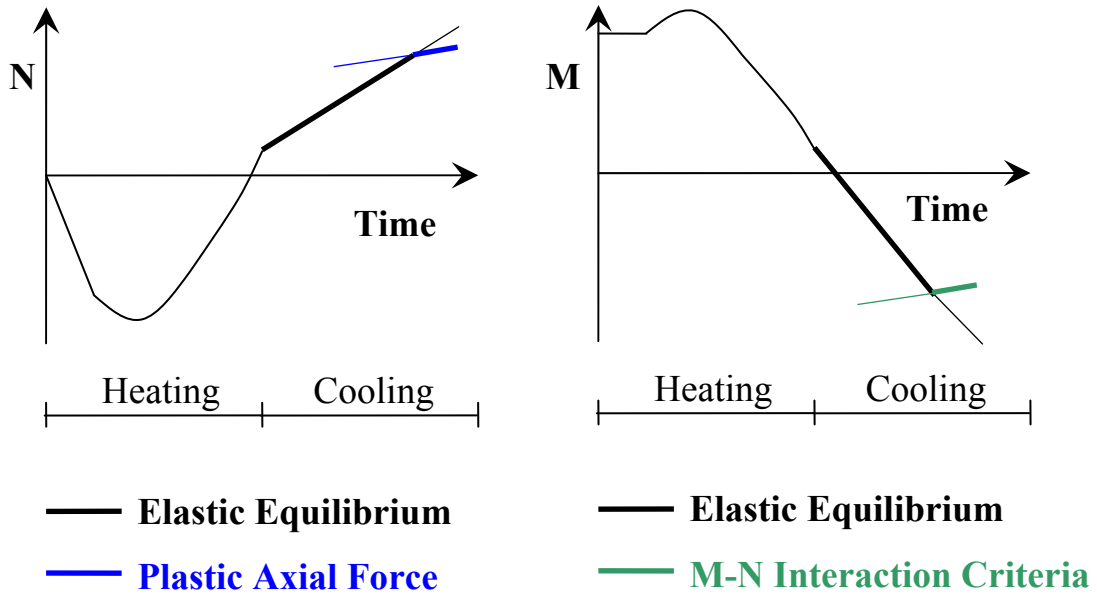

Figure 7-11 : Effect of plasticization on axial forces and bending moments

The method for predicting the internal forces and vertical deflections during the cooling phase requires knowing these results at the end of the heating phase. In the following paragraphs comparing the results given by SAFIR and by the analytical method, the internal forces and vertical displacements at $T = T_{max}$ are taken from SAFIR numerical simulations. The validation of the simplified method during the heating phase has already been done previously.

7.3.3 No rotational restraints

The internal forces are calculated in the reference case already considered previously for three couples of values (T_{max} ; T_{cool}). Tensile forces and sagging moments are positive.

	T_{max} = 400°C	T_{cool} = 20°C	T_{cool} = 20°C
	SAFIR	**SAFIR**	**Analytical**
N [kN]	-351.6	527	519
M [kN.m]	-114	-23.2	-22.4
δ [mm]	116	96	100

Table 7-3 : Comparison between numerical and analytical results (T_{max} = 400°C ; T_{cool} = 20°C)

When T_{max} is equal to 400°C, the cooling phase does not induce any plasticization in the mid-span beam cross-section. Even after the complete heating-cooling cycle, the axial force and the bending plastic moment are equal to the values calculated elastically. The equilibrium is

obtained when the vertical deflection is 100 mm.

	T_{max} = 600°C	T_{cool} = 20°C	T_{cool} = 20°C
	SAFIR	**SAFIR**	**Analytical**
N [kN]	20	752	737.2
M [kN.m]	-67.4	-75.6	-77.2
δ [mm]	284	199	206

Table 7-4 : Comparison between numerical and analytical results (T_{max} = 600°C ; T_{cool} = 20°C)

When T_{max} is equal to 600°C, the tensile forces remain lower than the axial plastic force during the whole cooling but the mid-span's bending moment calculated elastically is higher than the maximal bending moment respecting the M-N interaction criteria. Figure 7-12 shows a comparison between the mid-span's bending moment given by SAFIR and the moments calculated by use of the analytical method.

At T_{cool} = 300°C, the equilibrium is obtained at a vertical deflection that differs slightly from the results given by SAFIR. However, the precision on the internal forces N and M is good.

	T_{max} = 600°C	T_{cool} = 300°C	T_{cool} = 300°C
	SAFIR	**SAFIR**	**Analytical**
N [kN]	20	431.9	408.4
M [kN.m]	-67.4	24.0	37.3
δ [mm]	284	239	256

Table 7-5 : Comparison between numerical and analytical results (T_{max} = 600°C ; T_{cool} = 300°C)

Although the variation of curvature is approximately proportional to the vertical deflection, the "elastic" bending moment does not vary linearly during the cooling phase because the "equilibrium vertical deflection" does not vary linearly either. This is due to the fact that the Young's modulus considered in the equation is an average value between $E_{T=Tcool}$ and $E_{T=Tmax}$.

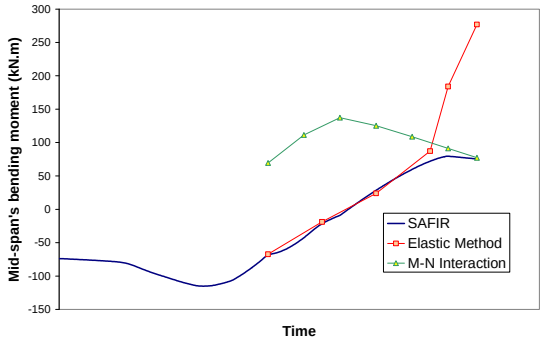

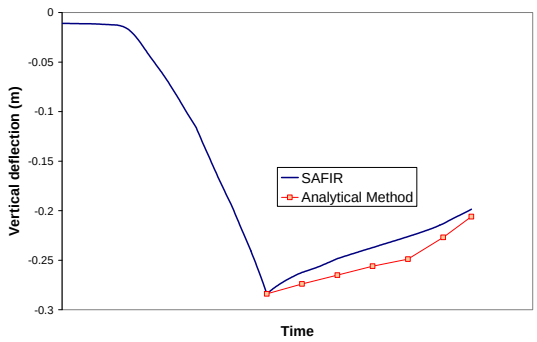

Figure 7-12 : Comparison between analytical and numerical results during cooling phase (T_{max} = 600°C)

7.3.4 Presence of rotational restraints

In presence of rotational restraints at the beam's extremities (K_R = 10,000 kN.m/rad), the evolution of displacements, axial forces and bending moments is also linear during almost the complete cooling phase. A slight variation of the slope of the vertical displacements is observed at the end of this phase (Figure 7-13) because of the plastic interaction between axial force and bending moment in both the beam's end and the mid-span's cross-section (Figure 7-14).

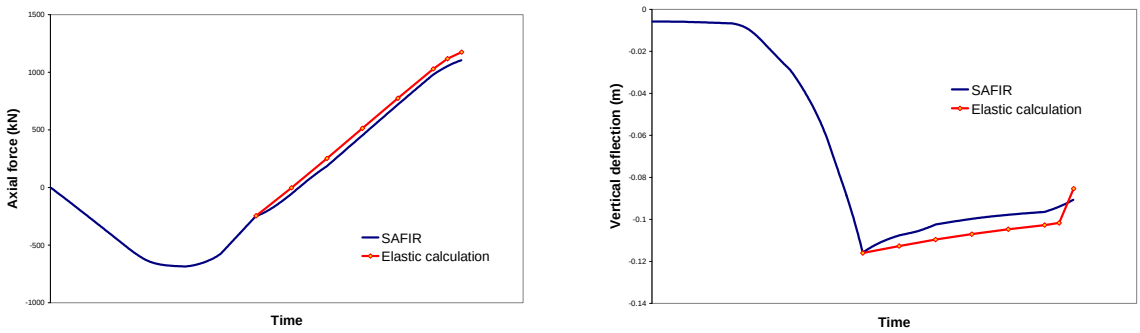

Figure 7-13 : Axial force (left) and vertical deflection of the mid-span section (right)

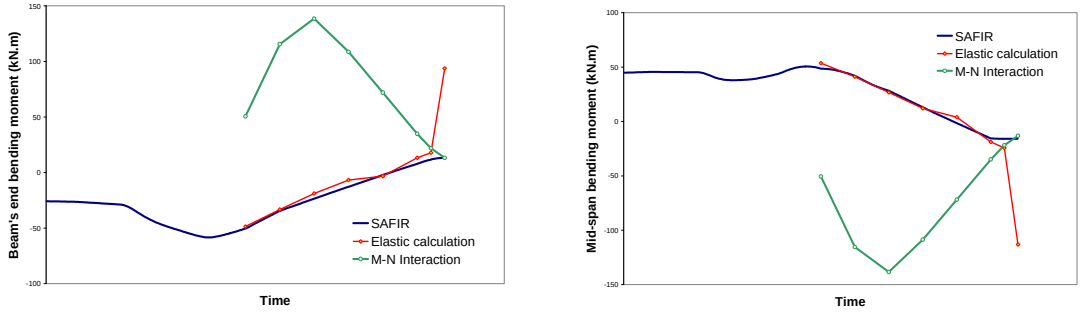

Figure 7-14 : Beam's end and mid-span bending moment (kN.m)

7.3.5 Influence of c_f and K'_A

New expressions of the coefficient c_f used to interpolate between simply-supported and fully fixed beam deflection profiles and of the fictive axial stiffness of the beam K'_A integrating axial restraints have been proposed by the author. The comparison between the results given by using the coefficients proposed by Wang and the new ones during the cooling phase is

exposed below.

In the reference case with rotational restraints, the difference between the coefficient c_f obtained with Wang's formula (c_f = 0.59) and the new formula (c_f = 0.32) differ much. However, the influence of this coefficient on the vertical deflections and axial forces is negligible. Indeed, the graphs are overlaid so that this is impossible to make a distinction. Concerning the bending moments in the mid-span and beam's end section, the difference is not as small but both coefficients give a good prediction (Figure 7-15).

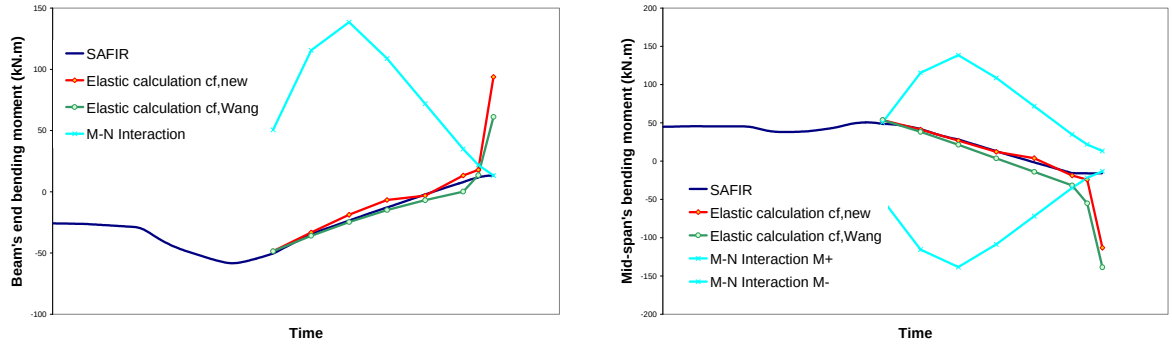

Figure 7-15 : Comparison between M_R and M_T calculated with $c_{f,Wang}$ and $c_{f,new}$

In the present work, a new axial stiffness of the beam K_A has been considered in order to take second order effects into account. The fictive axial stiffness K'_A (see 7.2.1.1) is defined as the ratio between the axial force and the variation of the beam length and is integrated the stiffness of the axial restraints. According to Wang's formula and the new formula, the beam axial stiffness K_A is respectively equal to 226 kN/mm and 180.2 kN/mm.

The precision on the axial force is improved with the new formula (Figure 7-16) but the difference is not significant because vertical displacements are not important and the behaviour of steel is elastic during the cooling phase. The precision is also a little bit higher in the evaluation of bending moments (Figure 7-17).

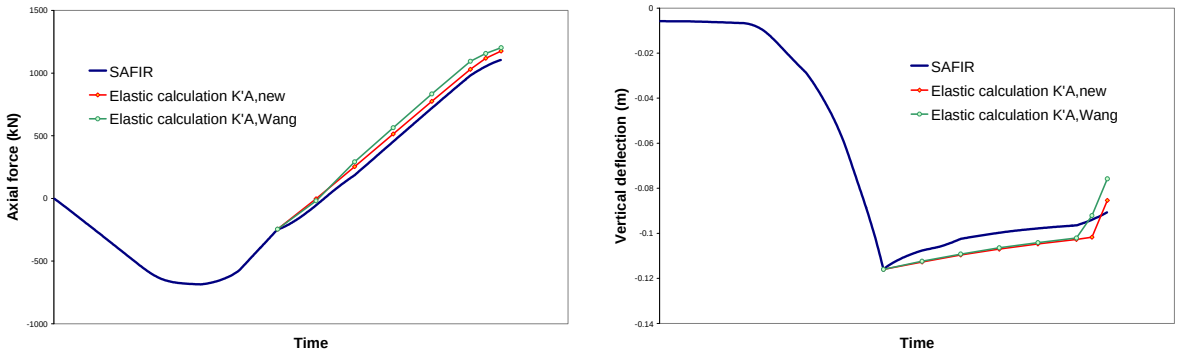

Figure 7-16 : Comparison between N and d calculated with $K'_{A,Wang}$ and $K'_{A,new}$

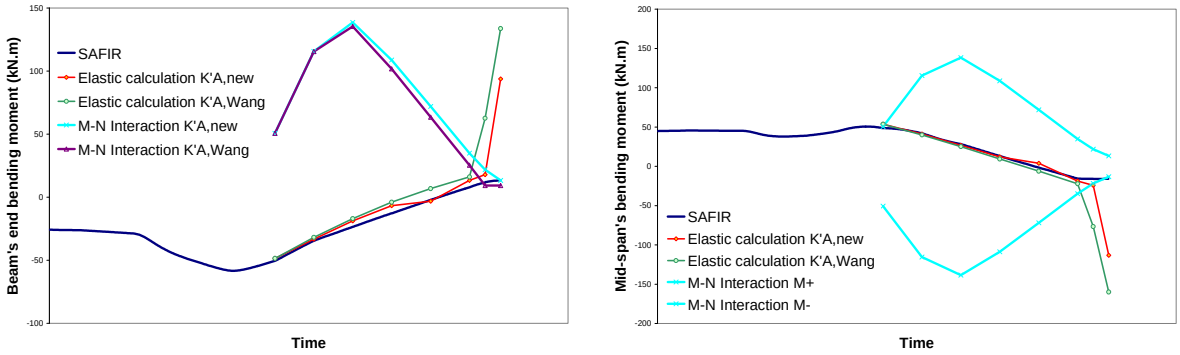

Figure 7-17 : Comparison between M_R and M_T calculated with $K'_{A,Wang}$ and $K'_{A,new}$

8 Conclusions and perspectives

8.1 Content

The structural behaviour of steel and steel-composite frames submitted to fire is usually studied during the heating phase, considering increasing temperature-time fire curves defined in the recent European standards. The presence of plasticity in restrained beams during the heating phase induces significant tensile forces during the cooling phase in these beams and beam-to-column joints. A research project focused on the behaviour of steel and composite connections under natural fire and funded by the Research Fund for Coal and Steel is currently in progress.

This work is a preliminary study aiming at determining the internal forces in axially and rotationally restrained beams and, consequently, in connections. This will represent a tool for the design of connections.

The achievement of this task has started with a validation of the numerical modelling of restrained beams under natural fire in the finite element program SAFIR. Although some variations have been observed between the experimental measurements and the results of numerical simulations, the correlation is good in general and the differences have been explained by experimental observations. As a conclusion of this study, the results SAFIR has been considered as a reference for the following analytical developments.

Then, some reference cases have been defined and analysed with precision to understand the main phenomenon having an impact on the behaviour of restrained beams submitted to natural fire. One-dimensional and two-dimensional analyses have been considered separately. The influence of the principal parameters has been investigated.

The most important part of the present work has consisted in the adjustment and the extension of a simplified method for the calculation of internal forces and vertical deflections of beams subjected to a heating-cooling cycle. In absence of vertical loading, a very simple formula has been proposed to evaluate the axial force created in axially restrained beams during a natural fire. The effect of vertical loading and rotational restraints has been considered by using an existing method, based on a general method exposed by Wang and integrating the second order effects. Three methods for improving this method have been proposed and discussed. Wang's method has also been extended to cooling phase.

8.2 General conclusions

The method developed in absence of vertical load is very simple of use and leads to very accurate results. However, the field of application of this method is limited because structural beams are always submitted to vertical loads. As an important simplification, neglecting the vertical loads is conservative because the vertical deflections allow some additional elongations in the beam and induce lower axial thrusts during both the heating and cooling phase.

Under vertical loads, Wang's method gives some very good results in elastic cases. This method is not easy to solve "by hand" but does not require much time in a computational calculation sheet. As underlined in this work, the way to consider of plasticity in Wang's method does not seem to be sufficient to get a good agreement with the results given by SAFIR. The main reason of this observation is probably due to the conservation of the Young's modulus in the terms relating to the axial and rotational stiffnesses of the beam. An adaptation has been proposed to solve this problem.

Two other modifications have been proposed in the scope of improving Wang's method. The first one integrates the influence of second-order effect on the axial stiffness of a beam and have only a significant impact when significant deflections are experienced. The second modification consists in the definition of a new factor for the interpolation between the deflection profiles of simply-supported beams and fully fixed beams in case of partial rotational restraints. The precision is not improved noticeably with this last modification.

The comparison of results given by the numerical simulations and the analytical method show a very good agreement in case of simply-supported beams, even when significant plastic deformations are obtained. Although several modifications making the resolution of the problem longer and more complicated than with the original Wang's method, the adapted analytical method gives sometimes less accurate results than expected in case of rotationally restrained beams. This is probably due to the difficulty to find the good deflection profile of the beam.

Finally, it has been shown that the behaviour of a beam is elastic during the cooling phase because the beam is unloaded during this period. Using the elastic Wang's method during the cooling phase is a good approximation and the consideration of the M-N interaction, that does not required much additional work, still increases the precision of the obtained results.

8.3 Perspectives

In the present work, several assumptions have been realised and the influence of these aspects should be investigated in future works. This method should also be used as a basis for the design of beams and connections under natural fire.

- Temperature distribution is usually not uniform. The upper beam flange is shielded by a concrete slab and this induces a thermal gradient in the profile. The relative thinness of the web with respect to flanges has also an influence on thermal distribution. The thermal gradient, especially at the beginning of the fire, involves additional deflections and new internal forces by second order effects. In his method, Wang simply proposed to add the thermal deflections to mechanical deflections. This would be useful if this still applies with the adapted method and during the heating phase.

- The present work only considers uniformly distributed loads. Other spatial distributions of load would lead to other deflection profiles. Wang also proposed a deflection profile for punctual loads.

- The rotational restraints caused by joint stiffness are usually not constant during the fire. The variation of internal forces and temperature distribution in the joints has a significant impact on the beam mechanical behaviour. The rotational stiffness of joints may also be strongly reduced in case of buckling in the lower beam flange due to excessive deformations in that zone.

- Finally, the final objective of the RFCS project is to produce some analyse the behaviour of connections under natural fire and to produce some design guidelines. To achieve this goal, the model of connections based on the Component Method should be improved or substituted because it does not allow integrating group effects. Given the importance of axial forces during both the heating and cooling phase and the difficulty to predict the distribution of forces in connections components, the present model can not take group effects into account.

9 References

[K.S. Al-Jabri and al., 1998] "Behaviour of steel and composite beam–column connections in fire", K.S. Al-Jabri, T. Lennon, I.W. Burgess, R.J. Plank, Journal of Constructional Steel Research 46(1–3), 1998.

[K.S. Al-Jabri and al., 2005] "Moment–rotation–temperature curves for semi-rigid joints". K.S. Al-Jabri, I.W. Burgess, T. Lennon, R.J. Plank, Journal of Constructional Steel Research 61:281–303, 2005.

[K.S. Al-Jabri, 2008] "Performance of beam-to-column joints in fire – A review.", K.S. Al-Jabri, J. Buick Davison, I.W. Burgess, Fire Safety Journal 43, 50-62, 2008.

[ASTM, 1998] "Standard test methods for fire testing of building construction and materials, American Society for Testing and Materials", ASTM-E119-98, Philadelphia, 1998

[F.M. Block and al., 2005] "High-Temperature Experiments on Joint Components - The Behaviour of the Compression Zone in the Column Web", F.M. Block, I.W. Burgess, J.B. Davison and R.J. Plank, Eurosteel 2005, 4th European Conference on Steel and Composite Structures, Maastricht, The Netherlands, 2005

[British Steel, 1982] "The performance of beam-to-column and beam-to-beam connections in the BS 5950: Part 8 – Fire Test.", British Steel, Swinden Laboratories, Rotherham, UK, Reports T/RS/1380/33/82D and T/RS/1380/34/82D, 1982.

[BSI, 2000] "Structural use of steelwork in building Part 1: Code of practice for design: rolled and welded sections", British Standards Institution (BSI), 2000

[O.S. Bursi and al., 2008] "Prefabricated Composite Beam-to-Column Filled Tube or Partially Reinforced-Concrete-Encased Column Connections for Severe Seismic and Fire Loadings", Final Report, RFS-CR-03034, O.S. Bursi, F. Ferrario, M. Haller, T. Lennon, L; Bianco, R. Mallardo, J.-F. Demonceau, J.-M. Franssen, J.-P. Jaspart, F. Hanus, A; Plumier, E. Bayo, J. Gracia, E. Alderighi, A. Braconi, W. Salvatore, in Press

[CEN, 1994] "ENV 1993-1-1:1992/prA2:1994, Eurocode 3: Part 1.1, Revised Annex J: Joints in buildings frame", European Committee for Standardization (CEN), Brussels, 2000

[CEN, 2002] "EN 1991-1-2, Eurocode 1: Actions on structures – Part 1-2: General actions –

Actions on structures exposed to fire", European Committee for Standardization (CEN), Brussels, November 2002

[CEN, 2003] "prEN 1993-1-8, Eurocode 3: Design of Steel Structures – Part 1-8: Design of Joints.", European Committee for Standardization (CEN), Brussels, December 2003.

[CEN, 2005] "EN 1993-1-2, Eurocode 3: Design of steel structures - Part 1-2: general rules Structural fire design", European Committee for Standardization (CEN), Brussels, April 2005

[F. Cerfontaine, 2004] "Etude de l'interaction entre moment de flexion et effort normal dans les assemblages boulonnés", F. Cerfontaine, Ph. D. Thesis, May 2004

[J.-M. Franssen, 2007] "User's manual for SAFIR 2007 – A computer program for analysis of structures subjected to fire", J.-M. Franssen, University of Liège, April 2007

[J.-P. Jaspart, 1991] "Etude de la semi-rigidité des noeuds pouter-colonne et son influence sur la résistance et la stabilité des ossatures en acier", J.-P. Jaspart, Ph. D. Thesis (in French), 1991.

[J.-P. Jaspart, 1994] "Numerical simulation of a T-stub – Experimental Data", J.-P. Jaspart, COST C1, Numerical Simulation Working Group, Doc C1WD6/94-09, 1994

[J.-P. Jaspart, K. Weynand and al., 1995-2000] "CoP – The connection program, Software to design joints in steel building frames", RWTH Aachen, MSM Liege, ECCS bv Hoofddorp, 1995-2000

[J. Kruppa, 1976] "Résistance au feu des assemblages par boulons haute résistance.", J. Kruppa, CTICM, France, 1976.

[R.M. Lawson, 1990] Lawson RM. "Behaviour of steel beam-to-column connections in fire.", Structural Engineering 68(14):263–71, 1990.

[L.C. Leston-Jones, 1997] "Elevated-temperature moment-rotation tests on steelwork connections.", L.C. Leston-Jones, I.W. Burgess, T. Lennon, R.J. Plank, Proc. Instn Civ. Engrs Structs & Bldgs, 122, 410-419, Novenber 1997.

[T.C.H. Liu., 1999] "Fire resistance of unprotected steel beams with moment connections", T.C.H. Liu, Journal of Constructional Steel Research 51 (1999) 61–77.

[T.C.H. Liu. and al, 2002] "Experimental investigation of behaviour of axially restrained steel beams in fire", T.C.H. Liu, M.K. Fahad, J.M. Davies, Journal of Constructional Steel

Research 58 (2002) 1211-1230.

[JIS, 1982] "Method of fire resistance test for structural parts of buildings", Japanese Industrial Standard, JIS A 1304, 1982

[H. Riaux, 1980] "Comportement à l'incendie d'assemblages simples boulonnés.", H. Riaux, PhD Thesis, INSA of Rennes, France, 1980.

[A. Santiago, 2007] "Experimental evaluation of the influence of connection typology on the behaviour of steel structures under fire", Aldina SANTIAGO, Paper submitted to AISC, 2007

[L. Simões da Silva and al., 2001] "A component model for the behaviour of steel joints at elevated temperatures", L. Simões da Silva, A. Santiago, P.V. Real, Journal of Constructional Steel Research 57 (2001), 1169–1195

[L. Simões da Silva and al., 2002] "Post-limit stiffness and ductility of end-plate beam-to-column steel joints", L. Simões da Silva, A. Santiago, P.V. Real, Computers and Structures 80 (2002) 515–531

[L. Simoes da Silva and al., 2006] "Experimental behaviour of a steel structure under natural fire.", F. Wald, L. Simoes da Silva, D. B. Moore, T. Lennon, M. Chladna, A. Santiago, M. Benes and L. Borges, Fire Safety Journal 41 (2007), 509-522

[S. Spyrou, 2002] "Development of a component-based model of steel beam-to-column joints at elevated temperature.", S. Spyrou, PhD Thesis, University of Sheffield, 2002

[Y.C. Wang and al., 2005a] "Analysis of catenary action in steel beams using a simplified hand calculation method, Part 1 : theory and validation for uniform temperature distribution", Y.Z. Yin, Y.C. Wang, Journal of Constructional Steel Research 61 (2005) 183-211.

[Y.C. Wang and al., 2005b] "Analysis of catenary action in steel beams using a simplified hand calculation method, Part 2 : theory and validation for non-uniform temperature distribution", Y.Z. Yin, Y.C. Wang, Journal of Constructional Steel Research 61 (2005) 213-234.

[B. Zhao and al., 2008] "Connections of Steel and Composite Structures under Natural Fire Conditions, Mid-term Report", RFSR-CT-2006-00028, B. Zhao, M. Roosefid, A. Breunese, G. Koutlas, G. Zilli, F. Hanus, J.-M. Franssen

10 Appendices

Appendix A Experimental Tests - Analytical calculation of joints resistance and initial stiffness

Beam		Column		Bolts		Plate		Geometry	
Type	UB 178 x 102 x 19	Type	UC 152 x 152 x 30	Type	M16	b_p [mm]	130	w [mm]	60
h_b [mm]	177.8	h_c [mm]	157.6	a [-]	8	t_p [mm]	10	e_{min} [mm]	35
b_b [mm]	101.2	b_c [mm]	152.9	b [-]	8	h_p [mm]	200	c_1 [mm]	51
t_{wb} [mm]	4.8	t_{wc} [mm]	6.5	diam [mm]	16	a_p [mm]	3	p_1 [mm]	40
t_{fb} [mm]	7.9	t_{fc} [mm]	9.4	A [mm^2]	201	a_{p2} [mm]	3.4	p_2 [mm]	58
A [cm^2]	24.26	A [cm^2]	38.26	A_b [mm^2]	157	β [-]	0.85	l_p [mm]	11
r_b [mm]	7.6	r_c [mm]	7.6	d_w [mm]	30	$f_{u,w}$ [N/mm]	430	$m_{colonne}$ [mm]	20.67
A_{vb} [cm^2]	9.85	A_{vc} [cm^2]	11.55	e_w [mm]	7.5	**Material properties**		$e_{colonne}$ [mm]	46.45
Material properties		**Material properties**		L_b [mm]	40.90	f_{yp} [N/mm^2]	327	$n_{colonne}$ [mm]	25.84
f_{yb} [N/mm^2]	327	f_{yc} [N/mm^2]	327	**Material properties**		f_{up} [N/mm^2]	430	m_{plat} [mm]	24.21
γ_{M1}	1	f_{uc} [N/mm^2]	430	f_{ub} [MPa]	800	γ_{M1}	1	n_{plat} [mm]	30.26
		E_c [N/mm^2]	210000	f_{yb} [MPa]	640				
		γ_{M1}	1	γ_{M2}	1				

Joint resisting moment

1. Row of bolts n°1

Column web in shear :	196.33	kN
Column web in compression :	204.75	kN
Column flange in bending :	169.32	kN
Column web in tension :	222.05	kN
End-plate in bending :	171.50	kN
Bolts in tension :	226.08	kN
Beam flange in compression :	329.69	kN
Beam web in tension :	239.97	kN

$F_{Rd,1}$ [kN] 169.32

2. Row of bolts n°2

2.1. Bolt considered individually

Column web in shear :	27.01	kN
Column web in compression :	35.43	kN
Column flange in bending :	169.32	kN
Column web in tension :	222.05	kN
End-plate in bending :	167.85	kN
Bolts in tension :	226.08	kN
Beam flange in compression :	160.37	kN
Beam web in tension :	220.91	kN

2.2. Bolt considered as part of a group (1+2)

Column flange in bending :	83.33	kN
Column web in tension :	81.61	kN
End-plate in bending :	91.25	kN
Beam web in tension :	133.43	kN

$F_{Rd,2}$ [kN] 27.01

3. Récapitulatif et Calcul du moment résistant

$F_{Rd,1}$ [kN]	169.32
$F_{Rd,2}$ [kN]	27.01

M_{Rdj} [kN.m]	25.20
M_{Rdw} [kN.m]	32.35

M_{Rd} [kN.m]	25.20
$M_{élast.}$ [kN.m]	16.80

Joint initial stiffness

$k_{eff,1}$ [mm]	1.31
$k_{eff,2}$ [mm]	0.76
$k_{eff,3}$ [mm]	1.41

z [mm]	107.74
$k_{eq,tr}$ [mm]	2.76
$k_{eq,comp}$ [mm]	2.14

Raideur initiale :	2940	kN.m/rad
Raideur idéalisée :	1470	kN.m/rad
Raideur sécante :	980	kN.m/rad

Appendix B Manchester Tests: Vertical Displacements, Axial Thrusts & Hogging Bending Moments

Vertical Deflection – k = 8 kN/mm

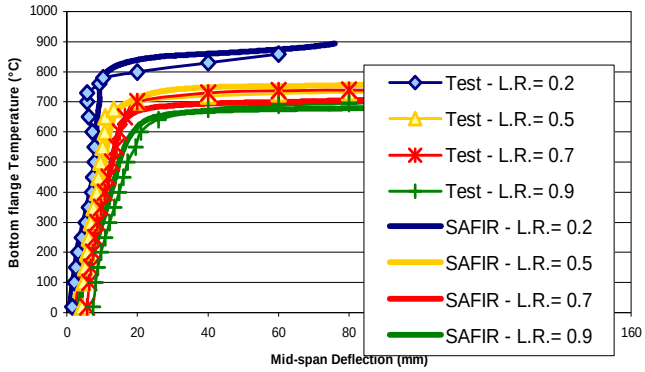

Axial Thrust – k = 8 kN/mm

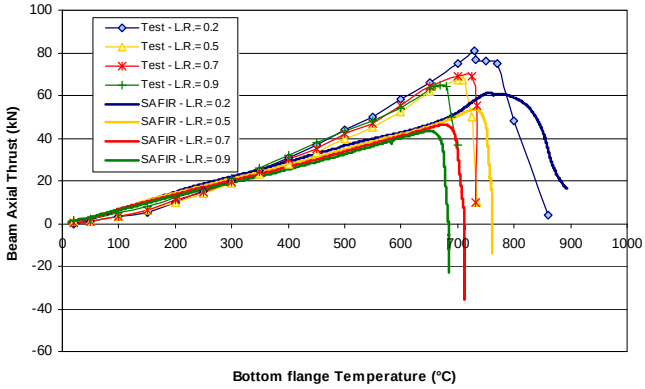

Hogging Bending Moment – k = 8 kN/mm

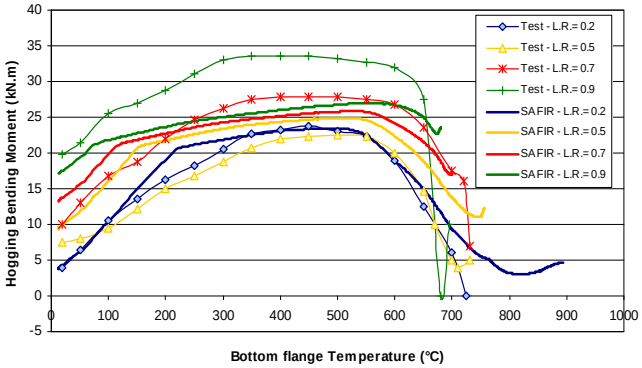

Vertical Deflection – k = 35 kN/mm

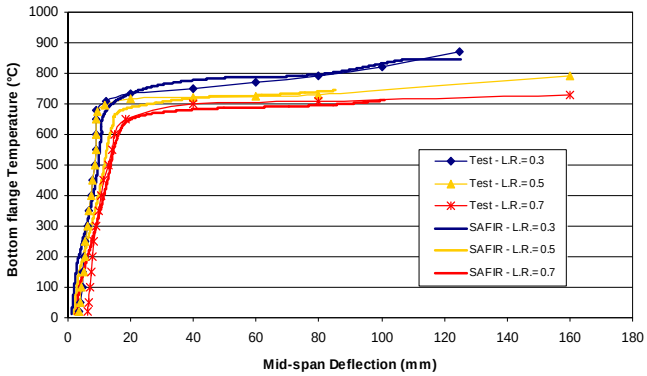

Axial Thrust – k = 35 kN/mm

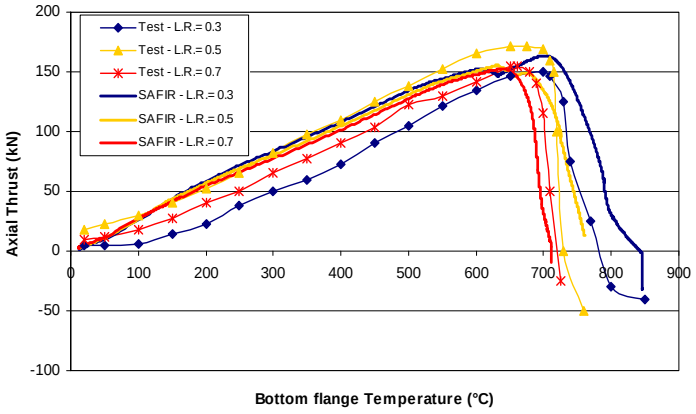

Vertical Deflection – k = 62 kN/mm

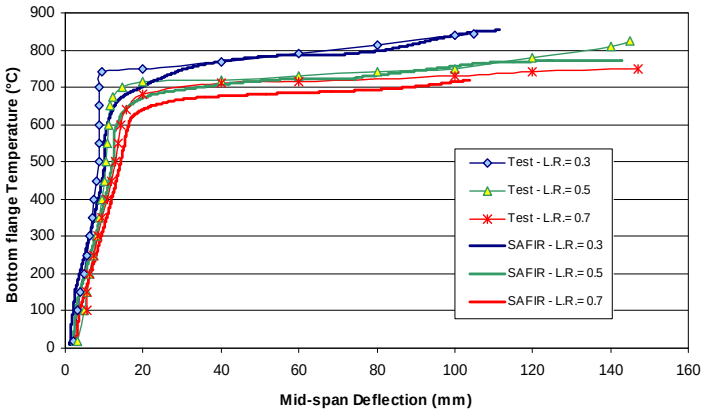

Axial Thrust – k = 62 kN/mm

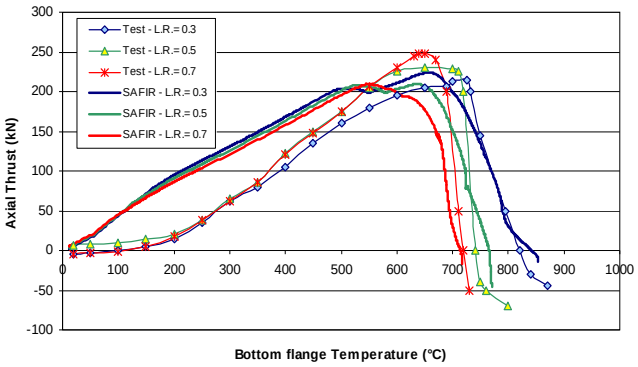

Hogging Bending Moment – k = 62 kN/mm

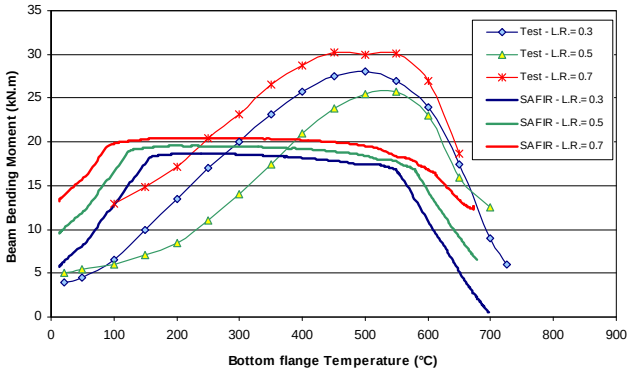

Appendix C COSSFIRE Tests - Thermal Analysis : Comparison between numerical results and experimental measurements

Test n°1

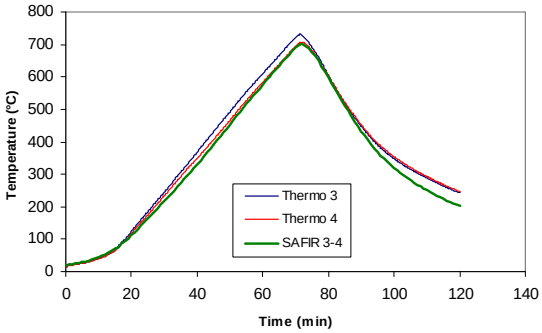

Plate (Beam side)

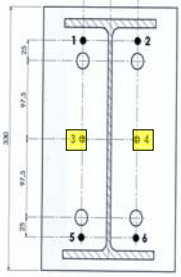

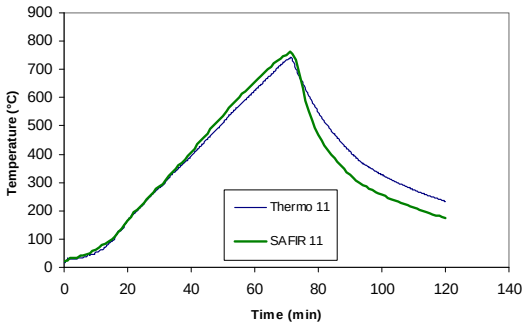

Beam (B1)

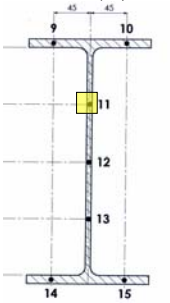

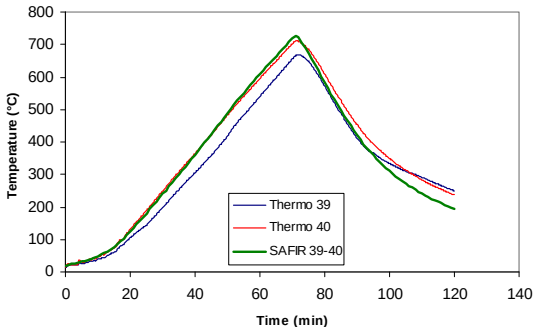

Bolts

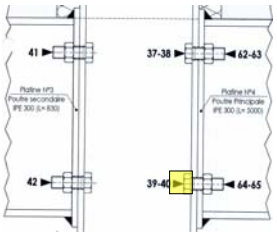

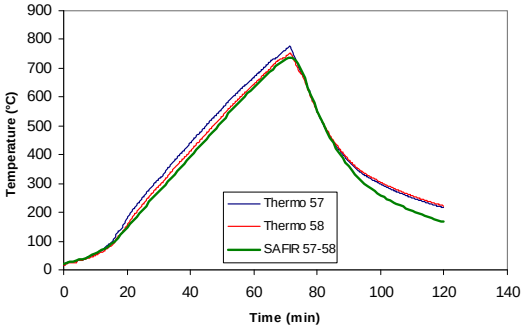

Column (C4)

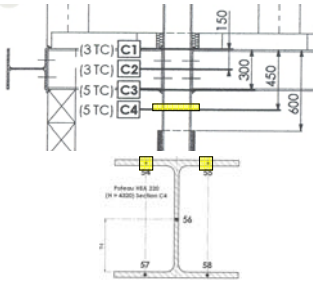

Test n°2

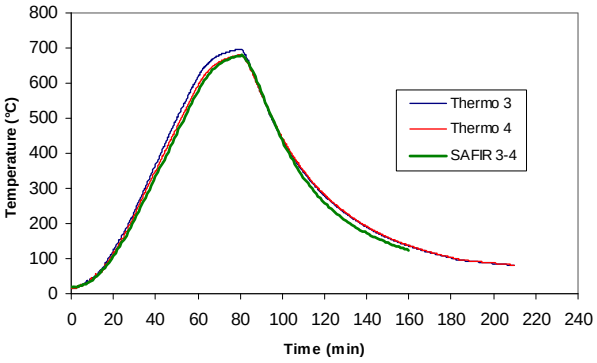

Plate (Beam side)

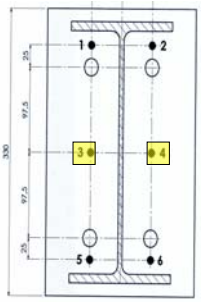

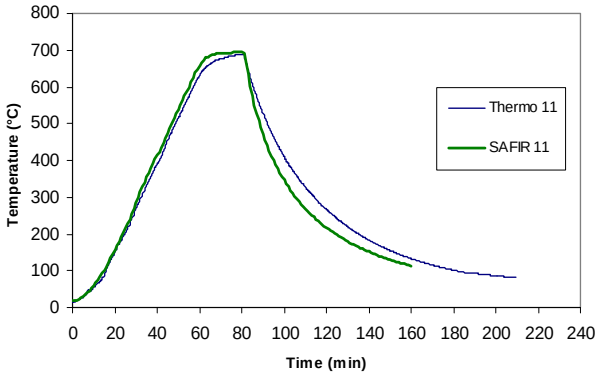

Beam (B1)

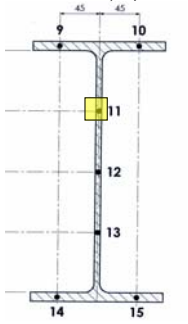

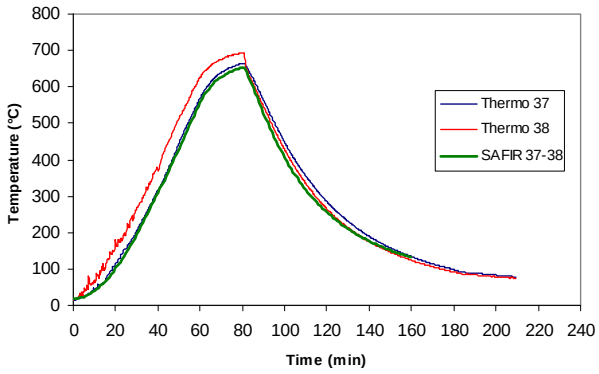

Bolts

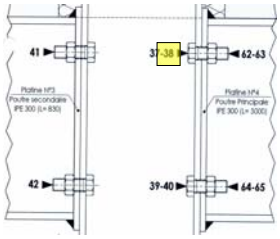

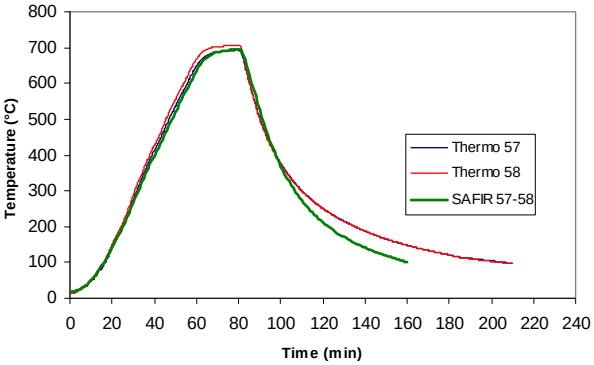

Column (C4)

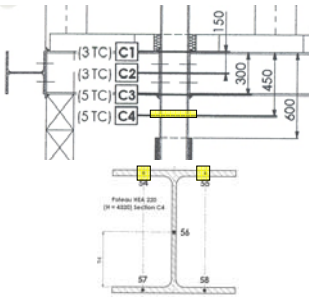

Appendix D Two-dimensional cases : parametrical analysis

i. Parameter n°1: Axial restraints

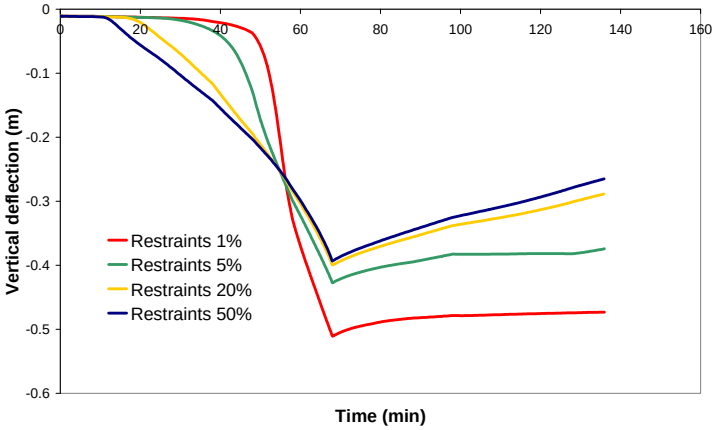

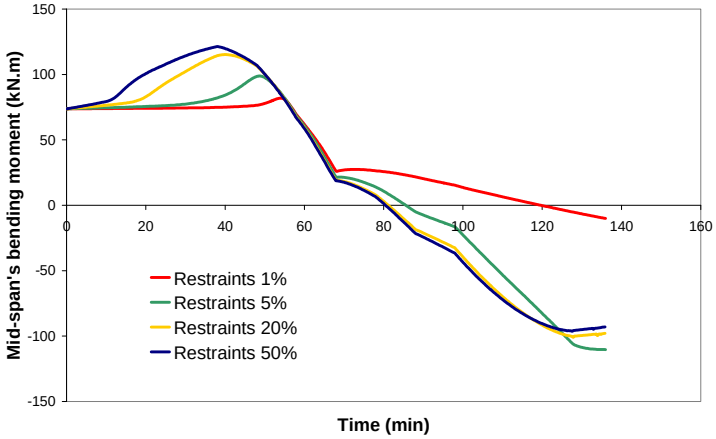

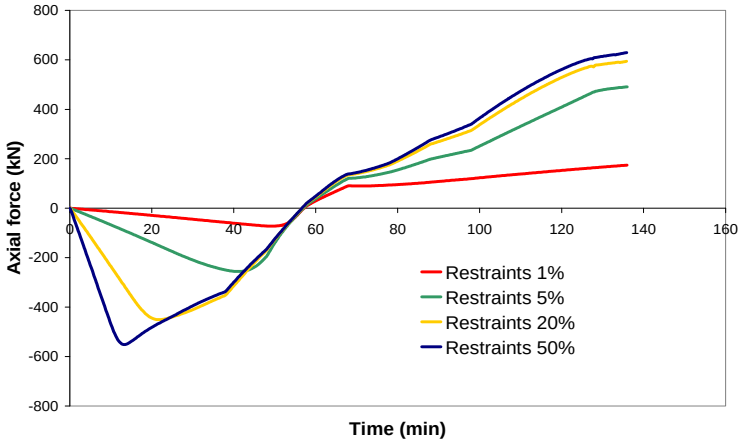

ii. Parameter n°2: Rotational restraints (At 600°C)

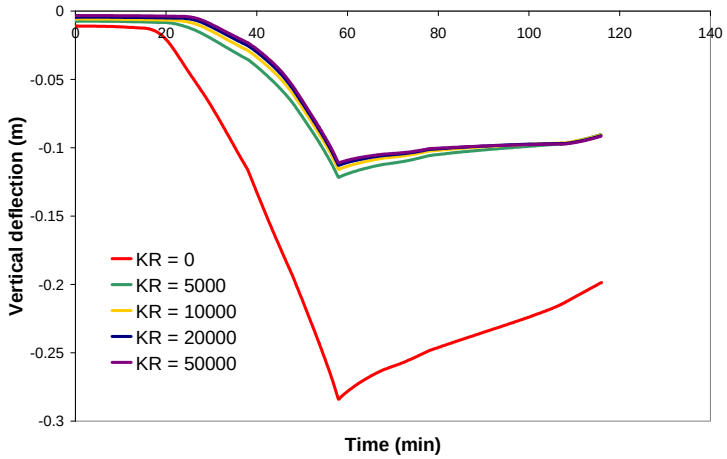

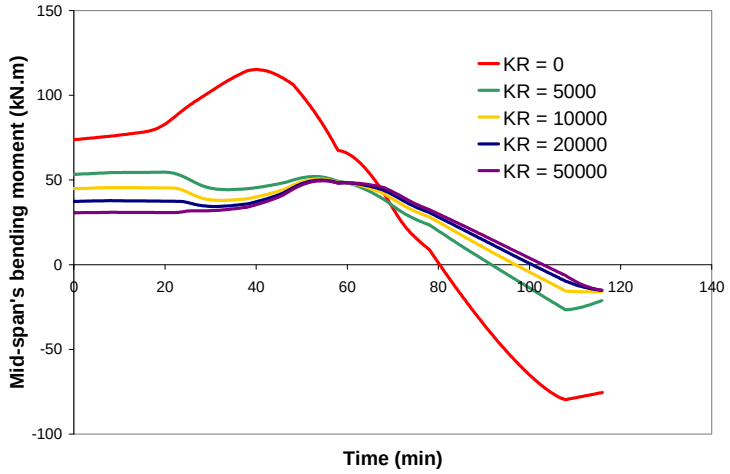

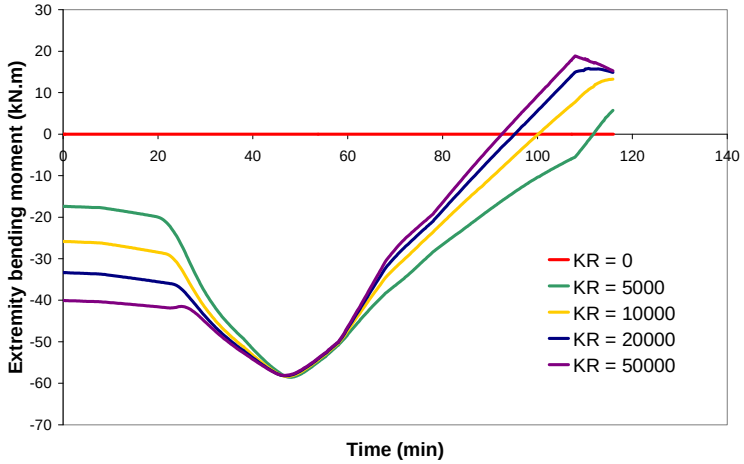

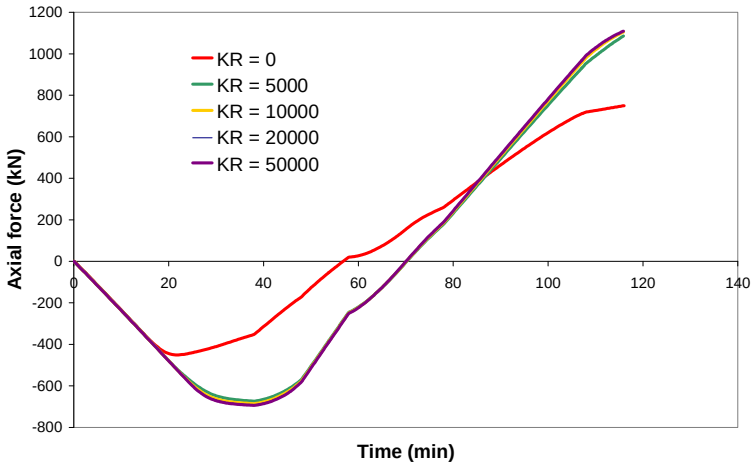

iii. Parameter n°3: Steel grade/Yield strength

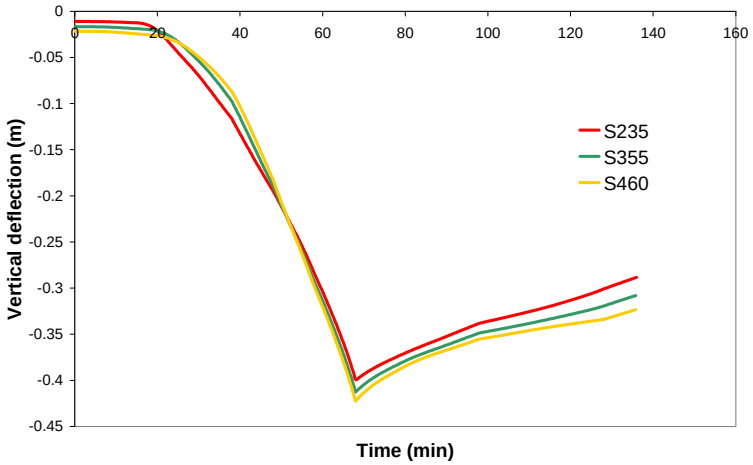

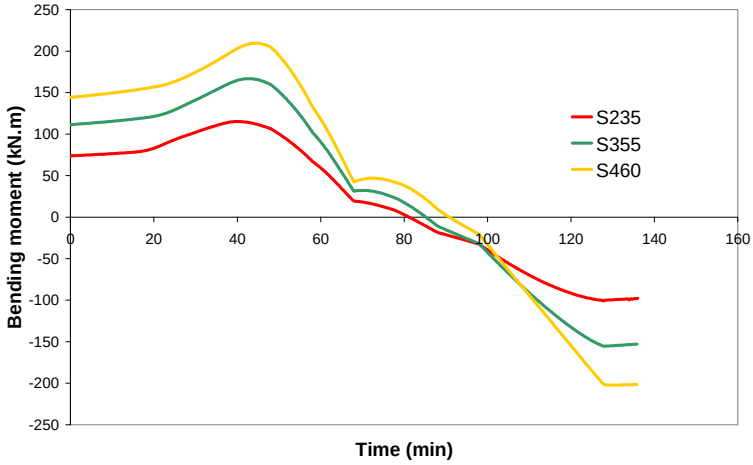

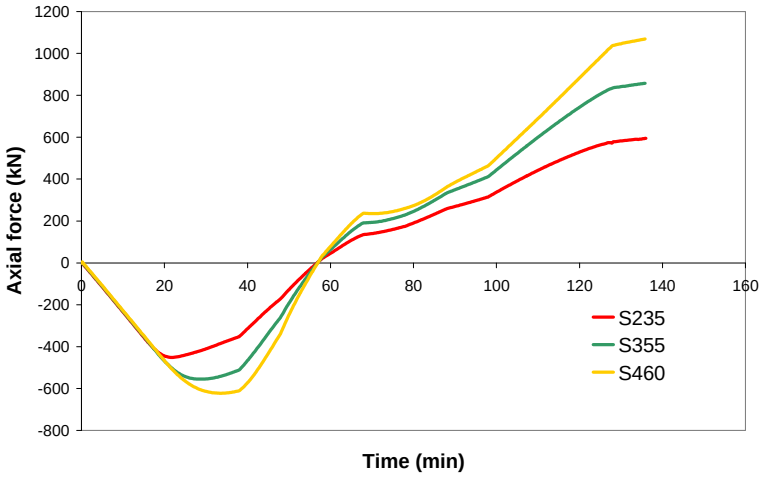

iv. Parameter n°4: Maximal temperature

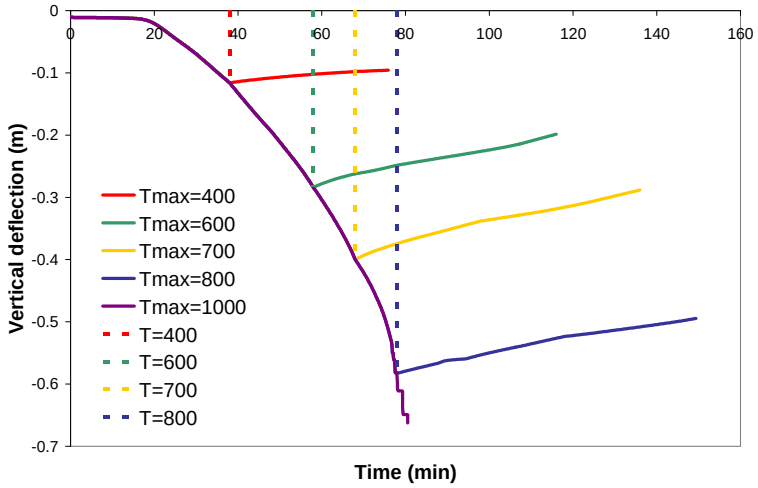

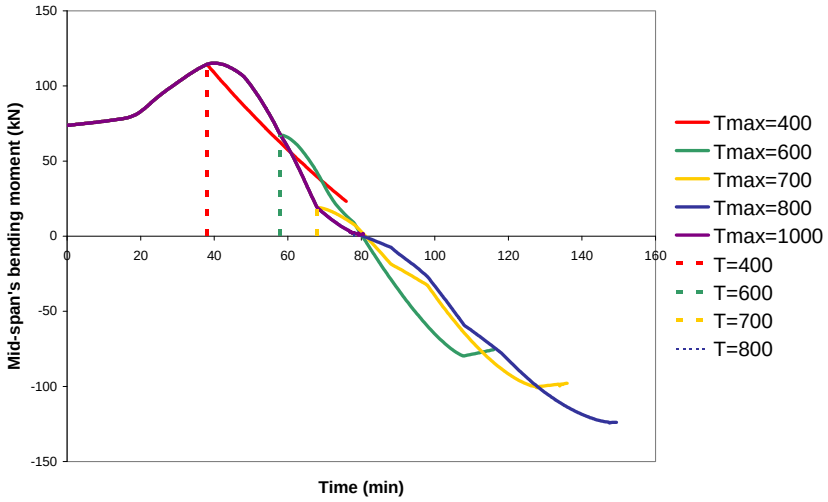

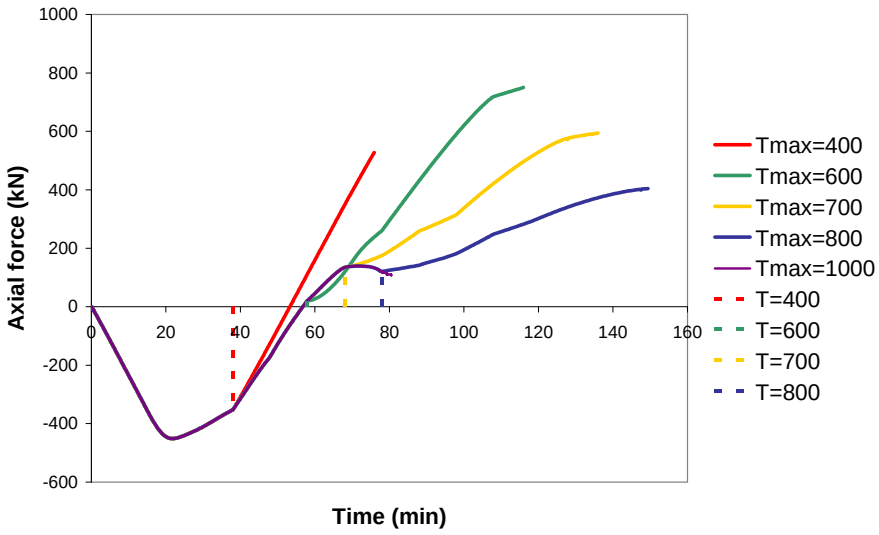

v. Parameter n°5: Beam Length

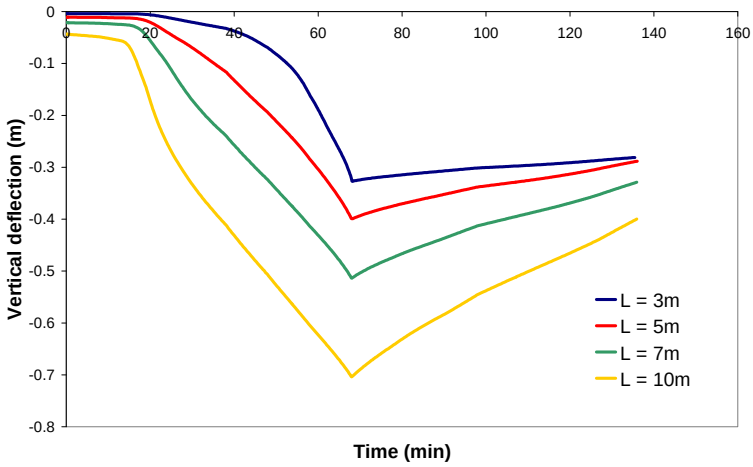

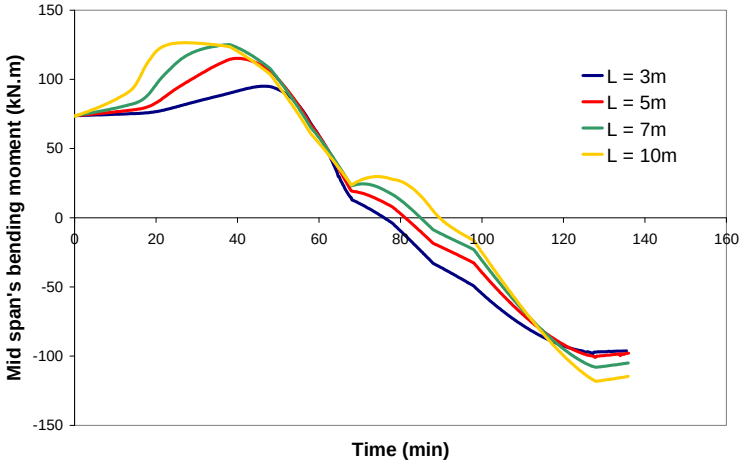

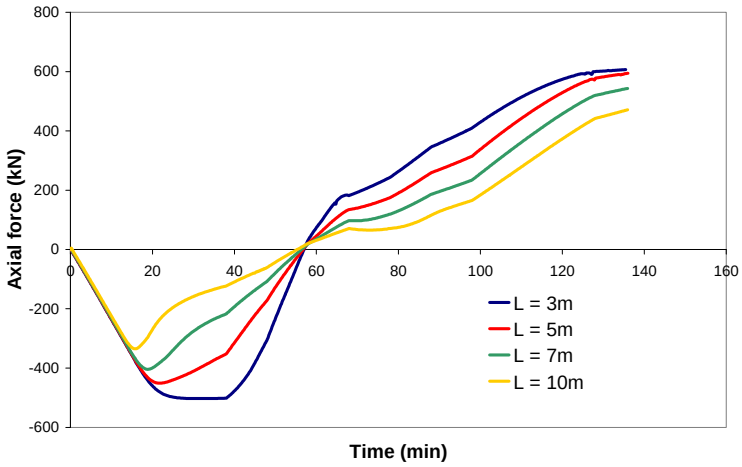

vi. Parameter n°6: Load Ratio

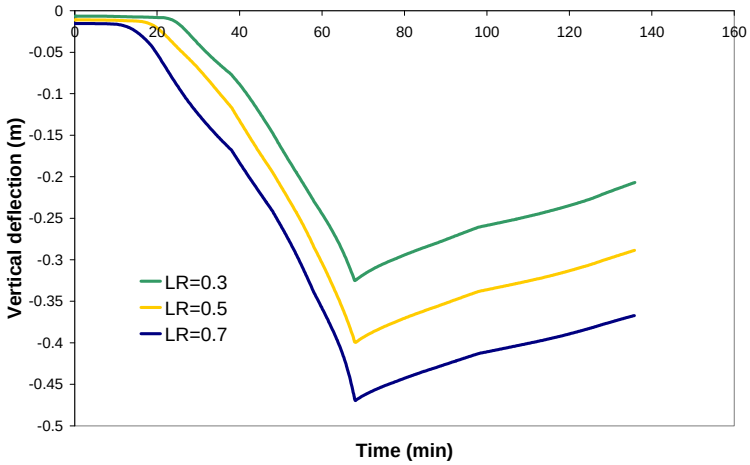

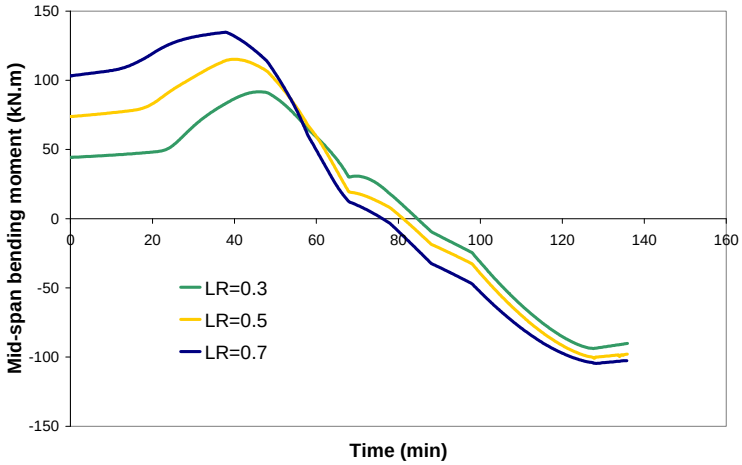

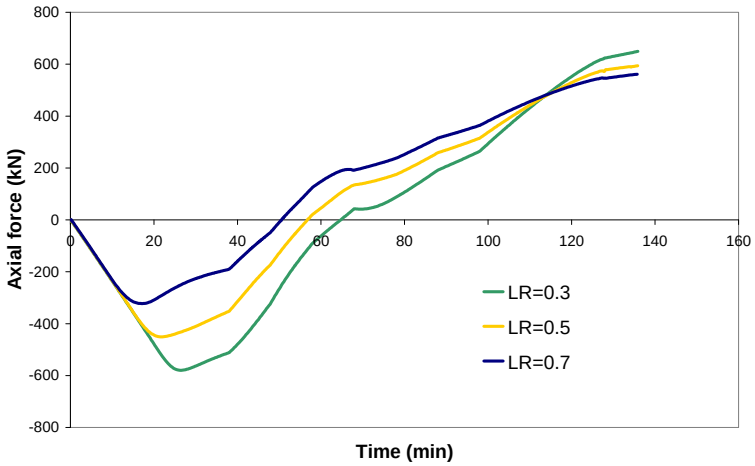
800
600
400
200
0
-200
-400
-600
-800
0
20
40
60
80
100
120
140
160
Axial force (kN)
Time (min)
LR=0.3
LR=0.5
LR=0.7

Appendix E Analytical calculation of the global rotational stiffness in a beam with two equivalent flexible supports.

The global rotational stiffness K'_R, defined as the ratio between the moment applied at a support and the rotation of this support, is calculated by adding the rotational stiffness of the flexible "loaded" support $K_1 = K_R$ and the rotational stiffness of the beam when the "loaded" support is substituted by a pinned support K_2.

The rotational stiffness K_2 is equal to the ratio between the unitary applied moment M and the rotation of the beam at the free support θ.

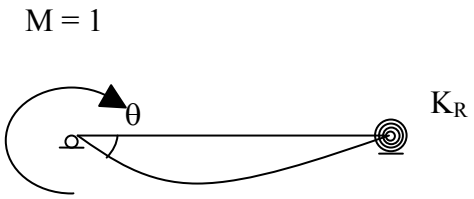

Figure D-1: Rotational stiffness K_2

This structural is calculated with the "Forces Method". The degree of hyperstaticity is 1. The bending moment at the flexible support is the unknown parameter but an additional equation is given between the bending moment and the rotation of this support.

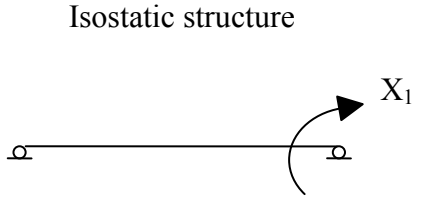

$$f_{11} = \frac{1}{3}\frac{L}{EI} \quad ; \quad f_{1P} = -\frac{1}{6}\frac{L}{EI}$$

$$f_{11} X_1 + f_{1P} = -\frac{X_1}{K_R}$$

$$\Leftrightarrow \; X_1 = \frac{\frac{L}{6EI}}{\frac{L}{3EI} + \frac{1}{K_R}}$$

Check: If $K_R = 0$ → $X_1 = 0$ OK

If $K_R = \infty$ → $X_1 = -1/2$ OK

The rotation θ of the free support is the superposition of the rotation under the unitary bending moment M and the hyperstatic bending moment. Thus, the rotational stiffness of the beam when the "loaded" support is substituted by a pinned support K_2 is:

$$K_2 = \left(\frac{L}{3EI} + \frac{\frac{L}{6EI}}{\frac{L}{3EI} + \frac{1}{K_R}} \right)^{-1}$$

and the global rotational stiffness K'_R is:

$$K'_R = K_1 + K_2 = K_R + \left(\frac{L}{3EI} + \frac{\frac{L}{6EI}}{\frac{L}{3EI} + \frac{1}{K_R}} \right)^{-1}$$

Appendix F Analytical calculation of beam axial stiffnesses accounting for second order effects.

The variation of the distance between beam extremities is obtained by use of the theorem of the unitary force:

$$F.d = d = \int_0^L \frac{M.M_1}{EI}\,dx + \int_0^L \frac{N.N_1}{EA}\,dx \quad \text{(influence of shear forces neglected)}$$

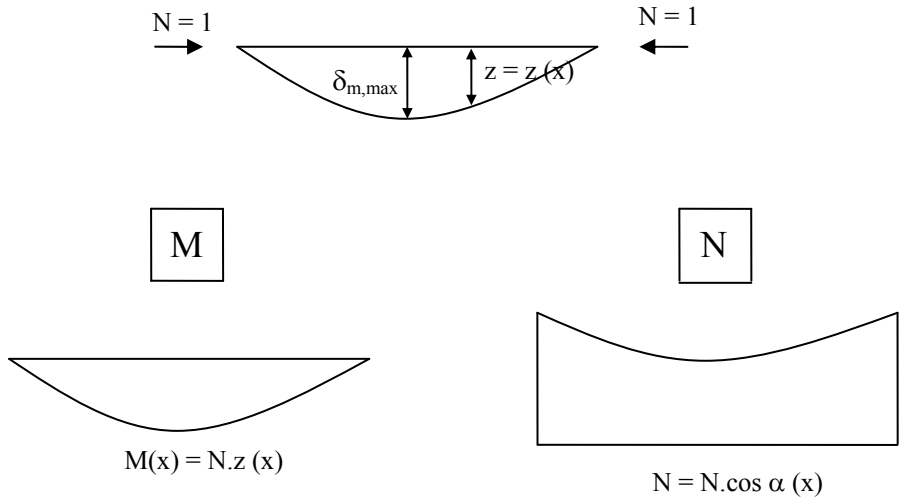

Figure E-1 : Bending moment and normal force including second order effects

Simply supported beam deflection profile

$$\int_0^L \frac{M.M_1}{EI}\,dx = \frac{1}{EI}\int_0^L \left(\frac{16\,\delta_{m,\max}}{5L}\right)^2 \left(\frac{x^4}{L^3} - \frac{2x^3}{L^2} + x\right)^2 dx$$

$$= \frac{1}{EI}\left(\frac{16\,\delta_{m,\max}}{5L}\right)^2 \int_0^L \left(\frac{x^8}{L^6} + \frac{4x^6}{L^4} + x^2 - \frac{4x^7}{L^5} - \frac{4x^4}{L^2} + \frac{2x^5}{L^3}\right) dx$$

$$= \frac{1}{EI}\left(\frac{16\,\delta_{m,\max}}{5L}\right)^2 \left[\frac{x^9}{9L^6} + \frac{4x^7}{7L^4} + \frac{x^3}{3} - \frac{4x^8}{8L^5} - \frac{4x^5}{5L^2} + \frac{2x^6}{6L^3}\right]_0^L$$

$$= \frac{1}{EI}\left(\frac{16\,\delta_{m,\max}}{5L}\right)^2 . L^3 . \left[\frac{1}{9} + \frac{4}{7} + \frac{1}{3} - \frac{4}{8} - \frac{4}{5} + \frac{2}{6}\right]$$

$$= \frac{3968\,.\,\delta_{m,\max}^2\,.L}{7875\,EI}$$

$$\int_0^L \frac{N.N_1}{EA}\,dx = \frac{1}{EA}\int_0^L \left(1-\left(\frac{16\,\delta_{m,\max}}{5L}\right)^2\left(\frac{4x^3}{L^3}-\frac{6x^2}{L^2}+1\right)^2\right)\,dx$$

$$= \frac{L}{EA}-\frac{1}{EA}\left(\frac{16\,\delta_{m,\max}}{5L}\right)^2\int_0^L \left(\frac{16x^6}{L^6}+\frac{36x^4}{L^4}+1-\frac{48x^5}{L^5}-\frac{12x^2}{L^2}+\frac{8x^3}{L^3}\right)dx$$

$$= \frac{L}{EA}-\frac{1}{EA}\left(\frac{16\,\delta_{m,\max}}{5L}\right)^2\left[\frac{16x^7}{7L^6}+\frac{36x^5}{5L^4}+x-\frac{48x^6}{6L^5}-\frac{12x^3}{3L^2}+\frac{8x^4}{4L^3}\right]_0^L$$

$$= \frac{L}{EA}-\frac{1}{EA}\left(\frac{16\,\delta_{m,\max}}{5L}\right)^2.L.\left[\frac{16}{7}+\frac{36}{5}+1-\frac{48}{6}-\frac{12}{3}+\frac{8}{4}\right]$$

$$= \frac{L}{EA}-\frac{4352\,.\,\delta_{m,\max}^2}{875\,EA\,.L}$$

Fully fixed beam deflection profile

$$\int_0^L \frac{M.M_1}{EI}\,dx = \frac{1}{EI}\int_0^L \left(\frac{16\,\delta_{m,\max}}{L^2}\right)^2\left(\frac{x^4}{L^2}-\frac{2x^3}{L}+x^2\right)^2\,dx$$

$$= \frac{1}{EI}\left(\frac{16\,\delta_{m,\max}}{L^2}\right)^2\int_0^L \left(\frac{x^8}{L^4}+\frac{4x^6}{L^2}+x^4-\frac{4x^7}{L^3}-\frac{4x^5}{L}+\frac{2x^6}{L^2}\right)dx$$

$$= \frac{1}{EI}\left(\frac{16\,\delta_{m,\max}}{L^2}\right)^2\left[\frac{x^9}{9L^4}+\frac{4x^7}{7L^2}+\frac{x^5}{5}-\frac{4x^8}{8L^3}-\frac{4x^6}{6L^2}+\frac{2x^7}{7L^2}\right]_0^L$$

$$= \frac{1}{EI}\left(\frac{16\,\delta_{m,\max}}{L^2}\right)^2.L^5.\left[\frac{1}{9}+\frac{4}{7}+\frac{1}{5}-\frac{4}{8}-\frac{4}{6}+7\right]$$

$$= \frac{128\,.\,\delta_{m,\max}^2\,.L}{315\,EI}$$

$$\int_0^L \frac{N.N_1}{EA}\,dx = \frac{1}{EA}\int_0^L \left(1-\left(\frac{16\,\delta_{m,\max}}{L^2}\right)^2\left(\frac{4x^3}{L^2}-\frac{6x^2}{L}+2x\right)^2\right)\,dx$$

$$= \frac{L}{EA}-\frac{1}{EA}\left(\frac{16\,\delta_{m,\max}}{L^2}\right)^2\int_0^L \left(\frac{16x^6}{L^4}+\frac{36x^4}{L^2}+4x^2-\frac{48x^5}{L^3}+\frac{16x^4}{L^2}-\frac{24x^3}{L}\right)dx$$

$$= \frac{L}{EA}-\frac{1}{EA}\left(\frac{16\,\delta_{m,\max}}{L^2}\right)^2\left[\frac{16x^7}{7L^4}+\frac{36x^5}{5L^2}+\frac{4x^3}{3}-\frac{48x^6}{6L^3}-\frac{16x^5}{5L^2}+\frac{24x^4}{4L}\right]_0^L$$

$$= \frac{L}{EA}-\frac{1}{EA}\left(\frac{16\,\delta_{m,\max}}{L^2}\right)^2.L^3.\left[\frac{16}{7}+\frac{36}{5}+\frac{4}{3}+\frac{16}{5}-8-6\right]$$

$$= \frac{L}{EA}-\frac{512\,.\,\delta_{m,\max}^2}{105\,EA\,.L}$$

Table of contents